FACULDADE DE ENGENHARIA DA UNIVERSIDADE DO PORTO

3D Breast Cancer Models: Multimodal Data Registration

Cátia Sofia Gonçalves Rodrigues

Integrated Master in Bioengineering

Supervisor: Hélder Filipe Pinto de Oliveira, PhD

Co-supervisor: Sílvia da Conceição Neto Bessa, MSc

September 16, 2019

3D Breast Cancer Models: Multimodal Data Registration

Cátia Sofia Gonçalves Rodrigues

Integrated Master in Bioengineering

September 16, 2019

Resumo

O cancro da mama é uma doença amplamente conhecida, principalmente em mulheres. Tem uma mortalidade consideravelmente baixa comparativamente com outras formas de cancro, no entanto é a forma mais comum nas mulheres, trazendo graves consequências a nível físico e psicológico. Esta baixa mortalidade deve-se maioritariamente à monitorização desde cedo de mulheres que se encontrem no grupo de risco para esta forma de cancro, dada a sua idade ou o seu histórico familiar, permitindo uma deteção precoce do cancro assim como um tratamento antecipado, que consequentemente será mais eficaz.

A maioria das pacientes necessita de realizar cirurgia mamária para a remoção do tumor, e esta cirurgia pode ter o propósito de remover a totalidade da mama ou apenas a zona onde o tumor se encontra e as suas redondezas. Os resultados desta cirurgia nem sempre correspondem ao que era expectável, e a mama pode de alguma forma ficar deformada após a cirurgia.

A presença de um modelo tridimensional da mama, que é específico à paciente, irá melhorar a comunicação entre a paciente e o clínico, permitindo uma visualização mais clara do modelo da mama e da localização do tumor, antes da cirurgia. Esta visualização permitirá uma melhor compreensão de como será a cirurigia e do que é que a paciente pode esperar desta. Estes modelos podem também ser usados para criar modelos biomecânicos ou modelos criados a partir de *Machine Learning*, que irão ajudar a prever as deformações que irão ocorrer na mama também. No entanto, estes modelos não são fáceis de obter, maioritariamente devido à natureza não rígida e deformável da mama.

Muitas técnicas de imagem são usadas na atualidade na deteção de cancro da mama, como ultrassons, mamografias e ressonâncias magnéticas, e esta última será usada na aquisição de imagens deste trabalho, pois fornece a informação interior da mama dividida por fatias que depois são usadas para construir um volume. Para criar este modelo, imagens de ressonância magnética e de superfície, e a sua correspondência serão feitas para combinar tanto a informação externa como a interna da mama. Os dados de ambas as modalidades não são obtidos com o paciente na mesma posição portanto, primeiramente deve ocorrer uma transformação de pose.

Apesar da mama ter um comportamento não rígido, o registo dos dados obtidos da ressonância magnética e da superfície irão incluir um registo rígido e não rígido. O registo rígido é um passo essencial para a boa performance do registo não rígido, tendo em conta que irá aproximar as duas nuvens de pontos e irá colocá-las no mesmo espaço. O registo rígido incluirá transformações como rotações e translações e a implementação do algoritmo *Iterative Closest Point*. O registo não rígido será feito pela implementação do algoritmo *Free Form Deformation*.

Pacientes provenientes de dois projetos diferentes serão usados para formar os conjuntos de dados usados nesta dissertação, que incluirá também um conjunto de dados para validação. Métricas como a distância Euclideana e a distância de *Hausdorff* são usadas para avaliar a precisão das transformações, no entanto essas métricas não consideram que os pontos estão na verdade a representar um objeto tridimensional, não sendo totalmente confiáveis. Para complementar estes

resultados, a visualização das nuvens de pontos e dos passos intermédios do registo é essencial para compreender qual será a melhor metodologia a implementar.

Um conjunto de dados de validação foi também criado com a intenção de validar as deformações induzidas na mama. Este conjunto inclui sete pacientes, com pontos de referência marcados com cápsulas de óleo de fígado de bacalhau. Os resultados mostram que a melhor implementação regista apenas uma mama de cada vez e não o torso completo e usa o paciente na posição vertical, depois da transformação de pose. O registo rígido inclui duas rotações, uma correção de orientação através do plano xy, uma translação através da zona do mamilo e a implementação do *Iterative Closest Point*. O registo não rígido será realizado usando a *Free Form Deformation* com uma grelha de pontos de controlo de [6,6,6].

Os resultados obtidos são bastante promissores para uma futura implementação em ambiente clínico, providenciando uma excelente ferramenta para ajudar tanto o paciente como o clínico, para respetivamente compreender e planear melhor as consequências da cirurgia mamária.

Abstract

Breast cancer is a widely known disease, mostly for its appearance in women. It has a considerable low mortality comparing to other forms of cancer, but it is the most common form of cancer in women, bringing meaningful physical and mental consequences for the patients. This low mortality is mainly due to the monitoring of the women who are above a certain age, or have a certain family history, which allows an early detection of the cancer as well as an early treatment, that is consequently more effective.

Most of the patients need to perform breast surgery to remove the tumour, and this surgery can be to remove the entirety of the breast or only the tumour and its surroundings. The outcomes of this surgery do not always match what was previously expected, and the breast can be somehow deformed after the procedure.

The presence of a three-dimensional breast model, that is patient specific, will improve the communication between the patient and the doctor, allowing a clear visualization of the breast and the tumor before the surgery. This visualization will allow a better understanding of how the surgery will be and what can the patient expect from it. These models can also be used to create biomechanical models or models created from Machine Learning, which will help predict the deformations of the breast as well. These models are not easy to be obtained, mostly due to the non-rigid and deformable nature of the breast.

A lot of imaging techniques are nowadays being used in the detection of breast cancer, as ultrasounds, mammograms and Magnetic Resonance Imaging, being the last one the one that is going to be used for the acquisition of breast images since it provides the interior information pf the breast divided by slices that can then form a volume. To create this model, images from Magnetic Resonance Imaging and surface data must be combined, and the matching will be done to combine both interior and exterior information of the breast. The data from both modalities is not acquired with the patient in the same position, so firstly a pose transformation must be performed.

Even though the breast has a non-rigid behaviour, the registration of the data from the Magnetic Resonance Imaging and the surface will include a rigid and a non-rigid registration. The rigid registration is an essential step to the good performance of the non-rigid registration since it will approximate both point clouds and place them in the same coordinate system. Rigid registration will include affine transformations such as rotations and translations and the implementation of a Iterative Closest Point Algorithm. Non-rigid registration is done by performing a Free Form Deformation algorithm.

Patients from two different projects are used to fill the datasets, that will also include a validation dataset. Metrics such as the Euclidean Distance and the Hausdorff Distance are used to evaluate the accuracy of the transformations, but these metrics do not consider that the points are actually representing a three-dimensional object so they are not fully reliable. So, to complement these results visualizing the final point clouds and the intermediate steps is essential to understand which is the best methodology.

A validation dataset was also created with the intention of validating the induced deformations in the breast. This dataset includes 7 patients, with reference points marked with codfish oil pills. The results showed that the best implementation registers a single breast at a time, and not the entire torso, and uses the patient in an upright position, after the pose transformation. The rigid registration will include two rotations, a correction of the orientation through the xy plane, a translation through the breast mounds and an Iterative Closest Points algorithm. The non-rigid registration will be performed using the Free Form Deformation algorithm with a [6,6,6] grid of control points.

The results obtained are very promising for a future implementation on a clinical environment providing a great tool to help both the patient and the clinician, to respectively understand and plan better the consequences of a breast cancer surgery.

Agradecimentos

Em primeiro lugar gostaria de agradecer ao INESC-TEC e ao grupo CTM pela oportunidade dada em realizar esta dissertação no contexto de um grupo tão completo e tão motivado. Um particular agradecimento ao meu orientador, o Professor Hélder Oliveira, por todo o apoio e motivação que me deu ao longo deste ano e por toda a flexibilidade mostrada, as suas ideias foram fundamentais para a boa realização desta dissertação. Um enorme agradecimento à Sílvia, minha co-orientadora, por toda a paciência para resolver as minhas dúvidas, pelo trabalho incansável e por todas as ideias e críticas extraordinárias que complementaram imenso este trabalho. Ainda dentro deste grupo gostaria de agradecer à Sara Oliveira por todo o apoio no tratamento dos dados e por me ter ajudado a descomplicar muita coisa ao longo deste trabalho, ao João Teixeira pela sua disponibilidade e ajuda e ao Henrique Carvalho pelo trabalho fornecido que me deu toda a base para esta dissertação e por todo o trabalho que fez desde o início da minha dissertação que deu mais qualidade aos resultados que aqui apresento. Dentro do projecto do BCCT.plan gostaria de ainda agradecer ao Doutor Pedro Gouveia por todos os dados fornecidos e apoio neste projeto, que foram cruciais para a realização desta dissertação e para os resultados obtidos.

À Adapttech, obrigada por acreditarem nas minhas capacidades e por me acolherem na empresa que mais parece uma família e que está sempre ansiosa por ver o meu sucesso e felicidade. Um particular agradecimento à Sofia pela ajuda enorme na minha integração como trabalhadora-estudante, pelo suporte dado e por me fazer sentir em casa.

Aos Catos, André, Luis, Hugo e Margarida, sou uma pessoa diferente graças a vocês, toda a vossa paciência comigo e todo o stress que passei convosco fizeram-me crescer imenso e fizeram-me não ter medo das coisas que me rodeiam, obrigada *for daring me to grow* e por terem crescido comigo, sou uma secretária orgulhosa. A todo o BEST Porto, obrigada por me proporcionarem as melhores experiências da faculdade, por me darem a oportunidade de conhecer o mundo e por me deixarem fazer parte da direção desta incrível associação. Serei uma alumna saudosa e deixarei parte do meu coração aqui, mas levarei memórias para uma vida.

À Rita, obrigada por toda a tua honestidade e por acreditares mais em mim do que eu própria, deste-me uma enorme motivação ao longo deste tempo todo. À Amélia por todas as conversas na varanda, todos os desabafos e chapadas de realidade, passe o tempo que passar sei que tenho em ti um poço de confiança. À Raquel, tenho o maior orgulho do mundo em ti e ao fim destes 14 anos de amizade, devo-te muitos dos momentos mais felizes e muita da minha recuperação em momentos tristes, obrigada por estares sempre lá, mesmo longe de mim. À Sónia, eu sei que me mandaste dormir durante estes 5 anos da faculdade, mas eu prometo que o vou fazer agora... O meu sucesso académico deve-se imenso ao teu apoio e à inspiração que me dava, obrigada por me chamares à realidade e por saberes sempre dizer o que eu precisava de ouvir. Ao João, por aguentares os meus devaneios e por seres sempre o meu porto seguro, obrigada por seres incansável e por tomares conta de mim (e por me alimentares também), mesmo quando eu não sabia que precisava que o fizessem.

À minha irmã, desculpa por não poder brincar mais contigo, por não ir ao teu primeiro dia na

escolinha e por ter de te deixar tanto tempo. Prometo que te vou ajudar a fazer os trabalhos de casa e que vou estar sempre lá quando precisares. E acima de tudo, à minha mãe, o meu maior exemplo e a responsável por tudo aquilo que consegui, só espero um dia poder ter tanta força como tu mãe. Isto é tudo por vós.

"We live on an island surrounded by a sea of ignorance. As our island of knowledge grows, so does the shore of our ignorance."

John Archibald Wheeler

Contents

List of Figures

List of Tables

Abbreviations

3D	3 Dimensional
BCS	Breast-Conserving Surgery
BCT	Breast-Conserving Therapy
CC	Correlation Coefficient
CT	Computerized Tomography
DoF	Degrees of Freedom
ECG	Electrocardiogram
FEM	Finite Elements Method
FFD	Free Form Deformation
FoV	Field of View
ICP	Iterative Closest Points
MRI	Magnetic Resonance Imaging
MSE	Mean Squared Error
NaN	Not a Number
PCA	Principal Component Analysis
PCL	Point Cloud
PET	Positron Emission Tomography
QoL	Quality of Life
RF	Radio Frequency
RMSE	Root-Mean-Square Error
ROI	Regions Of Interest
SNR	Signal-to-noise ratio
SSD	Sum of Squared Differences
TRE	Target Registration Error

Chapter 1

Introduction

1.1 Context

Breast cancer is a widely known disease, being one of the most common forms of cancer in women [1]. Its low mortality, compared to its incidence, is mostly due to all the methods of screening being implemented nowadays [2]. Women start being monitored, around the age of 40, and campaigns are made to raise awareness of how dangerous the disease is, and inform about the ways to monitor the breast's health, so the diagnosis is made early in order to increase the probability of success of the treatment. This process starts with self breast examination and clinical breast examination, for younger women, and goes on with the execution of a mammography (X-ray of the breast), when the patient reaches a certain age (that depends on the country). Considering some aspects like the clinical history of the patient, the density of the breast or an inconclusive result of the mammography, the patient may be advised to perform an MRI [2] in order to get a more accurate result of the breast analysis.

When it comes to the treatment it includes breast surgery to remove the tumour, if chemotherapy does not prove to be efficient. The surgery may require the removal of the entirety of the breast, which is called a mastectomy, or just a portion of it, which is called a BCS (Breast-Conserving Surgery). Mastectomy was previously almost the standard choice for all the patients going through breast cancer surgery, since the patients felt more safe and less scared of recurrence of the cancer. Now it is easier to localize the tumour in the breast and remove only that part and the surrounding tissues, which makes it unnecessary to remove the whole breast. The planning of this type of surgery and the accomplished result, may not match, which may come from the lack of experience of the surgeon or the location of the tumour in the breast.

Some deformations caused by breast cancer surgery can go against what was expected by the patient, and interfere in their personal and social life. The lack of satisfaction with their looks, that may have come from chemotherapy, will increase after surgery, along with depression, anxiety and feelings of sexual unattractiveness.

Currently, effort has been made in order to include the patient in the decision-making process, making her more aware of the risks and capable of deciding some aspects of the surgery, which in consequence will improve the acceptance of her own body after the surgery.

The next step should include the presence of 3D models of the patient's breast, combining the information gathered through radiological exams and data from the surface, to make the changes and deformations that will occur after breast cancer surgery, more visible to both the patient and the surgeon, involving the patient in the decision-making process and making them more comfortable and aware of the process.

1.2 Motivation

The task of creating 3D models of the breast is not easy due to the non-rigid and deformable nature of the breast. But nowadays, this task becomes necessary and useful, not only in the decision-making process of the breast surgery, but in other types of clinical applications, like in orthodontics [3] or in preoperative models of the liver [4], for example.

These models can then be used to create biomechanical models or models created from machine learning, which will help predict the deformations of the breast. This process allows a better and more clear visualization of the breast deformations after the surgery to the patient, allowing a more informed decision and consequently a more fitting surgery according to the patient's expectations.

1.3 Goals

The main goal of this dissertation is to create a 3D model of the breast, by registering images of different modalities, matching both the interior and the surface data of the breast. The 3D model could be created from only radiological modalities, but the combination of both radiological information and surface data, will allow not only a view of the outside part of the breast, but a view of the interior of the breast as well. This will allow not a generic model, but patient specific models.

This task can be difficult mostly due to the nature of the breast, since when acquiring images from the interior of the breast, the patient may be standing up or lying down, while in the acquisition of surface data, the patient is normally standing up. In both positions, the breast is shaped differently. So, for the matching of both radiological and surface data a pose transformation shall also be done, taking into account all the specifications of the characteristics of the breast.

1.4 Contributions

In this work, the dataset used will include more patients than the previous works, which means the algorithm will become more universal, since the range of breast sizes, shapes and deformities will be much wider. When using a larger dataset, problems that might not have been found previously, might now arise.

To infer the accuracy of the algorithm, a validation dataset will also be used, avoiding the problems inherent to the evaluation metrics normally used in Image Registration, such as the Euclidean Distance.

To approximate the results and the visualization to the reality the breast with the pectoral muscle on the back will be used, as well as the complete torso, instead of only using the frontal contour of the breast. The tumour will also be inserted in the breast, and the its behaviour thorough the algorithm will be analyzed.

The robustness of the algorithm will also be improved, mostly in the rigid registration approach.

The dataset augmentation, the introduction of a validation dataset and the study of different methodologies and their different varieties will make it possible to understand what is the best possible model to register data from different modalities, and which conditions. By understanding what is in fact the best model to register the breast with the information of different modalities, it is possible to create a patient specific 3D model and start planning further advances to create a model that is able to predict the deformations that the breast will go through when performing breast surgery.

1.5 Structure

The following document is divided in 6 chapters.

The second chapter, Breast Cancer, will refer to the basic principles of breast cancer, including the statistics (its incidence and mortality), proving that the stakeholder is numerous, how the treatment is performed, including radiological exams and the surgeries performed and how to gather information from the surface of the breast. This chapter frames the problem treated in this work in the current reality.

The third chapter, Data Registration, focuses on the current state of the technology, when it comes to the registration of images, going through all the steps of finding a 3D model of the breast with all the needed information. It includes the registration of radiological images, the registration and the reconstruction of the surface data, and subsequently its matching and validation. All the challenges of these steps are presented as well as some solutions found in the literature.

In the fourth chapter, Methodology, the Methodology used for the acquisition of the datasets and the image registration process is described..

In the fifth chapter, Results and Discussion, the final results are presented and in the sixth chapter, some considerations are made about the results and future needed work is defined.

Chapter 2

Breast Cancer

Among females, breast cancer is the most common form of cancer [1]. Its mortality is not the highest compared to other forms of cancer, due to all the screening methods and the awareness of the population that is made. These precautions include screening routines like breast self-examination, to young women, and clinical breast examination or mammography [2] to women over 40/50 years old.

There are two types of breast cancer, depending on where the cancer is formed[1]: ductal cancer, where cancer starts in the ducts that conduct the milk; and lobular cancer, where cancer starts in the milk-producing glands. Ductal cancer is the most common type of breast cancer.

2.1 Statistics

According to Globocan 2018 [5] (an online database providing estimates of incidence and mortality in 185 countries for 36 types of cancer, and for all cancer sites combined) among all new cancer cases during the year of 2018, 11.6% were breast cancer. That represents 2.1 million newly diagnosed female breast cancer cases worldwide, meaning that 1 in 4 cancer cases among women, will be breast cancer. Its mortality represents 6.6% of all deaths caused by cancer. This difference in the numbers of incidence and mortality, as shown in Figure 2.1, proves that the prevention of breast cancer using the multiple screening routines that are available, improves the mortality rates of breast cancer patients.

Yet, among females, breast cancer is the most commonly diagnosed cancer. According to National Cancer Intelligence Network [6], over 80% of women with breast cancer need to get through surgery in order to remove the tumour. In Europe, breast cancer occurs most commonly after the age of 72 [5].

Comparing to the global scenario, in Portugal there are over 6000 new cases per year (in a population of 5 million women in the country), and in terms of mortality, 4 women die every-day because of breast cancer[2]. Only 5-10% of these cases appear to have hereditary or genetic

[1] https://www.cancer.org/cancer/breast-cancer/about/what-is-breast-cancer.html

[2] https://www.ligacontracancro.pt/servicos/detalhe/url/programa-de-rastreio-de-cancro-da-mama/

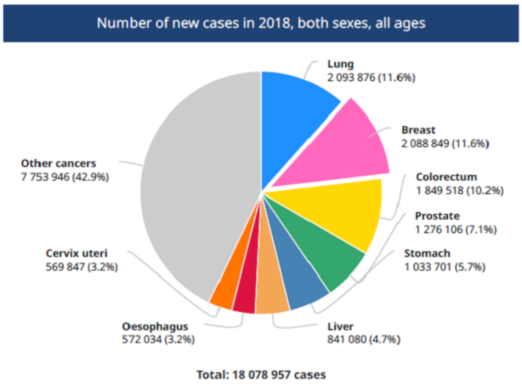

(a) Number of new cancer cases in 2018.

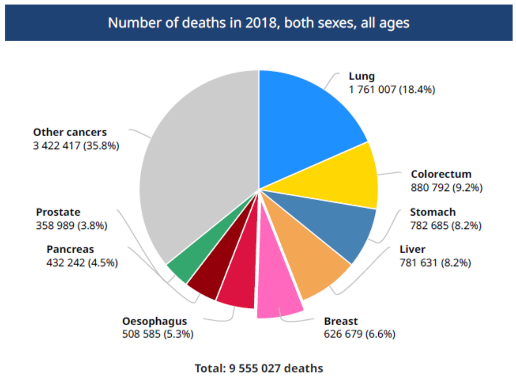

(b) Number of deaths because of cancer in 2018.

Figure 2.1: Statistics from Globocan 2018 [5].

influences, that need an earlier treatment comparing to other asymptomatic patients.

2.2 Breast Imaging

Screening for breast cancer has been proven to improve the mortality rates, by making the diagnosis and the control of the disease easier and affordable. Since 1990, breast cancer mortality has decreased by 30% [7] mostly due to the improvement of breast imaging techniques. Screening techniques come after self breast examination or clinical examination, when the results are positive or inconclusive for breast cancer. They are also included in some national plans for breast cancer prevention, for women above a certain age. They can be performed just by routine, in women that require it, because of their age or their family history.

2.2.1 Radiological Exams

The most common way to screen breast cancer is through radiological exams. Radiological exams are not as subjective as self breast examination or clinical examination, since they allow the visualization of the breast tissue and the possible anomalies.

2.2.1.1 Mammography

To check the health status of the breast, women are invited to perform mammography when they reach a certain age. Mammograms are the most common exam when it comes to breast cancer screening [7] and they can detect impalpable tumours.

In Portugal, the recommended age to start performing mammograms is at 40-45 years old, when there are no symptoms in the patient[3]. After the first exam, it is recommended that the patients repeat it every two years. It is also possible that women start doing mammograms earlier

[3] https://www.ligacontracancro.pt/servicos/detalhe/url/programa-de-rastreio-de-cancro-da-mama/

(but not earlier than 25 years old) if they have a history of breast cancer in their family (first degree family like mothers or sisters) [7].

Although mammograms show great results, women with higher density of breast tissue may have inconclusive results when performing mammography, and some supposed local cancers, can have a greater extension that is not seen in the mammography. The accuracy is also lower in young women and women with mutations that might lead to breast or ovarian cancer [8]. In those cases, other techniques are recommended in order to achieve accurate results.

Mammograms are also used to quantify the density of the breast [9], which is an indicative factor for the probability of developing breast cancer. Women with high mammographic densities have an increased risk of breast cancer, when compared with women whose breasts are composed mostly of fatty or adipose tissue. In Figure 2.2, there are 6 mammograms represented with different percentages of breast densities. This is an important characteristic when it comes to pose transformation and in the postoperative results of breast cancer surgeries.

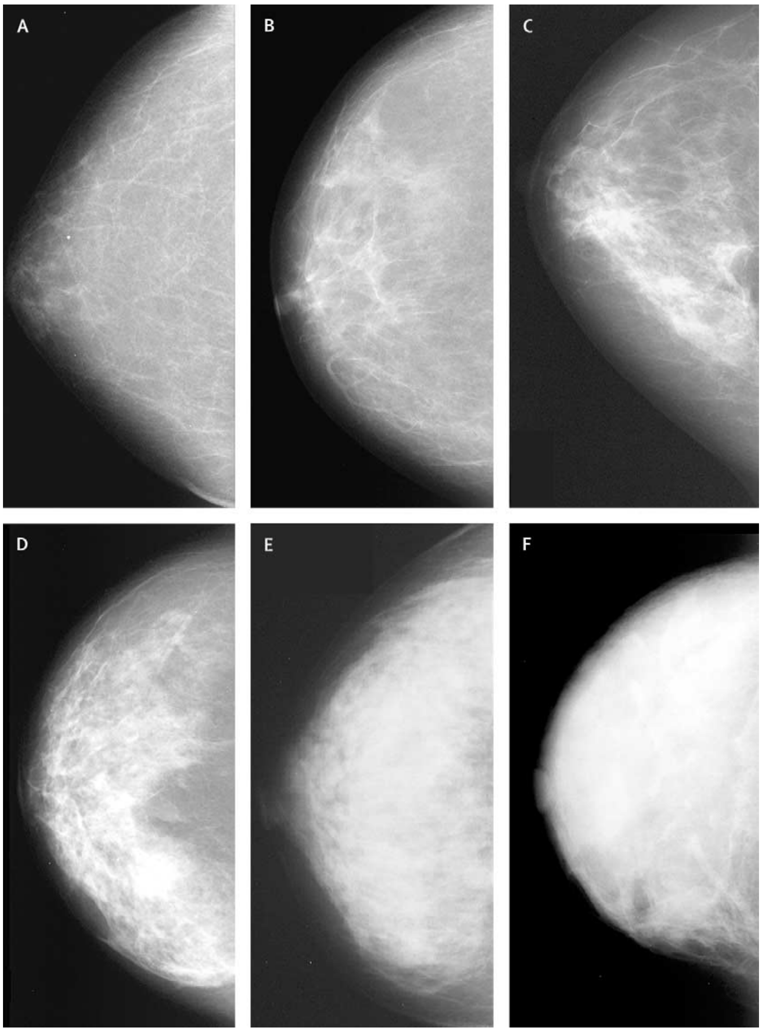

Figure 2.2: Categories of percentage mammographic density estimated by radiologists through mammograms A=0. $B =< 10\%.C =< 25\%.D =< 50\%.E =< 75\%.F =\geq 75\%$ [10].

2.2.1.2 Ultrasounds

Ultrasound exams can be used as an addition to mammograms for women with dense breast tissue [7]. Ultrasounds are widely used in medical imaging because they have no known risk to the patient, since they do not use radiation and for that they can be used in pregnant or young women. Ultrasounds can be performed regardless of the woman's age, which does not happen in mammograms [11].

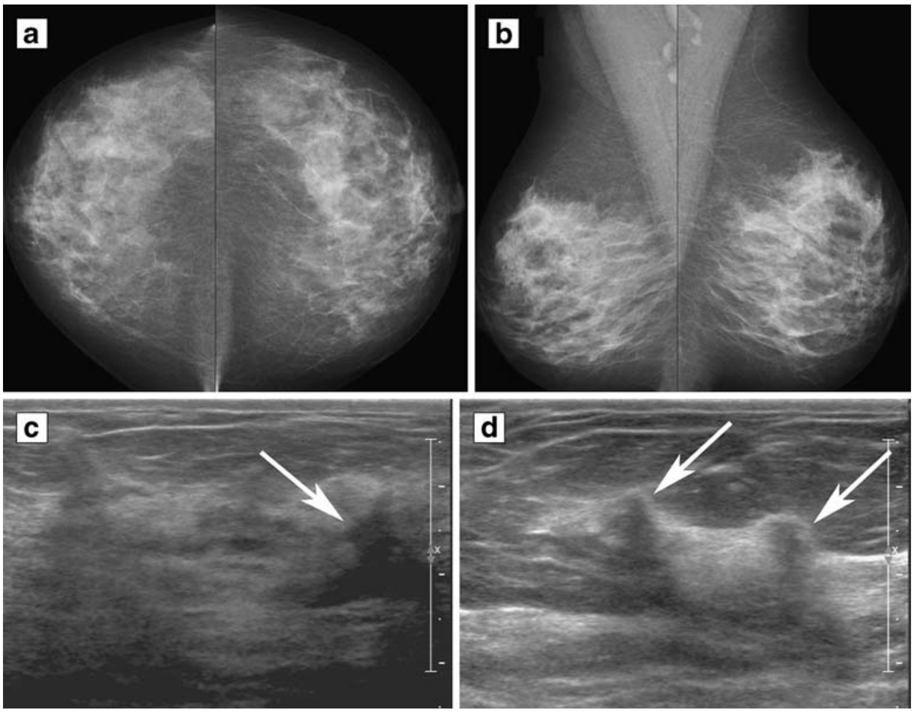

Figure 2.3: Selected images of a 54-year-old asymptomatic woman with dense breasts and no previous history of breast cancer. a) Craniocaudal digital mammograms are taken the same day as the ultrasound study. b) Mediolateral oblique digital mammograms are taken the same day as the ultrasound study. c) Transverse ultrasound image of the right breast; white arrow shows a 7 mm, grade I, stage 1, invasive ductal carcinoma. d) Ultrasound image of the left breast; two white arrows show 10 mm, grade I, stage 1, invasive carcinoma with lobular carcinoma in situ [12].

The ultrasound uses a transducer, that couples to the body with an acoustic gel. A pulse-like acoustic wave is produced, propagates through the body, and reflects when it finds reflecting surfaces and small scatterers. The transducer receives these waves and converts them into an electrical signal and amplifies, stores and displays them [13].

In Rotten *et al.*[11], it is shown that by combining both mammograms and ultrasounds, the percentage of false negatives is drastically reduced. When used in combination with mammograms, ultrasounds show great results in women with dense breast tissue since the diagnostic yield[4] increases from 3.6 per 1000, when only using mammography, to 7.2 per 1000, when using both combined. In Figure 2.3, this efficiency is proven since the invasive carcinomas are only shown in

[4]Diagnostic yield is the likelihood that a test or procedure will provide the information needed to establish a diagnosis.

the ultrasound, in a patient with high-density of the breast. The ability to find cancers smaller than 10 mm, is also greater when using both techniques combined [12].

2.2.1.3 Magnetic Resonance Imaging

An MRI scanner is composed by five parts, as represented in Figure 2.4:

1. The main magnet: superconducting, with coils of niobium-titanium wire, immersed in liquid helium around 4^{o}K;
2. A set of coils to provide a switchable spatial gradient in the main magnetic field, placed inside the bore of the magnet;
3. Resonators for the transmission and reception of radio-frequency pulses;
4. Electronics for programming the mining of transmission and reception of signals;
5. A console for viewing, manipulating and storing images: it allows the selection of the protocol, setting the gaining to the patient's electrocardiogram (ECG) and breathing (synchronizing the acquisition to the appropriate physiologic process), selecting the orientation of the scan plans to image, reviewing the images obtained and changing variables in the pulse sequence in order to modify the contrast between tissues.

The magnet, the gradient coils and the RF coils must be isolated from electronic noise, so they are placed in a copper-lined room, that acts as a Faraday cage. The patient undergoing this exam needs to be lying on a sliding table inside of a cylinder, under the effect of a magnetic field of 1.5 Tesla [13].

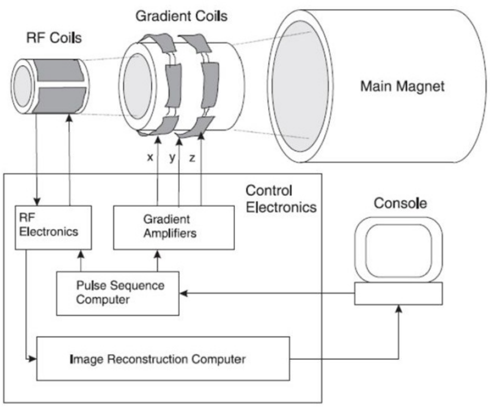

Figure 2.4: Block diagram of an MRI scanner [13].

MRI is performed in women with high risk of breast cancer, women who had breast or ovarian cancer before or neoplasia diagnosed by a biopsy, or in women with dense breast tissue as the only risk factor. It is used as an adjunct to the standard screening routines, like mammography or clinical examination. It can also be used to select the treatment for the patient [8]. It allows to see not only potential tumours but other kinds of lesions [14].

MRI has a very high sensitivity, but its specificity depends on factors like reader expertise [14], so it should be performed by someone with great knowledge of the necessary MRI techniques. If it is known that the woman has a mutation that will lead to a case of breast cancer, MRI shows greater sensitivity than mammograms, for example, as it is seen in Figure 2.5. But, due to the limited size of the opening, larger breasts might be compressed during the MRI.

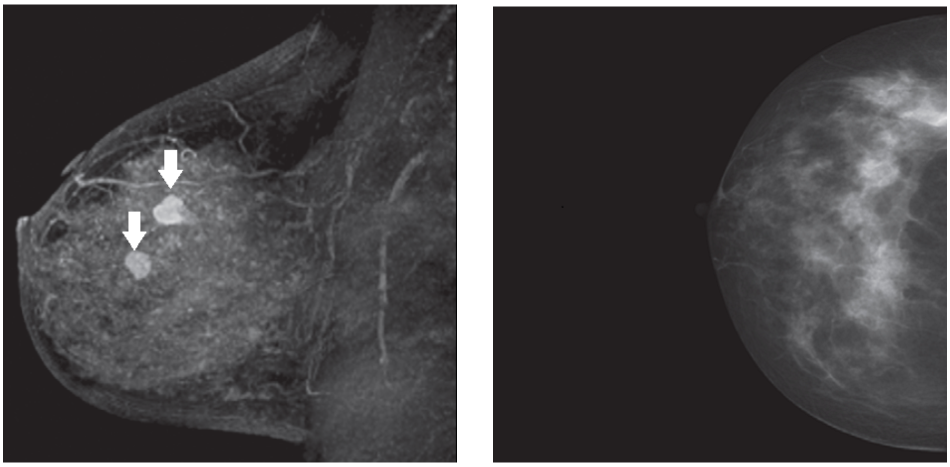

(a) MRI (b) Mammography

Figure 2.5: Multifocal carcinoma detected on MRI from a woman with no family history of breast cancer, but history of fibrocystic changes, and negative results after a mammography, proving that the accuracy of MRI is superior to the accuracy of the mammography [8].

Even though the MRI does not use any radiation, it might require the injection of a contrast agent which can be an inconvenient [15].

There are other imaging techniques being used nowadays, but still not so common, as Positron Emission Tomography (PET) and Computerized Tomography (CT). PET is currently being used in the detection of metastatic disease. It uses a radioactive substance that is injected and moves to places in the body where the cells are most active, especially highlighting cancerous tissue. PET is normally not used on the first stage of breast cancer since it does not reliably detect tumours smaller than 5-10 mm [16]. CT is also used to monitor the spreading of the cancer, and uses an iodinated contrast media in order to study the presence of axillary lymph nodes [17]. Both CT and PET can be used together to evaluate the staging of metastatic cancer.

2.2.2 Surface Information

Using 2D images of the breast is not the most intuitive way to show the patient how the surgery will be performed or what part of the breast is going to be removed since they do not allow the visualization of the deepness of the structures.

On the other side, 3D imaging is defined as any technique for recording visual information or creating the illusion of depth in an image [18]. A 3D representation also allows the visualization of the breast surface from multiple angles. The creation of a 3D model allows not only simple volumetric analysis but also, by using more sophisticated software, to perform quantitative measures on the breast and simulate post-operative outcomes [19].

The 3D construction that will allow the obtainment of the exterior information of the breast, can be divided into 3 phases [20] :

1. Data acquisition;
2. Processing;
3. Analysis.

Currently, most of the approaches for acquisition are mainly based on 3D laser scanners [19]. Laser scanning uses the triangulation principle, where a laser beam is projected on the patient's torso, and the reflected rays are captured by a detector that is sensitive to the orientation of those rays. The breast region of interest (ROI) can be marked on the patient before the scan or can be placed in the 3D image.

More generally, 3D reconstruction and measurement techniques can be divided in: contact and non-contact. Contact methods include coordinate measuring machines and rulers for example, while non-contact methods include photogrammetry and laser scanning. The non-contact methods can be seen in Figure 2.6.

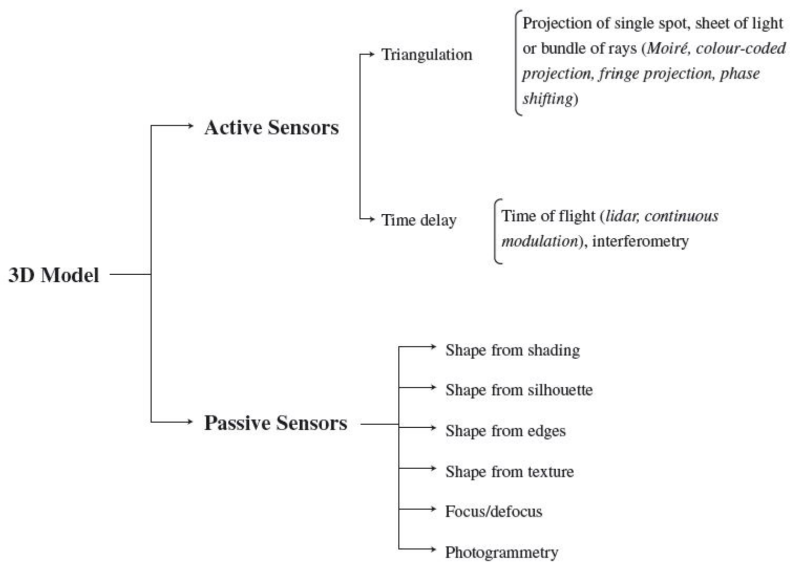

Figure 2.6: Three-dimensional acquisition systems for object measurement using non-contact methods [21].

Nowadays, the most used methods for 3D reconstruction are the non-contact ones, using active or passive sensors. The difference between the two type of sensors is mainly due to the time of processing of the 3D coordinates. While active sensors provide the 3D coordinates, necessary for the generation of the mesh, immediately, passive sensors need processing to derive the 3D coordinates. The collection of these xyz coordinates is called a point cloud.

Considering these two types of sensors, there are four methods that can be distinguished for object and scene modelling [21]:

1. Image-based rendering (IBR): creates novel views of 3D environments, using input images. This requires that the exact position of the cameras is known or that automatic stereomatching is performed.

2. Image-based modelling (IBM): mostly used for geometric surfaces. It uses 2D image measurements to recover 3D object information. Passive methods involve acquiring 3D measurements from multiple views. It uses projective geometry or perspective camera models.

3. Range-based modelling: captures 3D geometric information of the surface automatically. Uses active sensors and provides a very accurate result. The sensors use artificial lights or pattern projection.

4. Combination of images and range-based modelling: photogrammetry and laser scanning are combined in order to produce better results, in particular for large and complex architectural objects.

Usually, basic shapes use image methods, while more complex, detailed shapes use range methods.

After the acquisition the object needs to be sampled, being the number of samples directly proportional to the curvature, for example, a square only needs a few number of points, while the breast, needs a much higher number of points [20]. The acquired data also needs to be structured in order to form the polygonal surface of the mesh. To make it more realistic, the surface can be textured with data from images.

Most of the referenced systems can be bulky and not practical to use in a hospital, so there has been more investigation in smaller, more portable and cost-effective equipment. One of them is the Microsoft Kinect Device used for Xbox360, represented in Figure 2.7 [22]. It uses a pseudo-structured light scanning approach, where the distance to the objects in the field of view is calculated, possible because of its 3D depth camera, which enables the generation of a 3D colourized model [23]. Wheat *et al.* [23] tested the accuracy and repeatability of this system when imaging the breast. He used two calibrated Kinnects, the minimum number of cameras required to produce a complete point cloud. With the object in the FoV (Field of View) of both of the Kinnects, data from the RGB and depth cameras were obtained sequentially from both devices. Another advantage of this system is the acquisition time, which in this case was 2 seconds. After the acquisition, the point clouds were created, one for each Kinnect, using the depth data and the intrinsic parameters from the depth camera and using colour from the RGB camera, which is projected onto the points of the PCL, originating a coloured model. The software *Kinect for Windows* is free and allows the obtainment of the depth maps and consequently the point clouds of the object. Digital measurements of Euclidean and surface distances between landmarks showed great results when compared to manual measurements. But when more complex objects are being studied, some problems might arise. In the case of large ptotic breasts, the inframammary fold might not be captured [24]. A third Kinnect camera in a lower position in an upward view could be used to work around these problems.

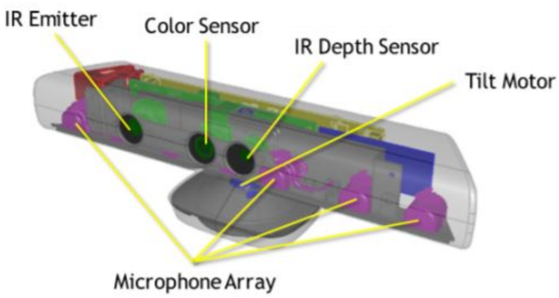

Figure 2.7: Microsoft Kinect Device.

2.3 Breast Surgery

The treatment of breast cancer always depends on the stage of the disease, and factors like[5]:

- The size of the tumor in relation to the size of the breast;
- The results of specific pathology tests;
- If the woman has gone through menopause already or not;
- The general health of the patient;
- Age;
- Family history.

In general, there are five treatment options, and most treatment plans include a combination of the following[6]:

- Surgery: involves removing the tumor and nearby margins;
- Radiotherapy: uses high-energy rays to kill cancer cells; may be used to destroy any remaining mutated cells that remain in the breast or armpit area after surgery, beginning 3-4 weeks after surgery;
- Hormone therapy: the pathologist will perform tests on the breast cancer cells to determine if they have receptors that feed on estrogen or progesterone, stimulating their growth; if the cells have those receptors, hormone therapy will be performed with blockers or inhibitors of those hormones;

[5] https://www.nationalbreastcancer.org/breast-cancer-clinical-trials
[6] https://www.nationalbreastcancer.org/breast-cancer-treatment

- Chemotherapy: uses a combination of drugs to either destroy cancer cells or slow down the growth of cancer cells. It can be used to shrink the tumour before surgery. It will be administered in short courses with several weeks in between, to allow the normal cells to recover;
- Targeted therapy: treatments that can attack specific breast cancer cells without harming normal cells, normally used in combination with chemotherapy; they have less severe side effects than standard chemotherapy drugs.

Surgery and radiation are considered local treatments, targeting just the area around the tumour, while the others are systemic, targeting the whole body with cancer-fighting agents. The medical team that is following the patient will choose a combination of treatments that are more effective for that specific case.

Surgery is likely to be part of any breast cancer treatment and it may also be considered to find out if the cancer has spread out to the lymph nodes, to restore the shape of the breast after removal or to relieve the symptoms of advanced cancer.[7]

Breast cancer surgery is performed with the goal of removing not only the tumor but also enough of the margin to be able to test for the spread of cancer. For that, the doctor analyses the results of breast imaging exams that the patient has performed, to decide on what type of surgery will be done and the amount of tissue that needs to be removed. Women with Stage 2 or Stage 3 cancer may receive chemotherapy before the surgery, which is known as preoperative or neoadjuvant chemotherapy[8], with the goal of reducing the size of the tumour before the surgery.

2.3.1 Types of Breast Cancer Surgery

When it comes to removing the tumour there are two types of surgery that are currently being performed, as represented in Figure 2.8 [9]:

1. Breast-Conserving Surgery (BCS): also called lumpectomy or partial mastectomy.
2. Mastectomy.

The main difference between these two types of surgery is the amount of tissue that is removed. In the first one, only the tumour and the surrounding tissue are taken out, but the volume of the breast that is taken depends on the location of the tumour. Lumpectomy is a first treatment option for some women with early-stage breast cancer. On the other side, mastectomy involves removing the entire breast (all of the breast tissue, nipple and skin and sometimes the surroundings as well)[10]. Very rarely, the muscles of the chest are also removed[11].

The surgeon recommends BCS if[12]:

[7] https://www.cancer.org/cancer/breast-cancer/treatment/surgery-for-breast-cancer.html
[8] https://www.nationalbreastcancer.org/breast-cancer-surgery
[9] https://ww5.komen.org/BreastCancer/Surgery.html
[10] https://www.cancer.org/cancer/breast-cancer/treatment/surgery-for-breast-cancer.html
[11] https://www.cancerresearchuk.org/about-cancer/breast-cancer/treatment/surgery/types-surgery
[12] https://www.cancerresearchuk.org/about-cancer/breast-cancer/treatment/surgery

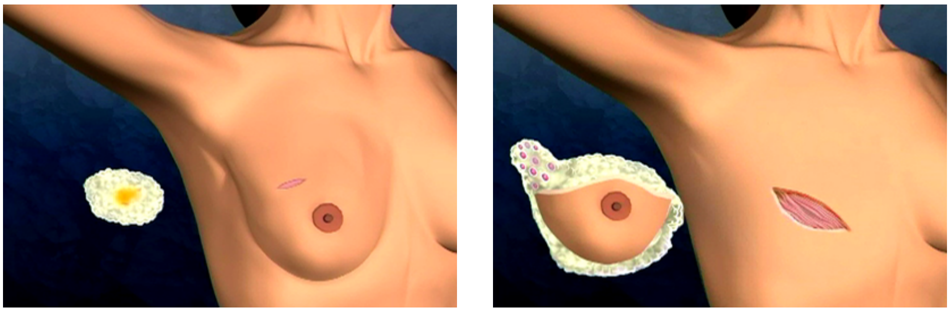

(a) Lumpectomy (b) Mastectomy

Figure 2.8: Breast Cancer Surgery.

- The size of the tumour is small, comparing to the size of the breast;
- The tumour is in a suitable position;
- The cancer is only in one zone of the breast.

And recommends a mastectomy if:

- There is a large lump (in a small breast);
- The tumour is in the middle of the breast;
- There is more than one zone where the cancer is;
- The patient has had radiotherapy in the past.

2.3.2 Surgery Planning

A breast surgical oncologist will advise the woman on the type of surgery that should be performed, but this decision can be discussed between both parts, in the case that both types of surgeries can be performed. The factors affecting the medical choice of surgery are[11]:

1. The size of the cancer;
2. The location of the cancer in the breast;
3. The size of the breast;
4. The patient's wishes.

BCS might sound like the best option since it does not require the entirety of the breast to be removed, but the patient will need radiation after the surgery. So the patient needs to deal with the radiation therapy and its consequences, and there is also the possibility that the breast looks too different or misshapen, particularly if a large portion of the breast is removed, which is the main factor of women opting to perform a mastectomy instead of a lumpectomy.

Doing a mastectomy may give the idea that the possibility of the cancer coming back is lower, but studies show that it does not have an influence[13]. Women choose to perform a mastectomy due to enhanced fear, because of family history, and give more value to that factor than to statistics, even if the doctor informs that both give the same chance of survival [25].

The choice of the patient goes between having only part of the breast removed, but having to do radiation therapy after, or removing the whole breast, giving the feeling that there is no chance of recurrence, and performing breast reconstruction surgery after.

2.3.3 Psychological Impact of Breast Cancer Surgery

After surgery, the breast may have a completely different aspect and shape, and that difference may cause the patient to feel less confident about their body, less attractive and more abnormal. If this surgery comes after treatment, the consequences of the surgery are added up to the previous consequences of radiation therapy like loss of muscle strength, depression and anxiety. These feelings may affect several aspects off the life of the patient, including her sexual life[14]. The sexual life of a patient may be affected not only by the lack of confidence, but also because the patient loses her sensations in the affected area. The social and family well-being deteriorate after the surgery, until at least six months after it [26]. Studies also show that women who have undergone mastectomy are more at risk for postoperative sexual dysfunctions, compared to women who have undergone BCS [27].

Studies show that women that have undergone BCS instead of a mastectomy, feel better about their body image after surgery [26]. These studies also show that some of the main concerns of these women are:

- Swollen/Tender arms after surgery;
- Worried-risk of cancer in the family;
- Worried-effects of stress on illness;
- Body image scale.

These concerns are mostly greater in women who have undergone mastectomy, but in a long term, it shows little influence in the quality of life (QoL) of the patient.

If it did not appear during the treatment, patients may suffer from depression and anxiety, due to the lack of confidence, the impact of the surgery on the daily life and relationships and the fear of recurrence [28].

After the surgery, the woman can make a reconstruction of the breast, or can choose to leave the breast the same way or use a prosthesis.

[13] https://www.cancer.org/cancer/breast-cancer/treatment/surgery-for-breast-cancer.html

[14] https://www.cancer.org/cancer/breast-cancer/living-as-a-breast-cancer-survivor/body-image-and-sexuality-after-breast-cancer.html

2.4 Summary

Taking into account all the mentioned aspects in this chapter, it is possible to conclude that breast cancer is a widely known disease, and the way of proceeding with diagnosis and treatment has been carefully studied through the years, to make the patient's life the most pleasant and normal possible. Different methods of diagnosis are done depending on the background and physics of the patient, and the type of surgery also depends on this. To make this process even more fluent and easy, with positive results, one of the suggestions is involving the patient more in the decision making process, suiting the results to the patient's expectations.

Chapter 3

Data Registration

In the previous chapter, the need to find a 3D model of the breast surface is explained because the stakeholder of this problem is numerous. The satisfaction of the patients after breast cancer surgery is not great and can be improved, using a 3D model of the breast that will be a huge step to improve the communication between the doctor and the patient. To do this, the breast surface needs to be registered, using a multiplicity of techniques, that are then combined. These techniques involve radiological modalities, and surface information, that after registration are matched to form the 3D model of the breast.

3.1 Overview

Registration is a fundamental task in image processing used to match two or more pictures taken, for example, at different times, from different sensors, or from different points of view [29]. To obtain a complete 3D model of the breast, several modalities and the information they provide must be combined. When it comes to breast cancer, data from radiological images and surface data should be combined since they provide information from both the inside of the breast and the outside, giving a complete model that is able to help both the patient and the doctor in the decision-making process. This matching presents some challenges, including:

- Patient change of pose during the acquisition of the radiological images;
- The deformable nature of the breast: its anisotropic and inhomogeneous tissue and its non-rigid behaviour [30];
- Different times of acquisition;
- Different points of view in theacquisition.

The final objective is to align images from two methodologies, using the same coordinate system. In order to perform this, some frameworks are normally used, including finding out the feature space, the transformation that needs to be done, the similarity measure (quality of matching) and defining a search strategy. To perform this, some transformations can be done [31]:

- Rigid transformations: that include rotations and translations of rigid objects. It is also used when there are only small changes in the object shape (for example, a sequence of MRI images) or in its intensity. It is widely used, because it uses few parameters, it is not too complex and it can approximate both images without having them changing their spatial relations.

- Affine transformations: that include, not only rotations and translations but scaling and shearing. It maintains the parallelism between lines, but not their lengths and angles. This type of transformation has more degrees of freedom (DoF) than rigid transformations.

- Projective transformations: used in tilted images. Straight lines are kept that way, but parallel lines are transformed in order to converge and then vanish. It behaves like a constrained-elastic transformation.

- Curved transformations: also referred as elastic, deformable, or fluid transformation [32], they may map a straight line onto a curve [33]. Gefen *et al.* [34] proposed a planar-to-curved surface alignment, matching data of 2D images with their corresponding images overlaid on a curved-surface within a volumetric image.

- Non-rigid transformations: these type of transformations are very challenging because they require a high number of DoF, being the computation time also high.

Rigid transformations include methods like PCA (Principal Component Analysis), ICP (Iterative Closest Points) and SVD (Singular Value Decomposition) [35].

PCA is a dimension-reduction tool, used to reduce a large set of variables to a small number of variables, mantaining the same information. It projects data on a new orthonormal basis in the direction of the largest variance.

ICP is a method proposed by Besl and McKay [36] where the transformation parameters of two point sets are calculated through the relationship between the corresponding matching points of two point sets to satisfy the given convergence precision, and finally the translation and rotation parameters between the two points are obtained to complete the registration process [37]. ICP uses convergence to the nearest local minimum of a mean square distance metric [35].

The ICP algorithm can be described as follows: Considering the rigid transformation T between the target point set S and the reference point set M, and assuming that the coordinates of the target point set S are $\{S_i|S_i\in R^3,\ i=1,2,...,N_S\}$ and the coordinates of the reference point set M are $\{M_i|M_i\in R^3,\ i=1,2,...,N_M\}$, in the k-th iteration, the coordinates of the corresponding point corresponding to the coordinates of the point set S are $\{M_i^k|M_i^k\in R^3,\ i=1,2,...,N_M\}$

The transformation matrix between S and M^k is calculated and the original transform is updated until the distance between the data is less than the given threshold τ. In the following points, the ICP algorithm will be described:

1. Calculate the $M_i^k\in M^k$ in the reference set M so that $\left\|M_i^k - S_i^k\right\| = min$;

2. Calculate the rotation matrix R^k and the translation vector T^k so that $\sum_{i=1}^{N} \left\|R^k S_i^k - M_i^k\right\|^2 = min$;

3. Calculate $S^{k+1} = S_i^{k+1} | S_i^{k+1} = R^k S_i^k + T^k, S_i^k \in S$;

4. Calculate $d^{k+1} = \sum_{i=1}^{N} \left\|S_i^{k+1} - M_i^k\right\|^2$;

5. If d^{k+1} is not less than the given threshold, repeat from (1) until d^{k+1} is under the threshold or the number of iterations is above k (the preset number of iterations).

Non-rigid transformations include transformations like [31]:

- Splines: splines are functions defined piecewise by polynomials. This type of transformation uses control points in the target and source images, and uses splines to define points away from these ones. Some of the most used splines are thin-plate splines and B-splines. Thin plate splines are used globally, meaning that one small change can introduce a greater transformation, which is not the desired situation in complex models. B-splines are used locally, because by changing one control point the transformation is only affected in the neighbourhood of that point. B-splines are very computationally effective;

- Elastic Models: use the source image as a linear, elastic solid image and deform it by using forces derived from an image similarity measure, stopping when the forces reach an equilibrium. It can not handle large deformations;

- Fluid Registration: works with highly localized deformations. Has a vast number of DoF;

- Diffeomorphic Registration: preservse the topology and prevents folding;

- Finite Element Method: widely used in biomechanics. It models the interrelation of different tissue types when applying displacements or forces. It helps to predict deformations and from that, derive or quantify tissue properties.

In breast image registration, the most suitable type of transformation is non-rigid, due to the nature of the breast. Given two images R (the reference image) and F (the floating image), that are defined in the grid Ω and mapping to the grey values $r,f = 1,...,n$, then the registration can be described by the following mathematical formula [38]:

$$\hat{T} = arg_{\tau} min S(R, F(\tau)) \tag{3.1}$$

Where τ represents the transformation space and S represents the similarity measure. If there is a perfect alignment between the two images $R(x)$ is equal to $F(\tau)$, $x \in \Omega$. The goal is to find the transformation that maximizes S, the similarity measure.

The framework of a non-rigid registration process is represented in Figure 3.1 [38]. As the floating image is being transformed, there needs to be an interpolation method, changing the floating image space into the coordinates of another image space. After that, the similarity between

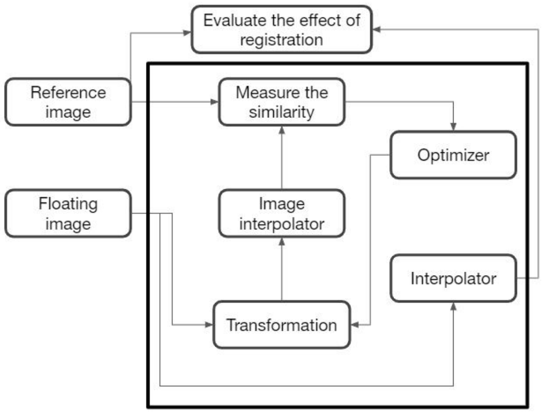

Figure 3.1: Framework of non-rigid registration.

the reference image and the floating image is measured, another τ is calculated, in order to improve the value of the similarity measure. This process is repeated until the value of the difference of two consecutive τ is lower than a specified threshold [38].

In order to define the model of deformation, there are two possible approaches: space transform models and physical based transformation models [38]. Space transform models include Free Form Deformation and Markov Radon Field Base Transform, both based on interpolation and approximation theories, that allow any kind of deformation. Physical based models can recover large deformations, but they have a high computational cost.

3.2 Registration of Radiological Images

Breast images acquired at the same or different times, or with different modalities are often combined in order to have a better visualization and diagnostic. This is often done with pre and post-contrast images of MRI exams [30], but it might be done with images from different modalities, for example: a mammogram and an MRI. Combining information from more than one modality, takes advantage of the information given by both modalities.

Registration methods can be classified as intra or inter-modality.

In intra-modality, the images that are suffering an alignment belong to the same modality, but are from different sessions or points of view, for example. In the case of different sessions, this task can become challenging because the anatomy of the patient might suffer some alterations due to the treatment of breast cancer, for example.

In the case of intra-modal registration, registration techniques can be divided into two categories: feature-based or intensity based, but both can be combined [30].

1. Feature-based: it requires the identification of landmarks in each of the mammograms. That task becomes difficult due to the nature of the breast and its compressibility (noticeable during the mammograms), being the landmarks non-rigid [39]. These control points can

be pointed out manually or automatically by finding, for example, the nipple in the mammograms or other boundaries. There is currently a lot of investigation being done in this area, for example: Vujovic *et al.* [40] with the objective of making a detailed comparison between mammograms of the same patient acquired at different screening to detect changes that are indicative of cancer, defined a 2 step strategy, being the first one analyzing each image independently in order to find potential control points, like the crossing of two elongated structures, and the second one being a correspondence between potential control points (a subset of control points is established using accumulator matrices and signatures, and those are able to find local patterns). A pair of reference points is used to reduce the number of false positive control points. Sivaramakrishna [41] proposed a textural approach, to register mammograms non-rigidly, where they are converted into texture maps where control points are selected. These techniques are only a small sample of all the approaches that have been investigated and more techniques are described by Guo *et al.* in [39].

2. Intensity-based: these techniques operate on the image pixel values [30]. Richard *et al.* [42] introduced a matching based on Regions of Interest (ROI), for mammogram registration, combining both feature and intensity based models and using an energy minimization problem with free boundary conditions.

Intra-modality registration in MRI is different from intra-modality registration in mammograms, since they provide different types of information. Mammograms show some difficulties in terms of accuracy due to the inherent compression of the breast during the exam. In the case of MRI, the entire 3D internal structure of the breast is provided. Firstly, the pre and post-contrast images need to be aligned or registered. Here the feature based selection has two stages: the selection of control points and their matching [30]. These points, can be registered manually, automatically from edges or breast contour, or randomly. Intensity based selection has been thoroughly studied. In MRI intra-modality registration, non-rigid approaches, like Free Form Deformation (FFD) have been used through many papers.

FFD is a modeling technique that enables the deformation of objects by deforming the space around them [43], and it was first described by Sederberg *et al.* [44]. Free Form Deformation means that whatever the object is, whatever its description and topology are, deformations are always possible [45]. Those deformations are defined by 3D splines, whose values are determined by the location of the control points. Describing the FFD, conventionally, is done by manipulating the control points. FFD has the advantage of being applicable to any parametric or polygonal model, not being restricted to any class of objects, since the FFD is based on the notion of deforming the underlying space. The deformation of the control points of an object, starts by assigning local coordinates to each of its points within the deformation lattice. Those local coordinates are defined by a parallelepiped-shapped lattice of control points, being their axes the orthogonal vectors s,t and u, as it can be seen in Figure 3.2 [43]. All object points within the space of the parallelepiped are assigned local coordinates through a mapping. Any point X with the coordinates (s,t,u) can be defined by [44]:

$$X = X_0 + sS + tT + uU \tag{3.2}$$

The (*s,t,u*) coordinates can be found by:

$$s = \frac{T \times U(X - X_0)}{T \times U \cdot S}, t = \frac{S \times U(X - X_0)}{S \times U \cdot T}, u = \frac{S \times T(X - X_0)}{S \times T \cdot U} \tag{3.3}$$

Taking into consideration that $0<s<1$, $0<t<1$, $0<u<1$. The lattice can be defined as:

$$P_{ijk} = X_0 + \frac{i}{l}S + \frac{j}{m}T + \frac{k}{m}U, \tag{3.4}$$

being $P_i jk$ the grid of control points, that form *l+1* planes in the *S* direction, *m+1* planes in the *T* direction, and *n+1* plates on the *U* direction.

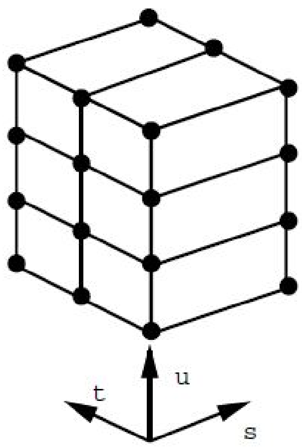

Figure 3.2: A lattice of control points. The s, t, and u vectors define the local coordinate system

When the control points are moved, it is possible to determine the new location of the object points, using a weighted sum of the control points. These weights are functions of the originally assigned local coordinates to the point. So, the positional change of the control points, changes the locations of the object points.

So, the deformed position can be defined as follows [44]:

$$X_{ffd} = \sum_{i=0}^{l} li(1-s)^{l-i}s^i \left[\sum_{j=0}^{m} mj(1-t)^{m-j}t^j \left[\sum_{k=0}^{n} nk(1-u)^{n-k}u^k P_{ijk} \right] \right], \tag{3.5}$$

Where X_{ffd} is a vector containing the Cartesian coordinates of the displaced point, and P_{ijk} is a vector containing the Cartesian coordinates of the control point.

Hsu *et al.* [43] uses as a deformation function a trivariate B-spline tensor product, since B-splines are greater in local control properties and desirable for both aesthetic value and for efficient computation with large control point lattices. B-splines also guarantee continuity when any of its control points are moved. Hsu *et al.* approach also allows both direct manipulation of the object and manipulation of the control points.

Rueckert *et al.* [46] found a new approach for the non-rigid registration of contrast-enhanced breast MRI using normalised mutual information. He proposed a technique that describes the global motion of the breast using affine transformation models, while the global transformation is described using spline-based FFD models. Schnabel *et al.* [47] presented a validation study for non-rigid registration of 3D contrast enhanced magnetic resonance images. In this work, it was used a Finite Elements Method (FEM), where biomechanical, physically plausible deformations are generated in order to simulate a gold standard[1] deformation vector field.

Inter-modality registration is used in order to combine information from more than one modality, information that is complementary. Since no modality is perfect, the ability to detect breast cancer can be improved when complementing information from more than one modality. The two most interesting and used modalities are definitely mammograms and MRI. Ruiter *et al.* [48] proposed an automatic approach. To overcome the deformation of the breast during the mammography it uses a a finite element model. It also imposes a deformation in the MRI images, in order to adopt the same configuration as in the mammography. After that deformation, a 3D projection of the MRI images is done, which enables a 3D visualization of the deformation in the breast caused by the mammography. This method is clarified in Figure 3.3 [48].

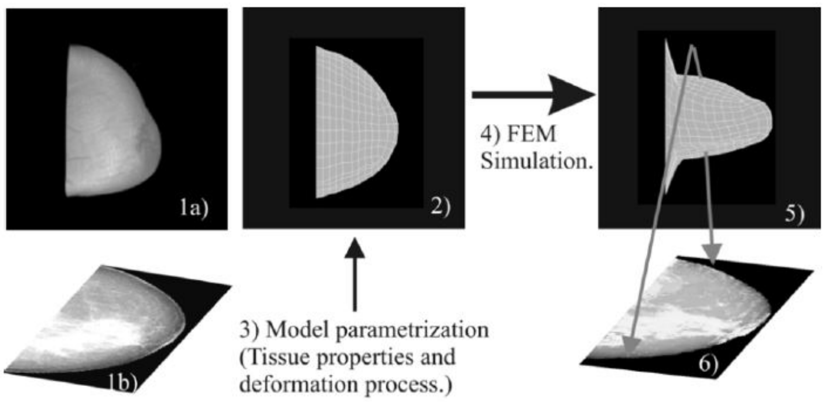

Figure 3.3: 1a) MRimage and 1b) Mammogram. 2) Finite element mesh of the patient's breast. 3) Definition of the tissue properties and the deformation process. 4) FEM Simulation. 5) Deformed finite element model. 6) Projection of a generated MR image of the deformed breast.

Kruger *et al.* [49] presented a method for analyzing 2D/3D intra-individual correspondences between mammography and MRI datasets, using an ICP-based B-spline registration to approximate the breast deformation differences.

Mertzanidou *et al.* [50] proposed an intensity-based image registration framework, where the biomechanical transformation model parameters and the rigid-body transformation parameters

[1] Gold standard refers to a benchmark that is available under reasonable conditions. It is not the perfect test, but the best one available that has a standard with known results

are optimised simultaneously to determine corresponding regions between an MRI and an X-ray mammogram.

3.3 Surface Registration

3D spatial information comes in the form of point clouds (PCLs), which is a set of data points in space. The process of surface reconstruction consists in converting PCLs to 3D surfaces and it can be more or less challenging depending on the technique used to acquire the 3D data. A point cloud is impossible to get from only one point of view, because normally the scanners have a limited field of view, and the structures can be quite complex as well. Another reason to implement multiple points of view is because there are areas in the breast that stay hidden, like the under breast area and the position of the patient may change during the acquisition. So, it is necessary to integrate information from multiple points of view [51]. The first step of reconstruction is registration and its goal is to find the Euclidean motion between a set of range images of a given object taken from different positions in order to represent them all with respect to a reference frame [51].

There are two types of registration, that can be applied to any kind of registration: coarse and fine registration.

- Coarse registration: searches for an initial estimate of motion between pairs of two consecutive 3D views, which leads to a complete registration. The distances between motions are minimized. Correspondences are made through points, curves and surfaces.

- Fine registration is used when a previous estimation of the motion is known and is used to start the iterations and converge to an accurate result. The iterations use a distance minimization function.

The second step is the surface reconstruction itself. Some approaches build a network of triangles over the existing vertices of the PCL, using algorithms like Delaunay triangulation. In Costa *et al.* [52] this algorithm is used in a coarse registration method based on tesselation, to extract robust keypoints from the RGB-D sensor information. For the fine registration an ICP algorithm is used to align the 3 different views.

3.4 Surface Radiological Matching

It is also necessary to combine the results of the registration of radiological images with the results of surface reconstruction to obtain a model that combines both the interior information of the breast and the 3D information of the surface, providing all the information possible which will improve the communication of the doctor with the patient in the decision-making process. To overcome this problem, both of the resulting models need to be represented in the same referential, that should be able to withstand deformation models. Taking into consideration that MRI provides 3D results, MRI information can be fused with PCLs to form a complete model.

While the acquisition of 3D data is performed with the patient in an upright position, the MRI is performed in a prone position, which makes it necessary to do a pose transformation in order to place both results in the same referential. Having the patient in a prone position causes the images to be mores susceptible to respiratory motion artifacts and it also reduces the visibility of the lesions, since the breast is more compressed [53].

There are some changes in the breast appearance when the position of the patient is different, the skin stretches, the ptosis of the breast is more or less visible and the boundaries of the breast move relatively to the skeletal structure, due to the change of gravity [54]. For example, having their arms up in an MRI changes the appearance and disposition of the patient's breast [55]. If it is possible to predict breast changes from a position to another, the task of predicting the result of a breast surgery becomes easier as well.

Surface radiological matching methods can be grouped in two types: physical and non-physical.

Physical models are used mostly to model breast deformities or to register volumes of images obtained in different positions [54].

Khatam *et al.* [54] uses physical models that are based on 3D stereophotography surface imaging (able to enhance the illusion of depth in the image) to determine the variation of breast skin deformation as the subject orientation is altered from supine to upright. In this work the skin is also considered a deformable and hyperelastic material. The back surface of the breast is defined by the surface of the chest wall (pectoral muscle), and it can be identified in MRI images. The breast tissue is considered to be hyperelastic as well. Here a simplified version of the skin's anisotropy is applied in order to make the calculations easier. The skin is considered to have little influence in supporting the breast, being the Cooper's ligaments and other connective tissues and the chest wall the main responsibles for that part. The ideal model, should not only predict the deformation of the breast, but the stretching of the skin as well.

Del Palomar *et al.* [56] proposes a method based on finite elements to establish a reliable simulation method that could predict a patient-specific outcome after breast surgery. They assumed that it can be assigned an average value of mechanical properties to the glandular and fatty tissue into the 3D image volume. They also made an effort to measure the skin deformation, with the focus of calibrating material properties of the skin, fat and fibroglandular tissues rather than exploring the inherent stretch variations on the breast surface.

In Eiben *et al.* [57], patient specific biomechanical models are used to provide an initial deformation of the breast (prior to registration), to make a prone to supine image registration of breast MRI. They use models to estimate the zero-gravity reference state, in order to perform the registration of the position configurations in this space.

There has been some investment in non-physical models, that are less complex, since physical models are not always suitable due to factors like their high computational cost. Behrenbruch *et al.* [55] uses non-rigid registration that is driven by the skin surface, and not by landmarks or other features, to make a prone to supine breast MRI registration for surgical visualization, using a tensor B-spline mesh to compute the deformation.

In Han *et al.* [53] in order to align prone and supine MRI breast images, biomechanical models using Finite Elements are used to initialize the subsequent non-rigid, intensity based registration at each iteration, providing a hybrid method.

These methods are still not common, specially when used to combine the registration of surfaces obtained from different points of view, or used in combination with physical models. In [58], an FFD algorithm is used to match both MRI and surface data. Firstly, the MRI data is represented in the following way: the Z-axis is positive in the inferior to superior direction, the Y-axis is positive in the anterior to posterior direction and the X-axis is positive from right to left. The surface data is represented in a different way when it comes to the Z and Y axis, as it was expected: Z-axis is positive in the anterior to posterior direction and the Y-axis is positive in the inferior to superior direction. The data from MRI is downsampled first and biomechanical simulations are

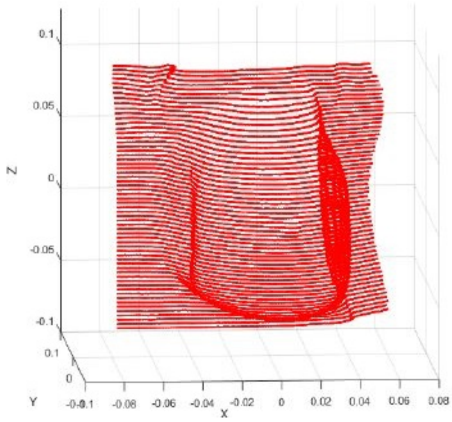

(a) Segmented MRI.

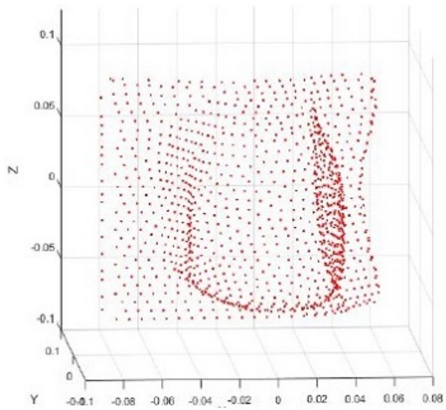

(b) Downsampled MRI.

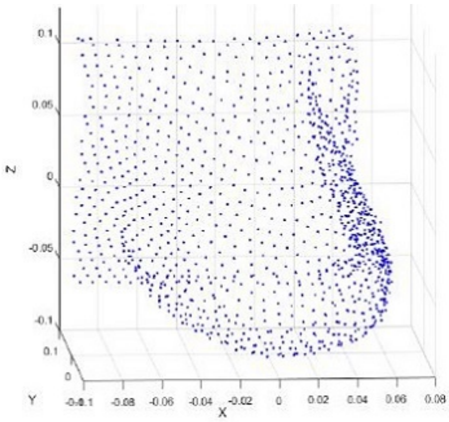

(c) MRI after biomechanical simulation.

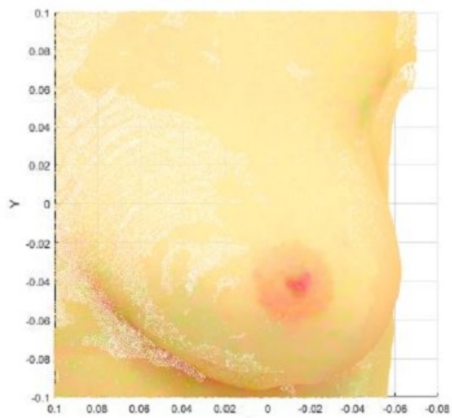

(d) Surface.

Figure 3.4: Comparison between segmented MRI data, downsampled MRI data, MRI data after biomechanical simulation and surface data [58].

used in order to transform the pose to the upright position. The described procedure is exemplified in Figure 3.4. It can be concluded from the results that data from MRI after the biomechanical simulation resembles the data from the surface, even though that the referential is still the same as it was previously. After that, a rigid registration approach is taken, and the data from MRI is treated in the following way:

1. Rotation: -90º in the X-axis and 180º in the Z-axis.
2. Translation: by detecting the breast mound, both in the MRI data and in the surface data.
3. Application of an ICP algorithm.

Since a rigid approach is not enough due to the deformable nature of the breast, a non-rigid approach is taken, using an FFD transformation that uses control points around the MRI (both normal and after the simulation) data to deform and match it with the surface PCL. The compared

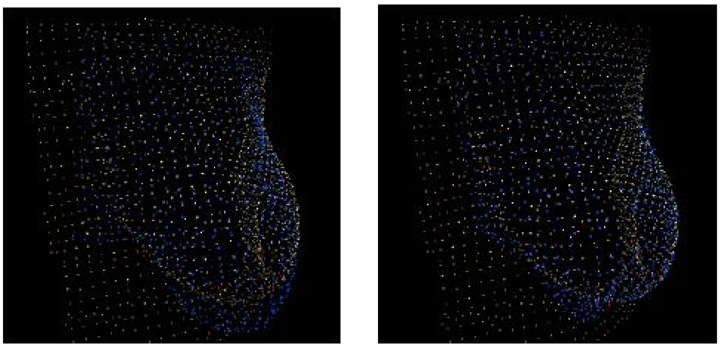

(a) After Rigid Registration. (b) After FFD.

Figure 3.5: Result of applying the FFD algorithm to the downsampled MRI (after biomechanical simulation) PCL of the patient with a [8 8 8] control point grid [58].

results between a rigid and non-rigid registration are presented in the Figure 3.5.

3.5 Validation Methods

In order to clinically implement a method, it needs to be correctly validated. This task is not easy, due to the lack of a ground truth, which does not allow the comparison of results. The ground truth that is normally used includes anatomical landmarks and external markers, for example [30]. Validation methods can be divided in subjective and objective methods, and the last ones can be either real or synthetic. Some of the mostly used tools for validation purposes are:

- Phantom studies [2]: since phantoms can be considerably still and can be displaced and rotated with accuracy, they can be used to calculate the accuracy of the registration. When non-rigid phantoms are used, it can be hard to calibrate the rotation or the displacement due to its behaviour, causing the same amount of compression not leading to the same breast image. Even though the above mentioned problems, phantom studies are widely used, because they era reusable and easy to access and they allow the control of the movement;

[2] A phantom is a specially designed object that is scanned or imaged in the field of medical imaging to evaluate, analyze, and tune the performance of various imaging devices.

- Calculation of the Euclidean distance: between certain features, like centroids of ROIs, breast contours or other landmarks;
- Subtraction of images: normally used in intra-modality registration and it can be applied to mammograms or MRI. Rueckert *et al.* [46] and Wirth *et al.* [59] used similarity measures like SSD (Sum of Squared Differences) and CC (Correlation Coefficient), in combination with the subtraction of images, for the validation of a non-rigid registration.

Schnabel *et al.* [60] used a validation method that includes finite elements to simulate physically plausible, biomechanical tissue deformations. When applying a certain range of displacements to finite elements models of different patients, it is possible to generate model solutions that simulate gold standard deformations. After that, deformed images are generated with a range of deformations, that are likely to occur in reality. The accuracy is quantified by co-registering the deformed images with the original, and comparing the recover voxel displacements with the simulated ones.

The most obvious method of validation, even though it is not accurate and it is the most subjective one, is visual inspection of the results by specialists.

3.6 Summary

Image registration is not an easy task and it has been the subject of many investigations due to the wide range of applications it can have. This task becomes even more difficult in the breast, where the tissue is non-rigid, deformable and changes appearance according to the position of the patient. This chapter came with the objective of clarifying the process of building a full 3D model of the breast, including not only the surface information, but the inside information of the breast. In order to build this model, there are a lot of steps that need to be made between the acquisition of the data and the achievement of the 3D model itself.

First, the information from radiological images needs to be registered and combined into the same referential. It is possible to use information from the same modality, acquired at different times and different points of view or from different modalities.

The data acquired from the surface, in the form of PCLs, also needs to be registered and reconstructed.

After that and finally, both data from the radiological images and from the surface can be combined in order to build the complete 3D model. Since the data is not acquired having the patient in the same position, there needs to be a pose transformation, using a physical or non-physical model. Physical models are more precise but have a higher computational cost.

So, in order to make the results clinically relevant and accepted, they need to be validated, a task that is not easy due to the lack of a ground truth or a gold standard.

Involving all steps, there is a distinction that is made almost through all of them, the difference between rigid or non-rigid algorithms, being the main difference between the number of DoF and the linearity of the transformations. The non-rigid algorithms are the less developed, but the most wanted ones, since most of the human tissues can be represented by a non-rigid behaviour. There are several assumptions or decisions made that can affect the final result, for example, when an initial pair of points is matched in two complementary PCLs, in order to begin an interpolation, the results can be affected depending on the point that is chosen. These processes need to be more accurate and similar to reality, as well as more automatic, so the human factor does not have to be considered.

There is a conclusion that can be obtained from the collected information: there is still no perfect model to solve the proposed problem, due to all the variables that need to be taken into account, which makes it necessary to have a deeper research into the subject.

Chapter 4

Methodology

In this Chapter, all of the datasets used will be presented, including the methods used for their acquisition and for their processing. The methodology followed to register the MRI and surface data, divided in rigid and non-rigid registration will also be presented. In the end, the methods used to process the data from the validation dataset will be explained as well as the evaluation metrics used to evaluate the process of registration.

4.1 Datasets

In the following subsections, the acquisition of the datasets used in the scope of this dissertation is described.

4.1.1 PICTURE dataset

In Carvalho *et al.* [58], a dataset with seven patients was used. This was the initial dataset, created with a subset of MRI data from the PICTURE project[1]. The PICTURE project was proposed with the aim of developing an accurate standardised method for objective cosmetic assessment that is cost-effective, simple to perform and insensitive to factors such as lighting, environment, patient position and operator variability.

For the acquisition of surface images a specific protocol was followed, specifying the following criteria:

- Optical Image Acquisition Camera, using the following methods:
    1. 2D Digital SLR Camera: for raw images and an HD video of the patient.
    2. Microsoft Kinect - 3DMK: RGB-D camera that is also a sensing system that captures RGB images along with per-pixel depth information.
    3. 3D MD Camera: used as a reference, can only be used by trained professionals with specialised equipment.

[1] https://www.inesctec.pt/pt/projetos/picture

- Patient Positioning: positioned with no jewellery or clothing, at a fixed point with her hands on her hips. The image must ensure anonymity of the patient.

  1. Using the 2D Digital Camera for the still photographs, the patient will stand at a fixed point and rotate 180° between lateral views, stopping for still photography at each 15°.
  2. Using the 2D Digital Camera or the Microsoft Kinect for video, the video images will be acquired continuously for a full 180° rotation between lateral views, performed as smoothly as possible.
  3. For the 3D MD Camera a single 3D frontal acquisition is acquired.

- Camera Mount: all cameras are mounted on a tripod or rig at an appropriate distance from the patient.

- Lighting and White Balance: no flash and light sources with known colour temperature. A still photograph and a short video with the patient holding a colour chart of neutral and standard skin tones will be acquired. An even illumination must be assured, with minimal asymmetry and production of strong shadows.

- Background: neutral to prevent reflections.

In this subset, 7 T1-weighted[2] MRI image sets were used, with 60 axial slides each, and a voxel resolution of 0.59 x 0.59 x 3 milimeters.

In Figure 4.1, an example of the surface and the MRI of one patient from the PICTURE project is shown.

From those seven patients, two only had data from one breast in the MRI, while the other five had both breasts. Testing with only seven patients is not very representative, since it does not provide a pool of data with a wide variety of breast shapes and densities that are useful to evaluate the transversality of the algorithm.

4.1.2 BCCT.plan dataset

BCCT.plan is a project that aims on the construction of a 3D tool that will help during the planning of the conservative treatment of breast cancer, enabling alternative surgical strategies and reducing the consequences of the current surgical strategies, when it comes to the appearance of the breast after the surgery. The dataset will contain radiological exams, annotated by radiology professionals and breast surface information.

[2] https://www.cancer.net/cancer-types/breast-cancer/stages
TNM system, the "T" plus a letter or number is used to describe the size and location of the tumor.
Tis: carcinoma in situ: the cancer is confined within the ducts of the breast tissue and has not spread into the surrounding tissue of the breast.
T1: tumor is 20 millimeters (mm) or smaller in size at its widest area.
T2: tumor is larger than 20 mm but not larger than 50 mm.
T3: tumor is larger than 50 mm.
T4: tumor has either grown into the chest wall, the skin or both. It can also be and inflammatory breast cancer.

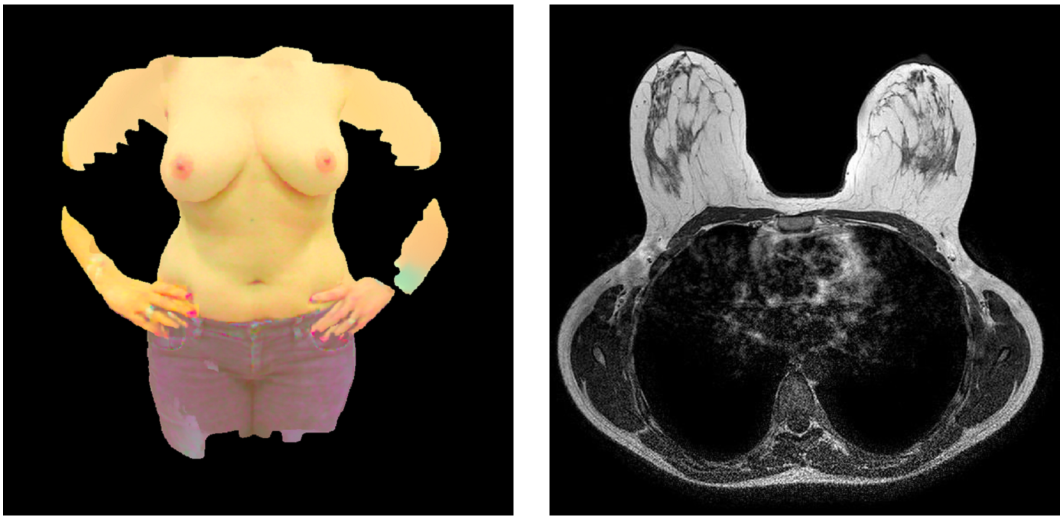

Figure 4.1: Scan and MRI data from the PICTURE project.

Patients with a Tis/T1-T3 breast cancer were proposed for Breast-Conservative Treatment (BCT refers to Breast-Conserving Surgery (BCS; ie, lumpectomy) followed by radiation therapy to eradicate any microscopic residual disease) at the Champalimaud Cancer Center between April 2017 and January 2019 for the BCCT.Plan project[3]. Contraindications included T4 cancers, inflammatory carcinoma and breast cancer recurrence post-BCT.

All patients were proposed for image capturing in the standing position with hands on hips.

The following data was acquired in all of the patients of this protocol:

1. Photographic data (2D images): photos of the patient from different angles using Canon EOS 1100D digital camera;

2. Surface data (2.5D and 3D images): surface scans of the patient capturing the size and shape of the breasts using Kinect Recording System by Microsoft® version 1.0 [61] and GoScan 20 3D by Creaform®;

3. Age, body mass index, bra and cup size;

4. Routine diagnostic images were collected (mammograms and ultrasound). MRI with gadolinium contrast was performed according to institutional protocols. Annotation, segmentation and volume computation of the tissue portions were performed and validated by two radiologists using the Horos® software v2.4.0. (breast contour, breast tissue including malignant tumor(s), pectoral major muscle, *Latissimus Dorsi* muscle anterior border: large, flat muscle on the back that stretches to the sides, behind the arm; sternum and clavicle).

In the MRI acquisitions, the protocol includes a pre-session acquisition with the patient in prone position with their arms alongside the body, and the session itself with the patient lying in

[3] http://medicalresearch.inescporto.pt/breastresearch/

prone position but with their arms raised. These sessions include the acquisition of T1 and T2 images, along with T2 images with fat suppression, diffusion weighted images and sagittal images with contrast.

In Figure 4.2, an example of the surface and MRI of a patient from the BCCT.plan project is shown.

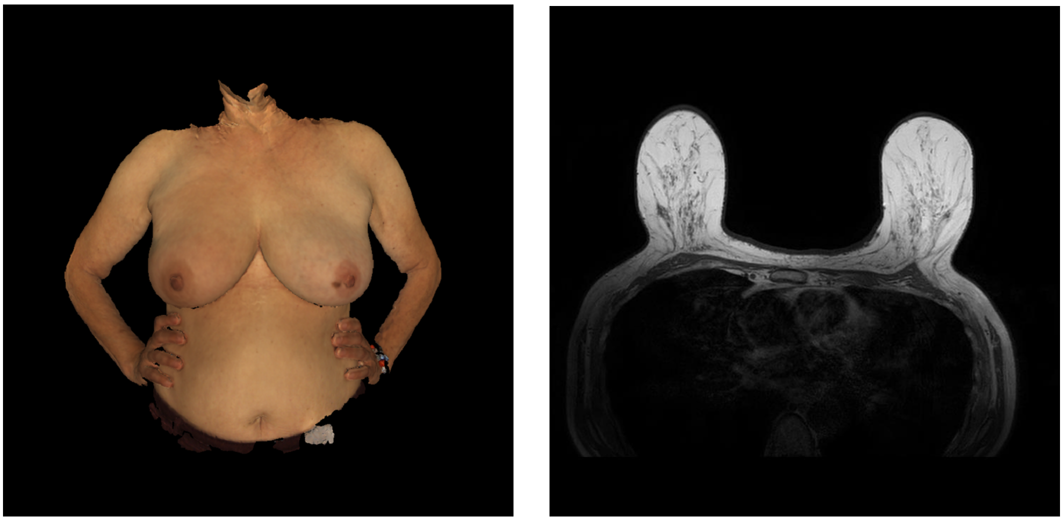

Figure 4.2: Scan and MRI data from the BCCT.plan project.

In the core of this project, an in-house software for annotation of the anatomical structures mentioned above was created. This software is called MARge and is able to create new labels for each one of the structures, change the annotation by slice, or use region growing in a set of slices. The MRI slices are seen in the axial view, but a sagittal and a coronal view are also displayed, as it can be seen in Figure 4.3.

From this project, ten patients were added to the previous dataset.

4.2 Pre-processing

After the annotations, the 2D slices of the MRI must be transformed into a 3D mesh, so the 3D mesh can then go through a pose transformation and be registered.

This transformation involves the following steps, also described in Figure 4.4:

1. **Definition of the contours of the breast**

   The breast anterior limit is defined by the skin, the posterior limit is defined by the interface with the pectoral muscle and the lateral limits are defined by the *Latissimus Dorsi* muscles. The top, bottom, frontal and back contours are created for each one of the breasts, since the pose transformation simulation can only be performed with an individual breast. That division is done vertically by the sternum. After the contours are created, their viability must

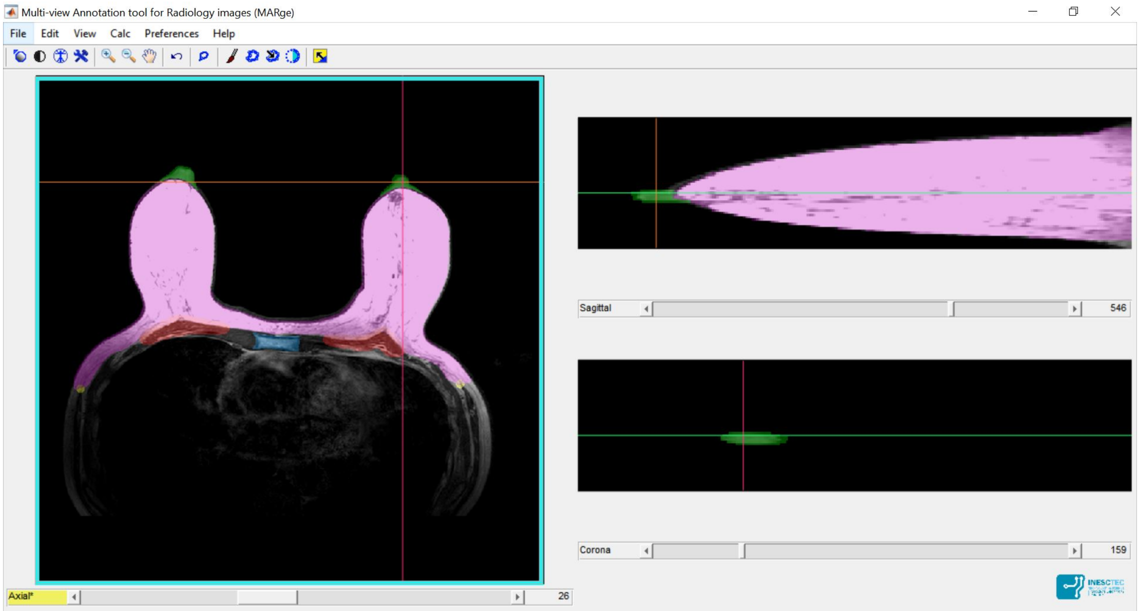

Figure 4.3: MARge Software. Pink: breast contour; Green: nipple; Red: pectoral muscle; Yellow: beggining of *Latissimus Dorsi* muscle; Blue: sternum. Axial view in the left, sagittal view in the top right corner and coronal view in the bottom right corner.

be asserted using the software Meshlab (the 1.3.3 version was used) and if some abnormality appears, the annotation should be corrected until the breast contours are viable.

2. **Point cloud creation**

   The contours are then merged into a single PCL for each breast by flattening all of the layers that define the boundaries of the breast. After its creation the number of points should be downsampled, to ensure that the PCL has less than 2000 points. Some PCLs were not able to complete the pose transformation step, most likely because the high number of points led to a high number of interior elements in the mesh, decreasing its size, which after some iterations would lead the derivatives to approximate to the zero value, ultimately leading to NaN values. In those cases, the number of points must be lowered.

3. **Surface mesh generation**

   To create the surface triangle mesh that models the skin, the Ball Pivoting Algorithm is used. The Ball Pivoting Algorithm joins three points in a triangle if a ball of a specified radius ρ touches them, without containing any other point [62]. After creating the surface mesh, some holes may appear if the Ball Pivoting algorithm was not able to join some elements because they were too distant from each other. Those holes can be filled by a tool provided by Meshlab. After filling those holes, some intersections may appear, and they have to be removed in order to create the 3D mesh. They can removed manually and filled again using Meshlab.

4. **Generation of the volume files**

Using the software Gmsh (version 4.3.0), a volume is added to the PCL which allows the 3D mesh generation.

5. **Creation of the files to the pose transformation**

   To represent the fat and fibroglandular tissues, a density factor is applied to all the breasts, in this case a density of 2 in a scale of 1 to 4 is assigned, where 1 is the lower density and 4 is the highest density [63], which corresponds to a b in a ACR breast density scale [64][4].

6. **Pose transformation**

   The MRI is obtained with the patient lying on a prone position, but to register this data with the data obtained from the scan, the patient must be on an upright position, and for that a pose transformation must be done. The upright position also allows a more natural and realistic visualization of the breast. The algorithm for the pose transformation is run on a PC virtual machine on VirtualBox and it will output the 3D mesh in the supine, unloading and upright positions. The model in prone position is converted to an unloaded state (a gravity-free reference state) , from which the supine and upright models are built. This simulator was provided by Vavourakis *et al.*[65].

The pre-processing pipeline here described is represented in Figure 4.4.

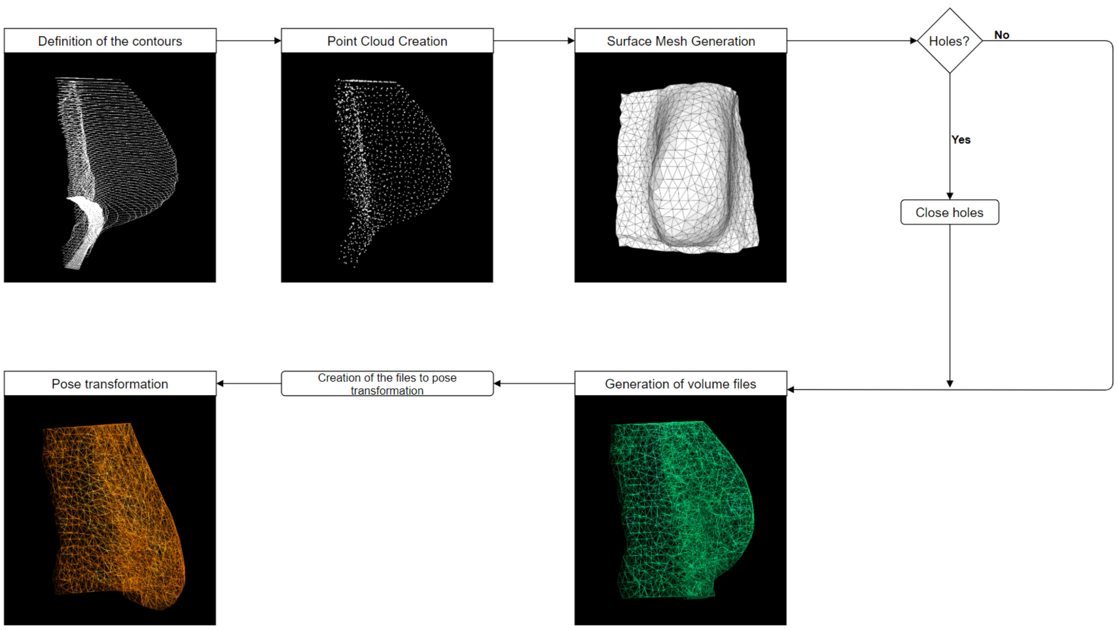

Figure 4.4: Pipeline of the pre-processing step.

[4]a: the breasts are almost entirely fatty
b: there are scattered areas of fibroglandular density
c: the breasts are heterogeneously dense, which may obscure small masses
d: the breasts are extremely dense, which lowers the sensitivity of mammography

4.3 Registration Strategy

The diagram presented in Figure 4.5 shows the entirety of the pipeline for the registration after the pose transformation of the MRI.

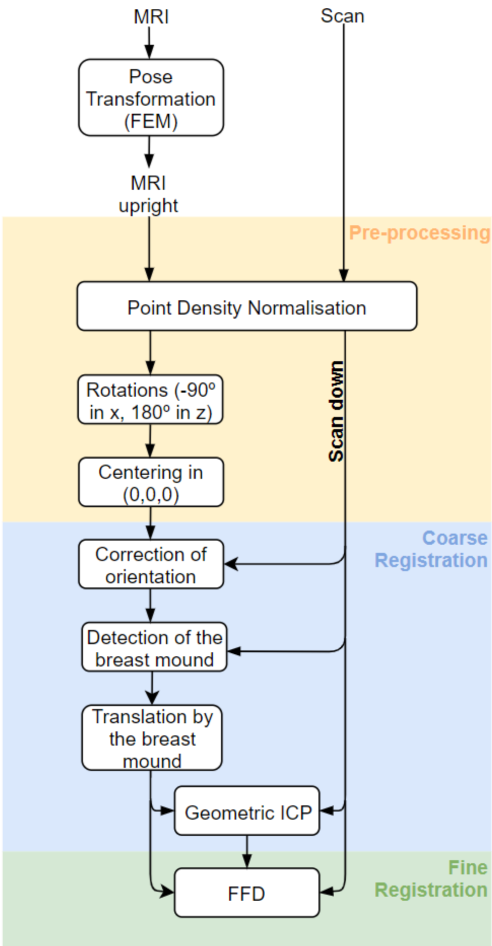

Figure 4.5: Pipeline summary for the registration of MRI PCLs and Surface PCLs.

The registration of the MRI point clouds will be performed in two different steps, starting by a rigid registration followed by a non-rigid registration. The rigid registration will also be divided in two steps: a pre-processing step that will place the two PCLs in the same space in order to successfully perform the second step, the coarse registration, that will approximate both of the PCLs through rigid transformations. Rigid transformations include pure rotations and translations, and these transformations are performed by specifying a matrix that moves the points in one point cloud to their appropriate positions in a second point cloud [66]. But the breast cannot be considered a non-deformable shape, so the rigid registration step is not enough to approximate correctly the shape of the breast obtained by the MRI with the one obtained from the surface, which justifies the non-rigid registration step. The rigid registration also assures better results in the following non-rigid registration, by placing the point cloud in the correct orientation and then approximating it to the target point cloud using points of reference or the distance between those points.

4.3.1 Affine Transformations

The MRI data comes in a different orientation from the surface, so a rotation is performed, given the surface as a reference.

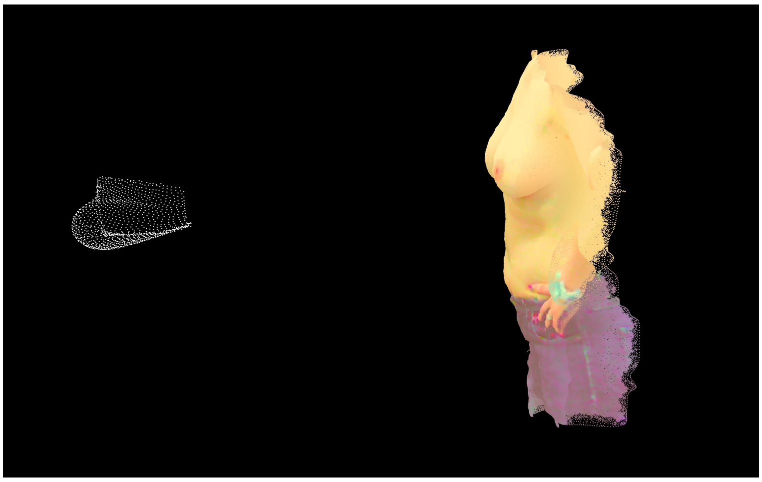

Figure 4.6: On the left: original MRI PCL. On the right: surface PCL.

To place the MRI in the same orientation as the surface, a rotation of -90° along the X-axis, followed by a rotation of 180° along the Z-axis is done.

Given the fact that some PCLs might come in a slightly different orientation due to the patient's position during the data acquisition, it is important to assure that both of the PCLs are oriented in the same way. For that, after centering them in the origin (0,0,0), both are aligned with the xy plane.

After the rotation, a translation is done to ensure that both point clouds, MRI and surface, are close enough before the ICP algorithm is applied. In order to make a translation, a reference point has to be found in both of the point clouds and in this case the chosen reference point was the nipple. The nipple is characterized by being the point with the highest curvature in the breast, but only defining it by that can be incorrect, since points in the abdomen of the surface can be detected as well. To eliminate the points that are not the nipple itself, only the point in the quadrant of the breast that has the highest curvature and the minimum value along the Z-axis is selected.

4.3.2 Geometric ICP

The Iterative Closest Point algorithm was proposed by Besl [67] and to use it both point clouds need to be close so it does not fall into local extremes, justifying the need of performing a rotation and a translation [37].

This algorithm is used to find the rigid registration between the target point set and the reference point set so that the two reach an optimal match.

The threshold for the distance between both PCLs was defined as a pair consisting of the Euclidean distance estimated between two translation vectors and the angular difference in degrees.

The algorithm stops when the average difference between estimated rigid transformations in the three most recent consecutive iterations falls below the specified tolerance value.

The results of the ICP algorithm are satisfactory in [58], but this algorithm is inefficient below the breast mound, which is where there is the highest density of points, by not being able to approximate this region in both of the point clouds, most likely because the algorithm falls into local extremes and does not make the correct match. By not making the a good approximation of the PCLs before the non-rigid registration step, the results will be worst, and those points will be matched with other surrounding areas that are closer to them, and not to the region below the breast mound as it should be.

He *et al.* [37] proposed a modified implementation of the ICP algorithm based on point cloud features, which includes features such as curvature, surface normals and point cloud density. In point clouds with irregular shapes, these features can reflect some basic shapes, which are critical for the correct representation of all of the characteristics of the point cloud.

In this case, the part of the breast that shows a greater inaccuracy is also the one with the highest curvature in the breast. This curvature reflects the concavo-convex degree of the point cloud surface. The remaining of the breast has a lower curvature, since it is a flatter zone of the breast.

This approach of the algorithm values the points with a curvature higher than a defined threshold, so they have more influence in the approximation of both of the point clouds and in the final result.

In order to calculate the curvature of all the points in the point cloud, a number of neighbours must be defined for each point. With the number of neighbours a covariance matrix of those neighbouring points can be calculated, which will indicate how similar the variances of features are [68]. From that covariance matrix, the eigenvalues (λ) and eigenvectors can be extracted. The curvature can then be calculated through the following formula:

$$Curvature = \frac{min(\lambda)}{\sum\lambda} \tag{4.1}$$

The number of neighbouring points chosen was 10 as it was recommended in He *et al.* [37]. To perform the ICP algorithm based on point cloud features, a threshold for the curvature must be chosen, but since this value can be subjective, all the points were ordered by their curvature value, and a percentage of those points was chosen and a subset was created.

When choosing that percentage, some values outside of the interest zone, located in the lateral borders of the breast were also being chosen, so the search for the points with the highest curvature was limited to the points below the breast mound point, which is the most problematic region. Since this area is very limited, the rest of the point cloud can have an unexpected behaviour, so a second subset is built with the rest of the point cloud, but only after applying a high downsampling to it, so the choice of feature points is not affected. By joining the two subsets of points, a set with a high density of points in the part with the most features and a low density of points in the part with the least features is achieved.

To give advantage to the points with the highest curvature, in the implementation of the ICP algorithm, the calculation of the error is changed in order to include the difference between the curvature of the matching points, so points with high differences in their curvatures will not be a match, avoiding the initial problem of having the points with the highest curvature not approximated to their correct matches. So, this error can be translated by the following adaptation of the RMSE error, considering $d^{m,s}$ the module of the distance between each point in the MRI and its closest neighbour in the surface:

$$Error = \frac{\sum_{i=1}^{n} d^{m,s}(i)}{n} + \frac{\sum_{i=1}^{n} \sqrt{(curvature_{m_n} - curvature_{s_n})}^2}{n} \tag{4.2}$$

Where m represents the MRI point cloud, s represents the surface and n the number of points that are being evaluated.

The error is used as a stop criteria along with the tolerance (a pair consisting of the Euclidean distance estimated between two translation vectors and the angular difference in degrees) and the maximum number of iterations.

4.3.3 Deformable Registration

The breast has a deformable nature with a non-rigid behaviour, and for that it is not enough to only use a rigid registration approach. The rigid registration works as a preparation step to the deformable registration, approximating both of the PCLs, providing a better environment for the deformable registration and leading to better results.

The deformable registration of the breast is performed using the FFD algorithm, explained in Section 3.2. As mentioned by *Carvalho et al.* [58], using a 3D grid of 8 points in each dimension ([8,8,8] grid) will improve the results comparing to using a smaller grid or a 2D grid, even though the computational time is increased by greater grids. To avoid even higher computational times, the number of points can be downsampled, having no great impact in the final results.

The tumour will also be inserted in the interior of the breast, in its correct position, which means that it will also be rotated and translated, but it will not go through the ICP algorithm. The data from the tumour is provided as a PCL for the patients of the BCCT.plan project (including the patients from the validation dataset). The goal is to understand the impact of the FFD algorithm on the tumour and to represent the 3D model of the breast with the tumour inside, improving the certainty of the doctor's approach on the Breast Cancer Treatment.

4.3.4 Closing the breast

In order to visualize the breast as a closed entity, the pectoral muscle will also be registered and used to complete the visualization of the breast.

The pectoral muscle has a rather low deformation when compared to the deformation of the breast itself [69], and for that its behaviour will be considered rigid.

To register this muscle, since its behaviour is considered rigid, a rotation and a translation will be performed. Unlike what happens on the breast, the ICP algorithm, that is part of the rigid registration step, will not be performed, since it would lead to wrong results, centering the pectoral muscle inside the breast.

4.4 Dataset Validation

A validation dataset is essential to understand the accuracy and validity of all the transformations that were applied to the breast. Since the evaluation metrics are not always a reliable source of understanding for the accuracy of the registration, and the visualization of all of the PCLs becomes difficult when the dataset has many patients, a solution was found to better understand what was indeed the best methodology for all of the patients.

The validation dataset was acquired in the same conditions as the BCCT.plan dataset, only adding 3D landmarks positioned at reference points, as shown in Figure 4.7. Those landmarks were positioned around the patients breasts with a black permanent marker before surface data registration (Figure 4.8 (c)). After that, liver cod oil pills were fixed above this reference points before MRI acquisition (Figure 4.8 (a),(b)). These landmarks can then be used, after the registration, to measure how further away the reference points are from each other, between the surface and the MRI, to conclude which of the points have the higher deformation and to understand what is the best methodology.

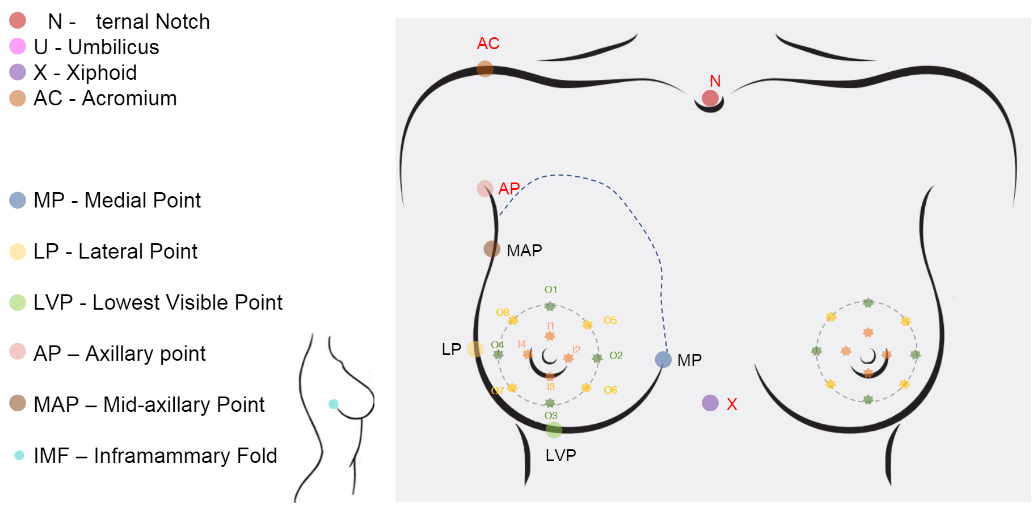

Figure 4.7: Reference points for the 3D landmarks, used both for the surface and the MRI.

The process used to annotate the slices of the MRI is almost the same as the one described in Section 4.1.2, with some changes due to the presence of cod oil pills. Those pills are annotated differently from the breast, and some caution needs to be made to guarantee they are intersecting the breast. Some of the pills, may be dislocated during the MRI, and those will not be considered. This dislocation is easily visible as it can be seen in Figure 4.9 in the pills surrounded by red.

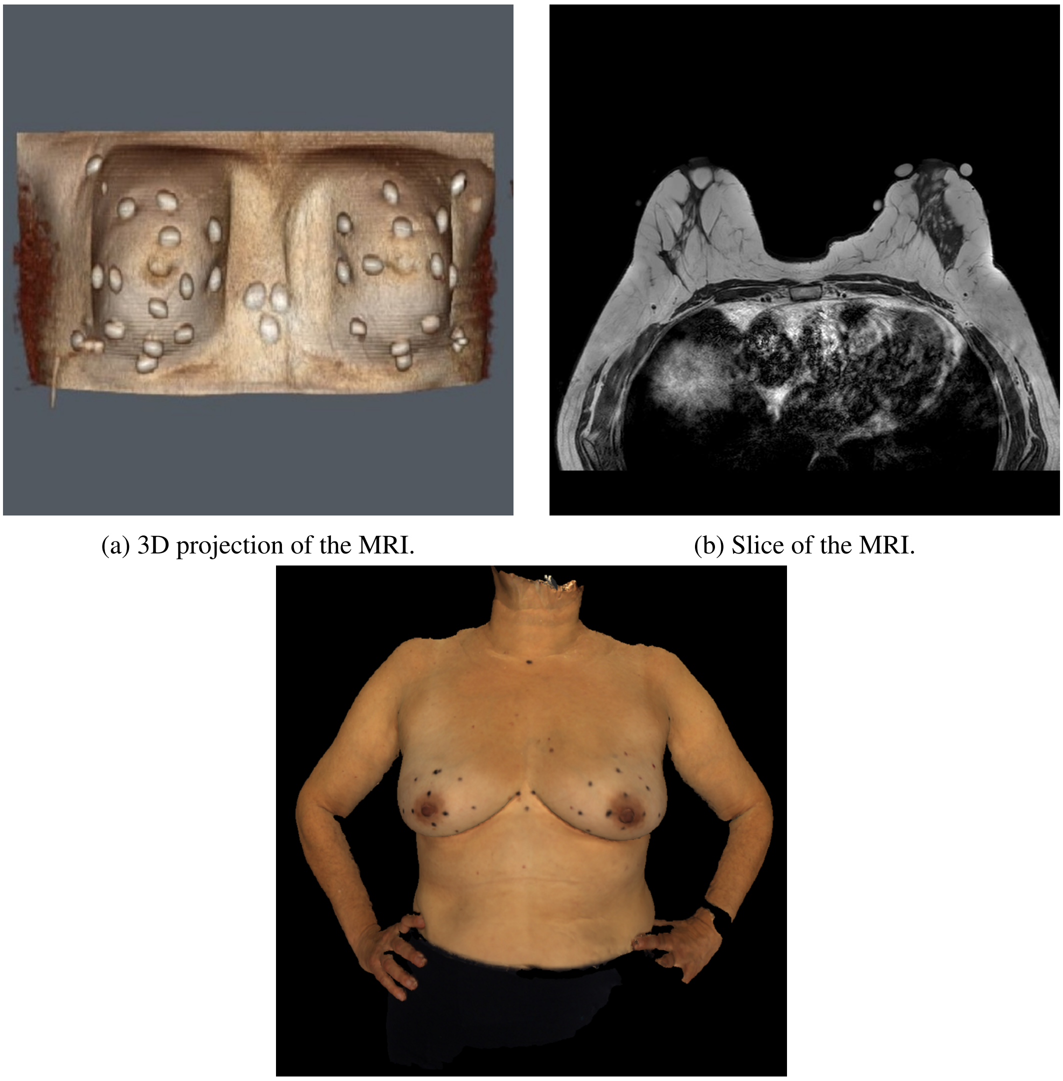

(a) 3D projection of the MRI.

(b) Slice of the MRI.

(c) Surface PCL.

Figure 4.8: MRI and Scan data with breast markers.

The reference points in the surface also need to be annotated. For that, the software Meshlab was used, and the reference points were selected and saved in a PCL. When selecting the reference points, there needs to be the least area of skin possible, selecting only the black area of the reference points. Figure 4.10 shows the selection of the reference points on the PCL.

After the annotation and selection of the reference points in both the MRI and the surface, a model with an assigned number to each one the reference points is created and the correspondences between the numbers and the landmarks, represented in Figure 4.7, is made. In Figure 4.11 and in Figure 4.12 the numbered reference points for the MRI and the surface, respectively, can be seen.

The pre-processing pipeline described in Section 4.2 is also followed for this dataset, but including the centroids of the landmarks in the PCL. These centroids are joined after performing the downsampling to assure that these points are not eliminated. Through all the steps it is important to verify that all the points of the centroids are being used.

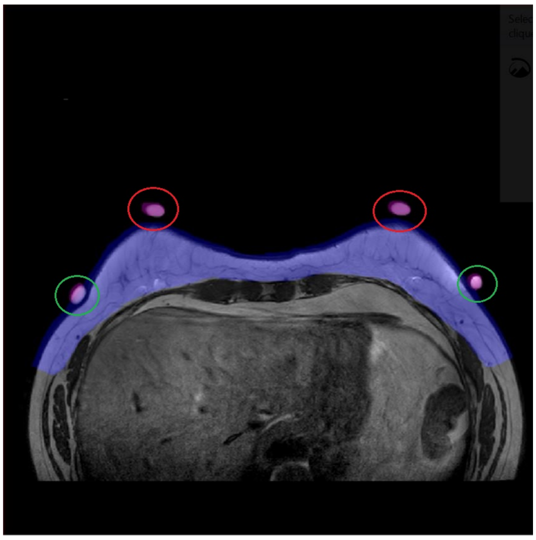

Figure 4.9: MRI slice with the cod oil pills showing in pink. Normal pills, intersecting with the skin are surrounded by green. Dislocated pills that show no contact with the skin are surrounded by red.

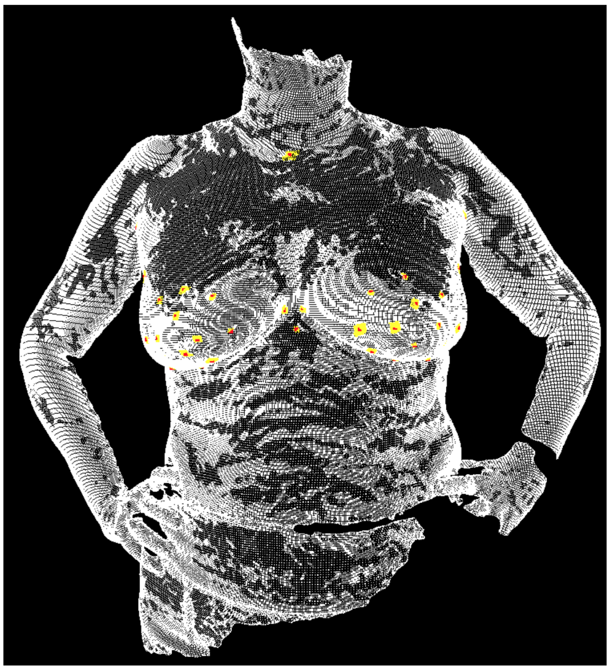

Figure 4.10: Reference points selected in the surface.

4.4.1 Evaluation Metrics

To evaluate the accuracy of the rigid registration, some metrics can be used to measure the distance between the two point clouds. The metrics used are point to point, which means that the distance is measured from each point in the reference point cloud to the corresponding point in the target point cloud, or vice versa, even if the two point clouds do not have the same number of points [70]. For each point in the reference point cloud, the nearest point, with the lowest distance,

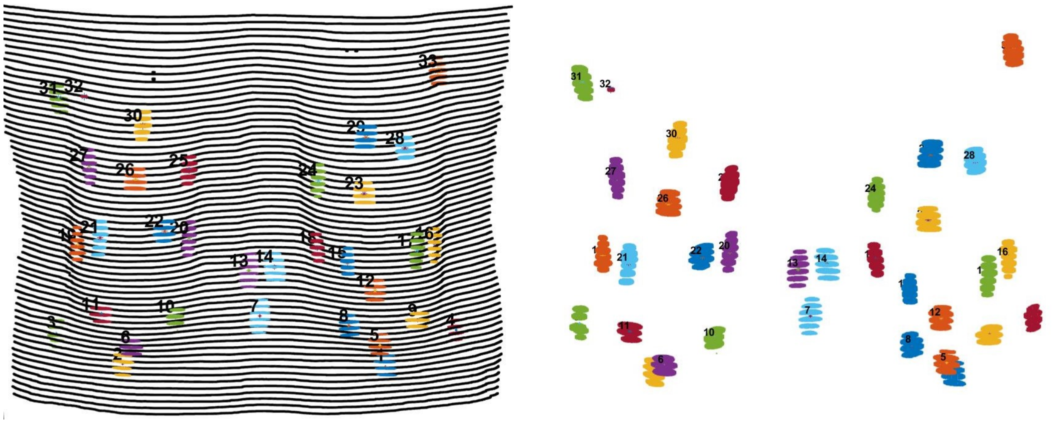

(a) Reference points with the breast contour. (b) Reference points without the breast contour.

Figure 4.11: Numbered reference points for the MRI.

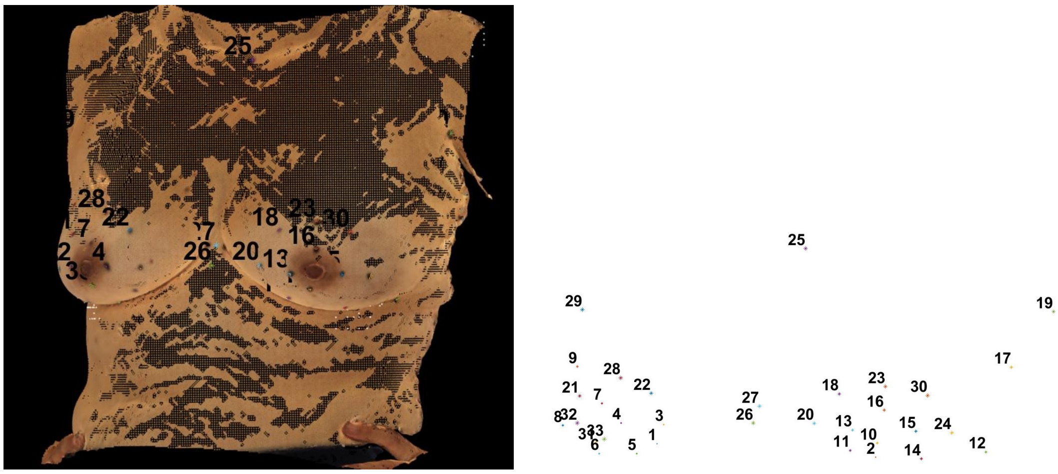

(a) Reference points with the surface. (b) Reference points without the surface.

Figure 4.12: Numbered reference points for the surface.

is found.

The metrics used are:

- Euclidean Distance: ordinary straight line distance.
- Hausdorff Distance: maximum distance between a point in the MRI and its closest point in the Surface, between all of the points [71].

$$Hausdorff\ Distance = \forall i \in M \max d^{M,S}(i) \tag{4.3}$$

The value of the Hausdorff distance is not a mean value and for that, it can be more sensitive to outliers.

In this case, the distance could be calculated in both directions (from the source to the target, or from the target to the source), but since the surface PCL has a bigger area, if the distance calculation is made from the surface to the MRI PCL, the errors will be much higher [72].

However, these metrics cannot be completely reliable, since they do not consider that the points are actually representing a 3D object surface and they can not fully express the user experience quality [70].

4.4.2 Target Registration Error

The anatomical landmarks used in the validation dataset can be called fiducial points. The Target Registration Error (TRE) measured at a given point, relative to some given origin, is the distance after registration between the anatomical landmark in one space and the corresponding anatomical landmark in the other space, in this case, between the surface and the MRI [73]. The TRE works as a method to measure the registration accuracy, as it will measure the difference between the same landmark, allowing a conclusion about the efficacy of the algorithm.

The final TRE is calculated as the mean square of all the TRE values calculated for all the fiducial points.

4.4.3 Summary

To summarize, the dataset now has 24 patients, corresponding to 46 breasts, since in the PICTURE project two of the patients only have one breast. Those patients were obtained from 3 different projects, and one of them provided a set of patients for validation using reference points in both the surface and the MRI that can then measure the validity of the algorithm.

Figure 4.5 summarizes the pipeline followed for the Registration Strategy. The MRI is acquired in prone position, and a Finite Elements Method is used to transform this pose into an upright pose. Even if the MRI is in the same pose as the surface PCL, their orientation still needs to be change accordingly. For that, the MRI PCL is rotated 90^{o} in x and 180^{o} in z, and then both of the PCLs are centered in the origin (0,0,0) and aligned with the xy plane to correct bad positioning that might have happened during the acquisition of the data. To finish the affine transformations, a translation is applied after finding the breast mound in the surface and in the MRI, using this point to perform the transformation. Before the deformable registration is done, and to assure the closest approximation of the points using a rigid registration, the ICP algorithm is performed, with a different approach that values the points with the highest curvature. To finalize the pipeline, the Free Form Deformation is used to register the breast in a non-rigid approach.

Chapter 5

Results and Discussion

In this section the results of the methodology presented in Chapter 4 will be shown. Tables for all the patients (5 patients from PICTURE project, 10 patients from BCCT.plan project and 7 patients from the validation dataset) will be presented, but the figures will only be represented for one patient, the first one, unless told otherwise, for situations when a worst or best case is worth showing. Distances will be presented in millimeters. The two patients from the PICTURE project with only one breast will be discarded for this analysis, since they present no relevant characteristics and they could not be used when comparing the use of the entire torso with the use of a single breast. For simplification purposes, patients from the PICTURE project will have the numeration from 1 to 5, patients from the BCCT.plan project will be from 6 to 15, and patients from the validation dataset will be from 16 to 22. The left and right breast will not defined by their laterality and they will take the numeration of 1 and 2.

Besides the results obtained from the rigid and non-rigid registration, the influence of some factors in this registration will be studied, such as:

- Using the complete torso of the patient, comparing to registering only one breast at a time. Previous results presented by Carvalho *et al.*[58] only performed the registration for one breast. The results showed that there was a gap between both breasts at the end of the pipeline, because they were both registered individually. Using the complete torso will also provide results that are more close to reality.

- Using the breast with the pectoral muscle in the back. The pectoral muscle has a proximate to rigid behaviour so it will only go to the rigid registration, but visualizations with the pectoral muscle will be provided in order to see the breast as a closed entity.

- Inserting the tumour inside the breast and understanding its behaviour.

- The behaviour of the algorithm with the breast in a prone position, with no pose transformation.

All of the options that are available to perform the algorithm are shown in Figure A.1 in Appendix A, but only some of them will be performed and analyzed on this Chapter. All of the results discussed in this Chapter are shown in Appendix A with full description for each patient.

The algorithm used to generate these results was run on Matlab R2019a.

5.1 Rigid Registration

5.1.1 Affine Transformations

As it was mentioned in Chapter 4, to correctly align both the PCLs, some affine transformations are performed, that are summarized in this list:

- Rotation of -90º along the X-axis, followed by a rotation of 180º along the Z-axis;
- Center in the origin (0,0,0);
- Alignment with the xy plane;
- Translation through the breast mound.

The correct alignment of the breast with the xy plane places the MRI in a more correct position, aligned with the scan, and consequently closer to it. A representation of this correction can be seen in Figure 5.1. After the correction of the orientation, the breast is considerably closer to the scan.

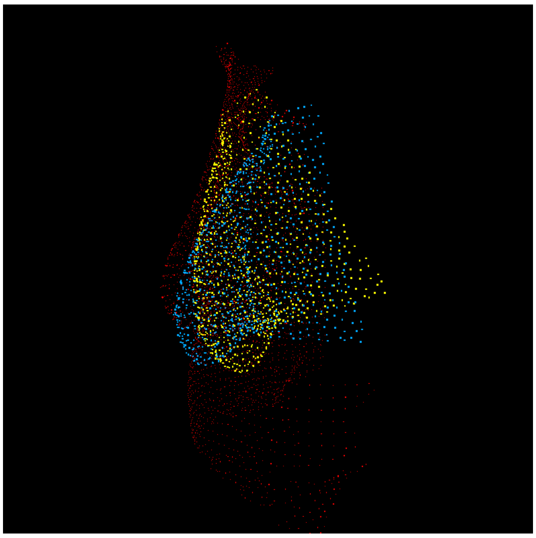

Figure 5.1: Correction of the orientation. The PCL in red represents the scan, while the PCL in blue represents the MRI after being rotated and centered in (0,0,0) and the yellow the MRI after the correction of orientation using the xy plane.

The translation through the breast mound can be done using the entirety of the torso to perform the translation, eliminating in that way one of the degrees of freedom associated to this transformation. To use the complete torso, the breast mounds of the scan and the MRI are calculated separately for the left and right breast. After that, the mean value of the breast mounds is calculated for the MRI and the scan and the translation is made using these two points.

An example of a well performed translation is shown in Figure 5.2(a), where the breast mounds are correctly identified in both the MRI, in red, and the scan, in blue. Figure 5.2(b) is an example of a badly done translation, where the breast mounds are detected in the stomach area below the breast. A bad detection of the breast mounds and consequently a bad translation can lead to wrong results after the ICP, since the breast is not well positioned.

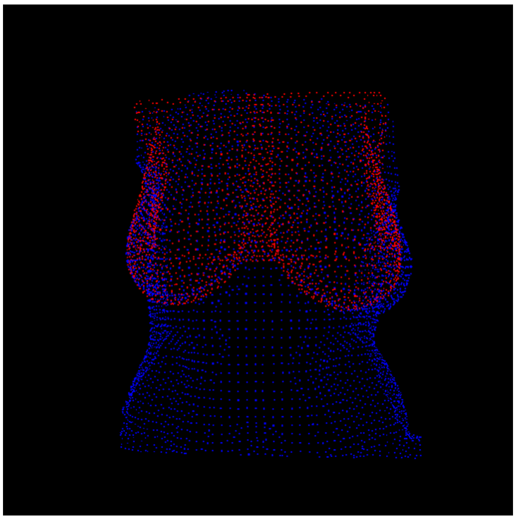

(a) Patient 15, after translation.

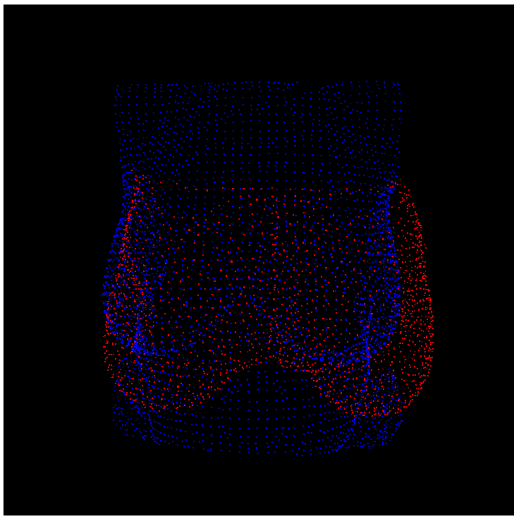

(b) Patient 1, after translation.

Figure 5.2: Results after translation.

5.1.2 Iterative Closest Point Algorithm

When comparing the results after the implementation of the rigid registration, it is important to use both numerical and visual results. The results for the normal ICP are represented in Figure 5.3, divided by each dataset. This implementation was followed by [58], but since the date of his publication some improvements have been made to the algorithm, and so the results were produced again.

To understand the relevance of the visual results for the approval of the evaluation metrics, some visual results will be presented considering the metrics shown in Figure 5.3, with the best and worst Euclidean distances, respectively. Patient 16 has a great fitting to the surface, which shows by its low error and by Figure 5.4(a), but both breasts still have a gap between them, so its orientation could still be improved. On the other side, patient 6 that has a higher error, besides also having a gap between both breasts, it shows a worst fitting to the surface. The ICP is not able to correctly orientate the breast after the translation by the breast mound, so the right breast has almost a 90º difference from what should be its position.

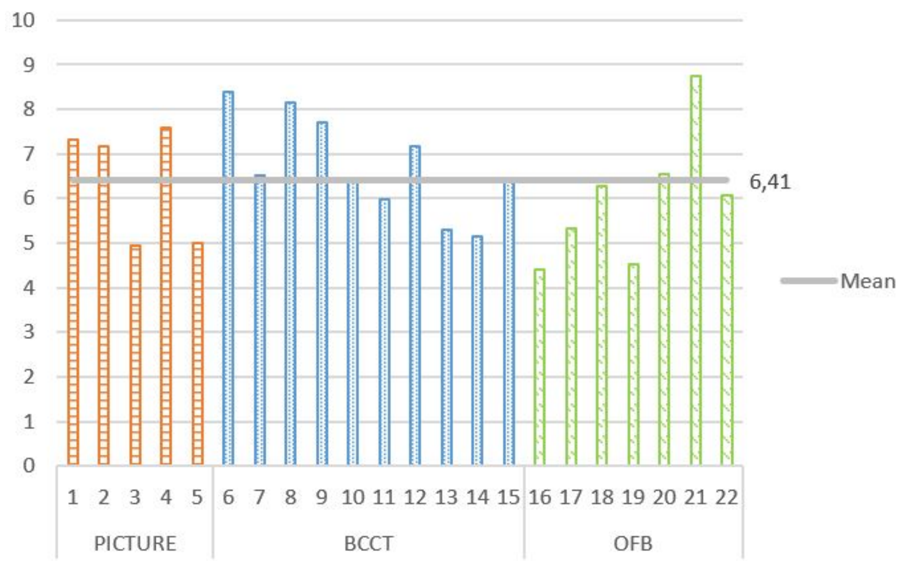

Figure 5.3: Euclidean distances after the normal ICP.

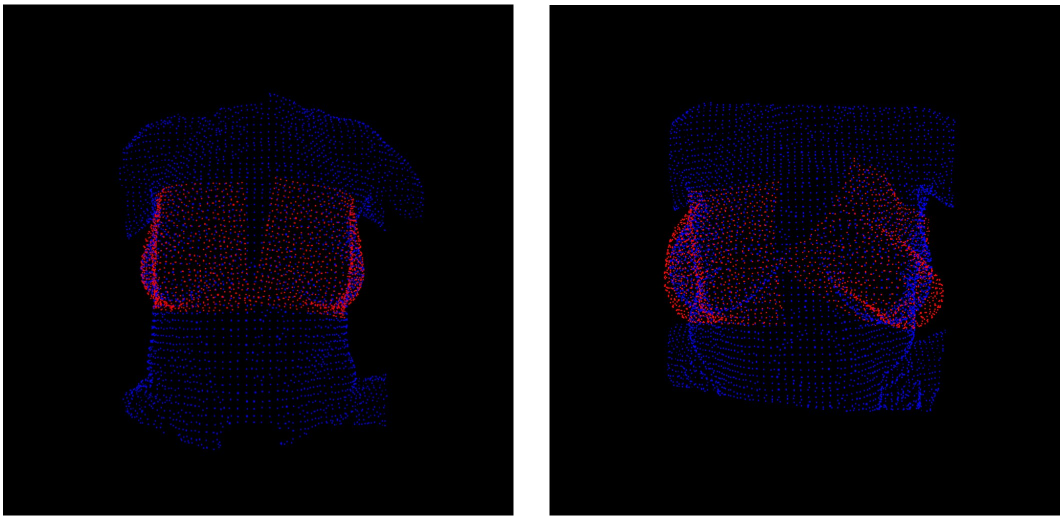

(a) Patient 16. (b) Patient 21.

Figure 5.4: Results after the normal ICP.

When comparing the results obtained from the implementation of the geometric ICP, shown in Figure 5.5, with the results obtained from the implementation of the normal ICP, it can be concluded that the mean Euclidean Error is 1.19mm greater than the error obtained with the normal ICP.

In Figure 5.6, the best and worst results of the geometric ICP can be seen, respectively in 5.6(a) and 5.6(b).

The goal of this implementation is to give more weight, and consequently more impact, to the points below the breast mound that do not get proximate enough to the surface PCL. The points in this area were chosen by selecting the points below the breast mound and joining them with a

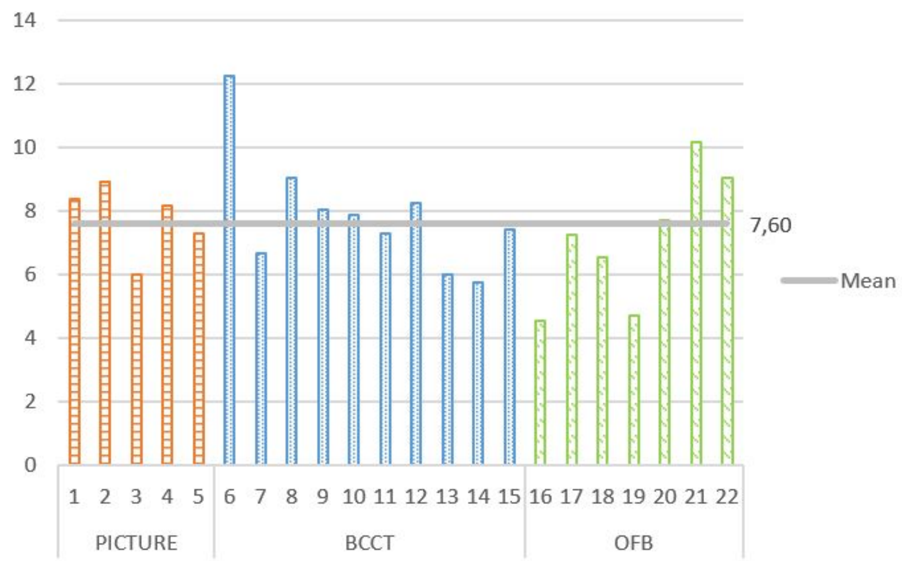

Figure 5.5: Euclidean distances after the geometric ICP.

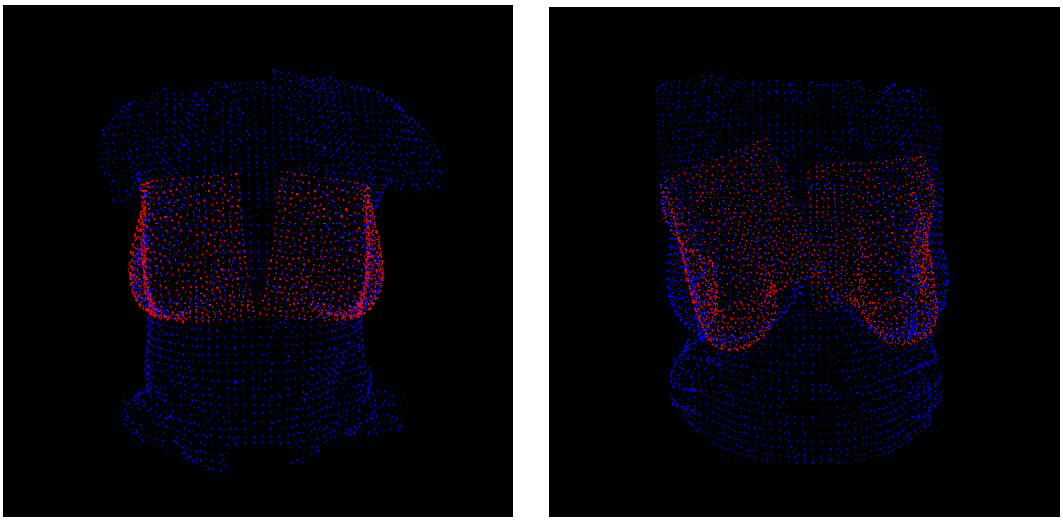

(a) Patient 16. (b) Patient 6.

Figure 5.6: Results after the geometric ICP.

very downsampled PCL of the MRI to guide the points outside of this zone. This will give a better approximation for the points below the breast mound and consequently a better orientation to the points in the superior part of the breast.

This can be proved by comparing Figure 5.7 and Figure 5.6(b) that represent the same patient after the normal and geometric ICP, respectively. In the case of the normal ICP the points of both breasts are further apart in the sternum zone, and there can be seen that in the MRI PCL, below the breast mound the points are not close enough the surface. In the case of the geometric ICP, the ptosis of the breast is more correspondent to the surface and that will lead to a better fitting of the MRI, approximating both breasts in the sternum. It is also necessary to keep in mind that the geometric ICP will have a greater impact in breasts with a bigger ptosis.

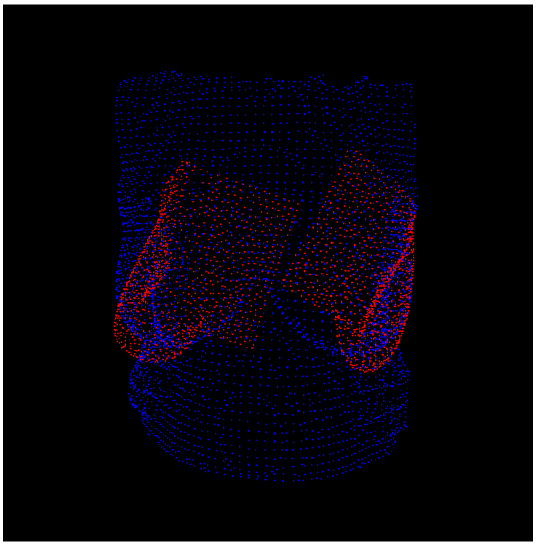

Figure 5.7: Patient 6 after the normal ICP.

The number of points below the breast mound can be arbitrary, so a study was made in order to understand what number would bring the best results. 4 percentages of points with the highest curvature below the breast mound were chosen: 40%, 60%, 80% and 100%. Figure 5.6 shows the results when using 100% of the points below the breast mound, while the Tables for the rest of the percentages are shown in Appendix A.

When comparing the 4 percentages used, the mean value of the Euclidean error for the 80% and 100% is the same (7.60mm), but the standard deviation and the minimum and maximum values are higher for the 80% case. In the 40% and 60% cases, the mean Euclidean error is greater than in the 80% and 100% case. So, for the geometric ICP, the totality of the points below the breast mound will be used as weighted points in its implementation.

When performing the ICP algorithm with the complete torso, the breast will no longer get separated in the sternum zone, automatically preventing greater displacements between the both PCLs that lead to unrealistic behaviours. An example of the usage of the torso is presented in Figure 5.8 also for the patient 6. The results are rather similar for the normal and geometric ICP, but in the geometric ICP the MRI is closer to the surface in the area below the breast mound especially for the left breast.

Figure 5.9 represents the ideal approximation before the deformable registration, forthe patient 20 after the normal and geometric ICP, mostly in 5.9(b), which will consequently improve the results after the FFD.

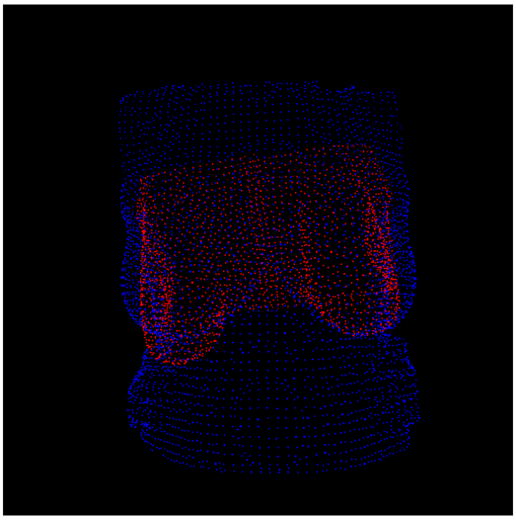

(a) Normal ICP with complete torso.

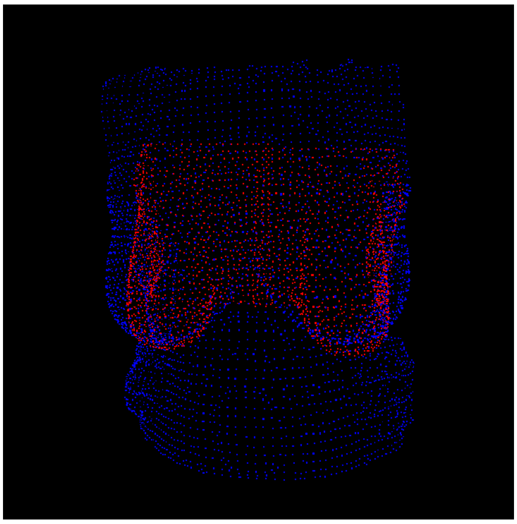

(b) Geometric ICP with complete torso.

Figure 5.8: Comparison between the normal and geometric ICP for the patient number 6 using the complete torso.

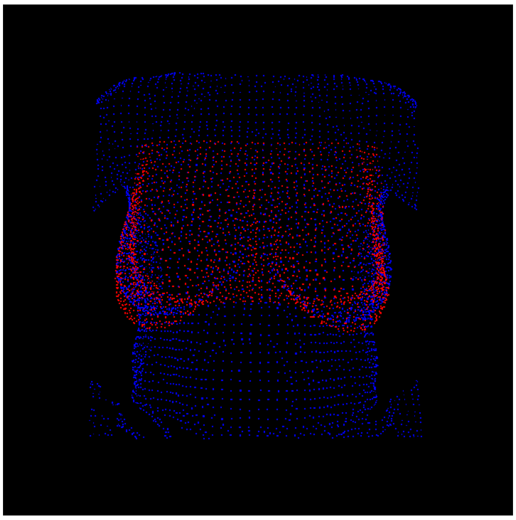

(a) Normal ICP with complete torso.

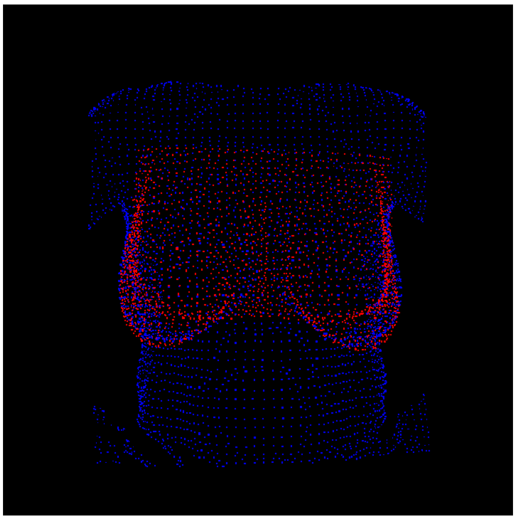

(b) Geometric ICP with complete torso.

Figure 5.9: Comparison between the normal and geometric ICP for the patient number 20 using the complete torso.

5.2 Deformable Registration

5.2.1 Free Form Deformation

The non-rigid registration is performed using the FFD with an [8,8,8] grid, with a threshold for the error of 1×10^{-7} mm and 250 iterations as stop criteria. When analyzing the final results for the patients registered using the normal ICP, one breast at a time, five patients present a very high Euclidean error (high discrepancy when comparing to other values) after the non-rigid registration, when comparing to other patients.

The best and worst of these four cases can be seen in Figure 5.10, respectively.

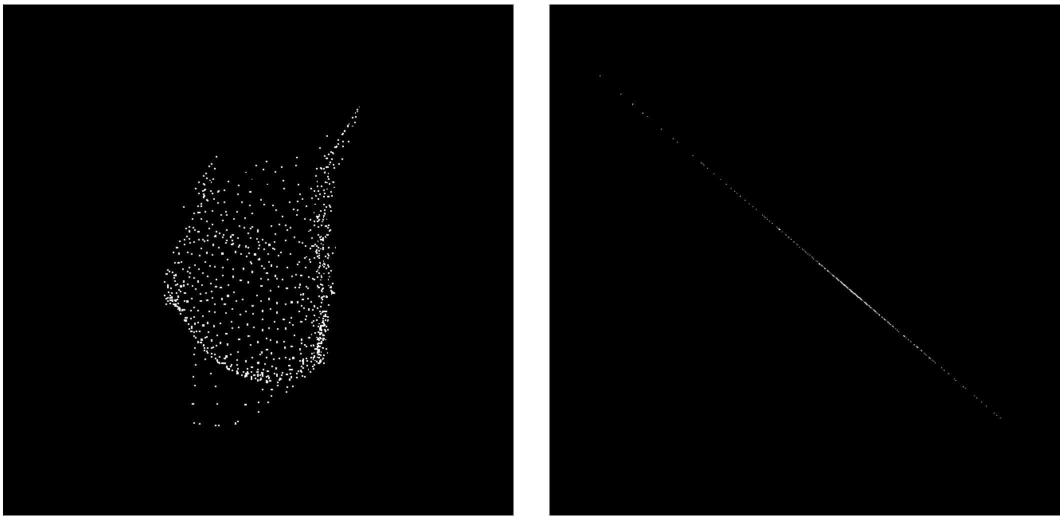

(a) Patient 22, breast number 2.

(b) Patient 17, breast number 2.

Figure 5.10: Deformed breasts after the complete registration, using normal ICP and a single breast.

While in Figure 5.10(a), the shape of the breast is still recognizable, although it has many dispersed points, in Figure 5.10(b), there is no recognizable shape and the breast is completely disintegrated. The complete desintegration of these breasts during the FFD algorithm, might be due to the lack of proximity between both PCLs and the bad positioning of the MRI after the rigid registration step. The detection of the breast mound is not robust enough and sometimes the breast mound is mistakenly chosen by some points below the breast mound, namely in the stomach area.

In fact, when looking at the PCL of patient 6, for example, after the ICP algorithm implementation in Figure 5.11, it is noticeable that the PCL is deviated and in a more lateral position. The same does not happen to patient 22 and 17.

The reason for the deformation in these other breasts, that belong to the BCCT.plan and the validation dataset, can be behind the surface PCL. For these datasets, the acquisition was made with the scanner GoScan 20 3D by Creaform, while in the PICTURE project the acquisitions were made with the Microsoft Kinect - 3DMK. Even though the GoScan is a more robust and expensive scanner, it fails to register all the parts of the surface, mostly in the inframammary fold region, while the Kinect is able to capture all of the surface.

The lack of precision of the GoScan is seen in the surface of patient 18 represented in Figure 5.12. A reconstruction of this hole can be done, using the software Meshlab, which will cover the hole. But, even after the hole is covered, the point density in the region of the hole will be very low comparing to the rest of the PCL, making the PCL non-uniform in terms of density.

The results after the elimination of these 4 patients can be seen in Figure 5.13.

Results of the non-rigid registration using the geometric ICP only have one patient with deformations after the pipeline, that is shown in Figure 5.14.

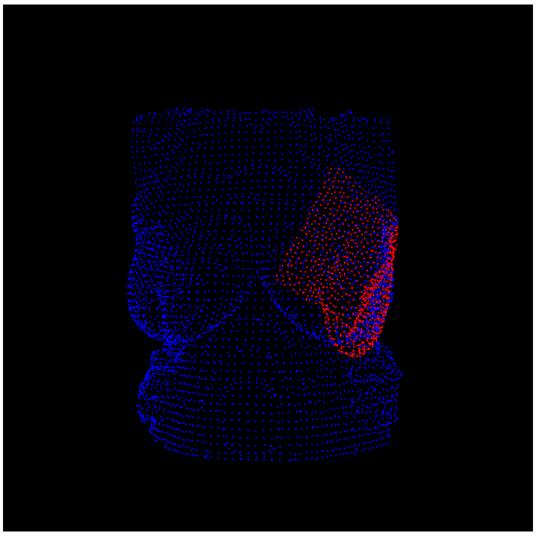

Figure 5.11: Patient 6, after a normal ICP implementation.

Figure 5.12: Surface of patient 18.

Figure 5.15 shows the Euclidean distance after the FFD when using the geometric ICP, after eliminating the patient with a deformation. The mean value for this Euclidean Distance is 0.93±0.24mm and is very similar to the one presented in Figure 5.13 of 0.91±0.18mm, although thislast one does not represent as many patients.

Figure 5.16 shows the difference, after the non-rigid registration, between the implementation of the normal and the geometric ICP, in the first patient,which has a below the mean error. In Figure 5.16(a), there is wider gap between the both breasts, while in Figure 5.16(b) there is an overlap between the both PCLs.

In summary, the results using the normal implementation of the ICP, and a single breast registration, show some anomalies in 5 of the 22 patients, due to factors such as a bad positioning and presence of holes in the surface PCL, which in combination with the unpredictability of the FFD

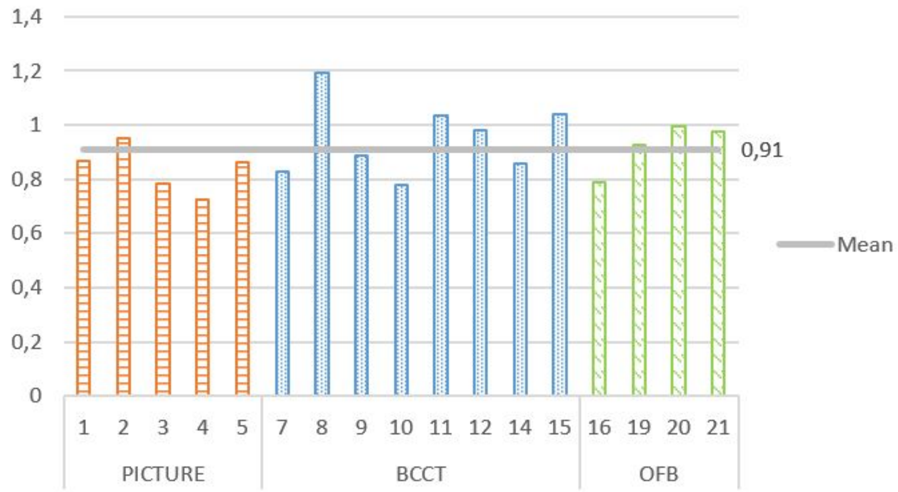

Figure 5.13: Euclidean Distance after the FFD using the normal ICP.

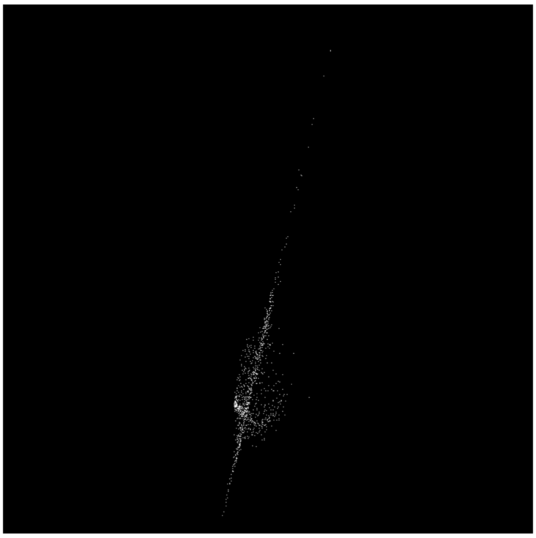

Figure 5.14: Breast number 2 of patient 18 after the non-rigid registration using the geometric ICP.

algorithm will lead to worst results. To understand if changing the implementation of the FFD algorithm will have an impact on these results, a trial was made using a smaller 3D grid of [6, 6, 6] instead of the [8,8,8] grid that was previously being used.

The results for the non-registration using the normal ICP and a 3D grid of [6,6,6] points to the FFD are shown in Figure 5.17, for both the normal and geometric ICP. Even though the mean value is higher using this grid, there are no exceptions of patients with deformations, which makes it a safer option than the two options mentioned above.

5.2.2 Algorithm with complete torso

When testing with the complete torso, the resulting PCLs show no deformations such as the patients with a [6,6,6] grid, although the mean values of the Euclidean distance are higher. PCLs

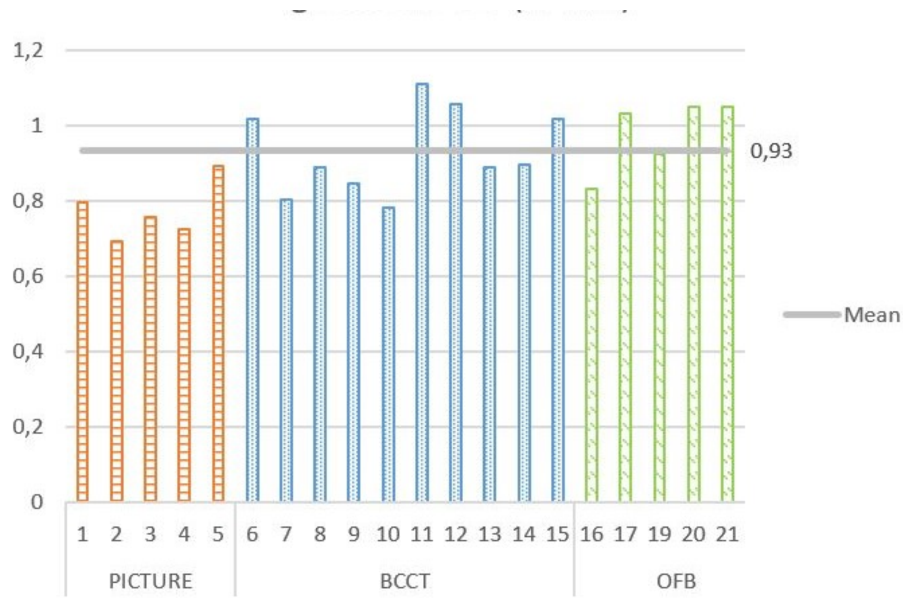

Figure 5.15: Euclidean Distance after the FFD using the geometric ICP.

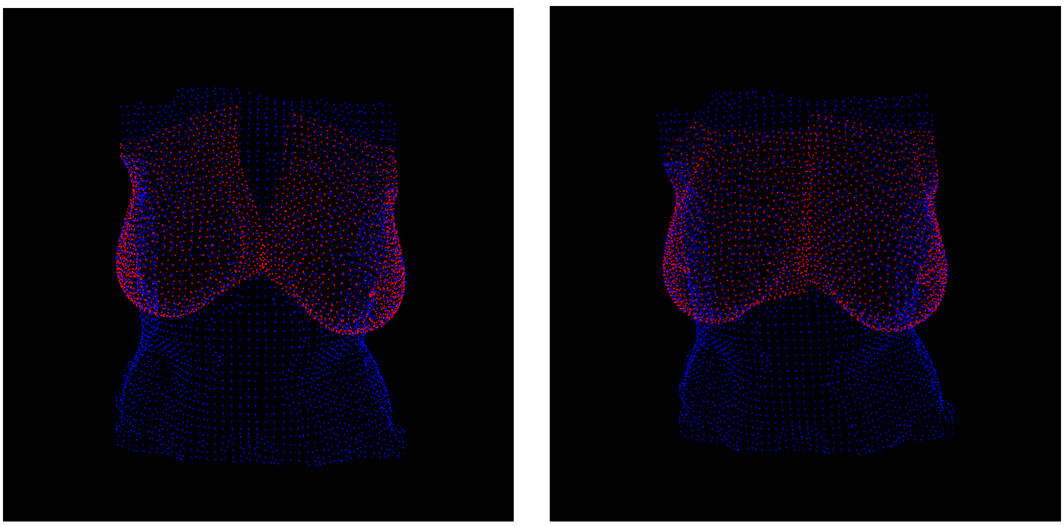

(a) Normal ICP. (b) Geometric ICP.

Figure 5.16: Results after the non-rigid registration for the normal and geometric ICP.

after the non-rigid registration show although a higher density of points between both breasts, as it is represented in Figure 5.18. This happens if the points are not well aligned with the surface before the non-rigid registration. Those points will be matched with the surrounding areas since they are the closest.

The same problem is not so visible when implementing the geometric ICP. When using the geometric ICP the points are normally closer to the breast in the region of the points below the breast mound, before the non-rigid registration, and so the results will be better in terms of dispersion of points, comparing to the normal ICP, as it can be seen in Figure 5.19.

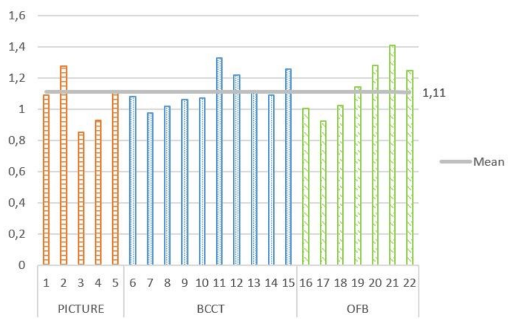

(a) Normal ICP.

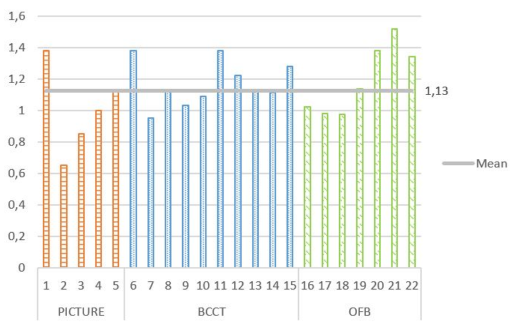

(b) Geometric ICP.

Figure 5.17: Results after the non-rigid registration for the normal and geometric ICP using a grid of [6,6,6] points in the FFD.

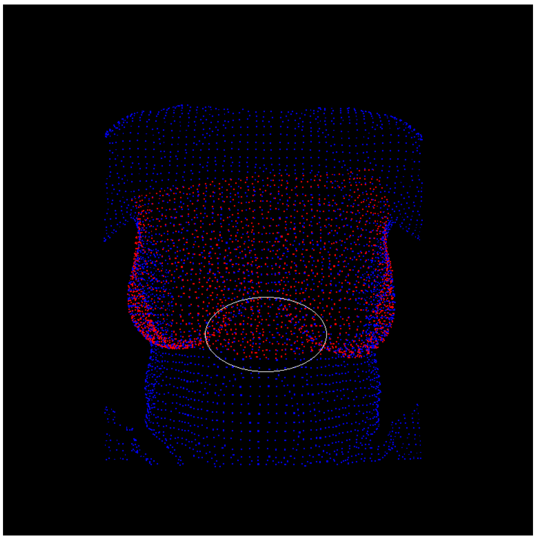

Figure 5.18: Complete torso after the non-rigid registration for patient 20 with normal ICP.

5.2.3 Insertion of the tumor

The influence of the FFD algorithm on the tumor was also studied. The tumor does not go through the pose transformation algorithm and is kept at the same position of the MRI acquisition. In terms of registration, the transformations applied to the breast will also be applied to the tumor, which means they will not be accountable when it comes to find what transformations need to be done, but they will have to go through those transformations.

A schematic of the localization of a tumor done by a clinician involved in the BCCT.plan project is presented in Figure 5.21 for patient 21.

Figure 5.22, shows the tumor before and after the registration respectively. The registration will approximate the tumor towards the skin as it can be seen in Figure 5.22(b). Considering that the data is mirrored in Figure 5.23, comparing to Figure 5.21, it can be concluded that the tumor also suffers some lateral movement to the right.

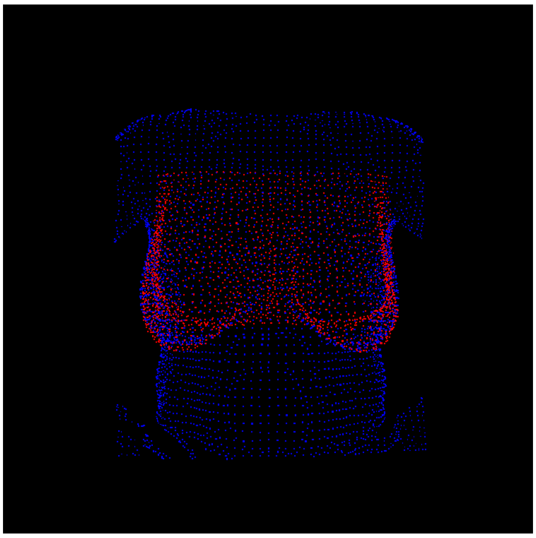

Figure 5.19: Complete torso after the non-rigid registration for patient 20 with geometric ICP.

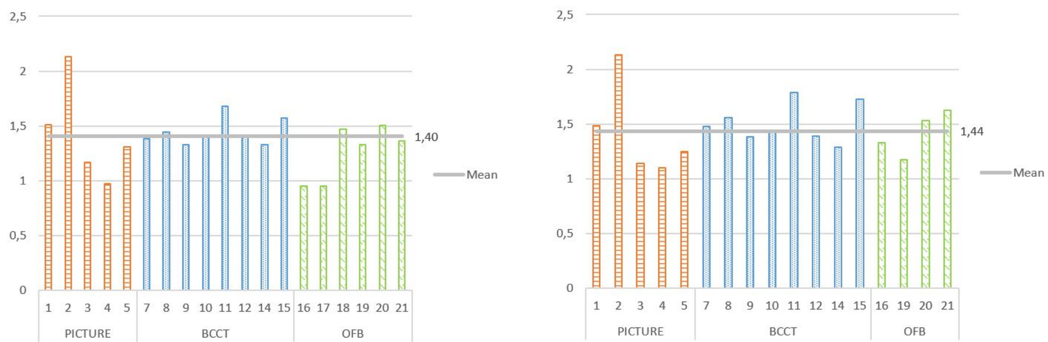

(a) Normal ICP. (b) Geometric ICP.

Figure 5.20: Results after the non-rigid registration for the normal and geometric ICP using the complete torso.

5.2.4 Insertion of the pectoral muscle

To visualize the breast as a closed entity, the pectoral muscle was also registered. The pectoral muscle went through the rigid registration, but it did not go through the non-rigid registration, otherwise it would deform the points of the muscle towards the breast. It can be considered that the pectoral muscle has a rigid behaviour, since the pose transformation of the breast will not affect the pectoral muscle.

Visualizations of the torso before and after the registration with the pectoral muscle are provided in Figure 5.24 for patient 20. As it can be seen, the pectoral muscle shows a constant behaviour through the registration and shows no changes or strange behaviours.

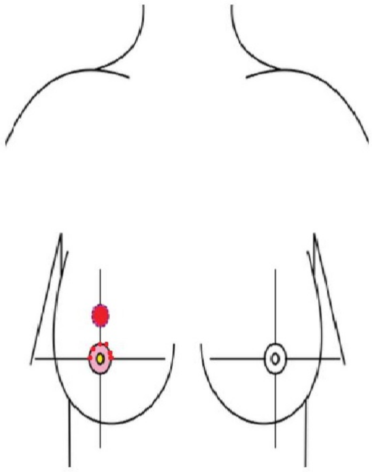

Figure 5.21: Representation of the localization of the tumor of patient 21.

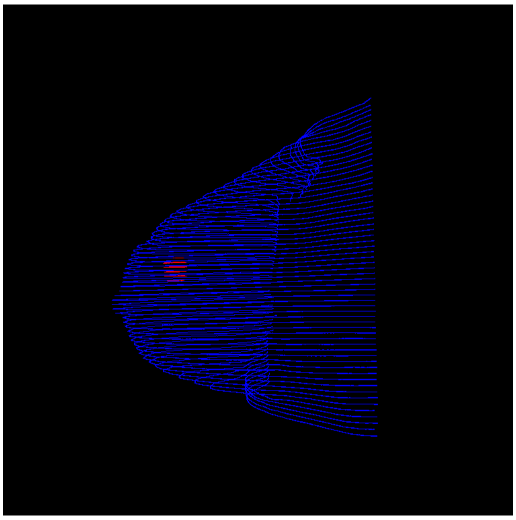

(a) Frontal contour of the breast before the registration with the tumor.

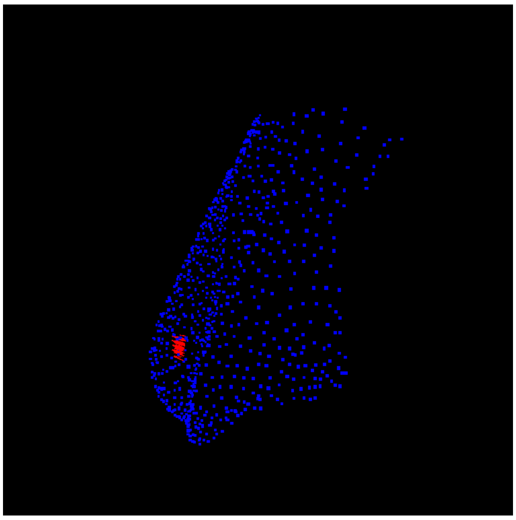

(b) Breast after the FFD with tumor.

Figure 5.22: Patient 21 with tumor.

5.3 Validation Dataset

The purpose of the validation dataset is to understand the accuracy of the algorithm and to understand its viability by analyzing the correspondence between the same breast markers in different modalities, in this case the MRI and the surface. The following methodologies will be tested:

1. Normal ICP, with single breast and a grid of [8,8,8] points for the FFD;

2. Geometric ICP, with single breast and a grid of [8,8,8] points for the FFD;

3. Normal ICP, with the complete torso and a grid of [8,8,8] points for the FFD;

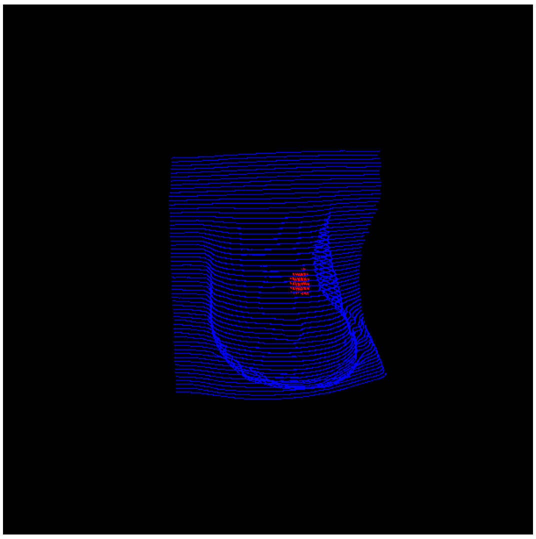

Figure 5.23: Representation of the localization of the tumor of patient 21 on a frontal view.

4. Geometric ICP, with the complete torso and a grid of [8,8,8] points for the FFD

5. Normal ICP, with single breast and a grid of [6,6,6] points for the FFD

6. Geometric ICP, with single breast and a grid of [8,8,8] points for the FFD

Testing with a [6,6,6] grid for the FFD, using the complete torso was not done, because the torso has many more points than the single breast, so it should be registered with a bigger grid.

Each one of the breast markers has 11 mm of diameter, but only their centroid will be considered. When analyzing the distances presented here for the validation dataset, it must be considered that the distance is to the centroid of the reference and not its borders, which can lead to greater distances.

The reference points represented in Figure 4.7 of Chapter 4, have different displacements considering factors such as the size of the breast and the position of the patient. For example, if the breast is large, the MAP reference point will have a higher displacement, since the compression of the breast will also be much greater during the MRI. The MRI will also deform the breast towards the middle of the torso.

The displacement of the more external points such as MAP, AP, LP will be higher than the displacement of more medial points such as the MP, since the breast will be more compressed on the sides during the MRI. In the supra-internal part of the breast (points such as I1, I2, O1, O2), the displacements will be normally inferior comparing to the infra-external part of the breast (points such as I3, I4, O3, O4). MAP distances can be uncertain due to the difference of the arms position during the surface data acquisition and MRI.

Graphics in Figure 5.25, show the value of TRE distributed by breast markers and by patient. The x-axis shows all of the breast markers, while each coloured bar represents one of the seven patients. In these graphics the mean value for each breast marker is also marked through the red circles and the mean value for all patients and all breast markers is represented in a black dashed

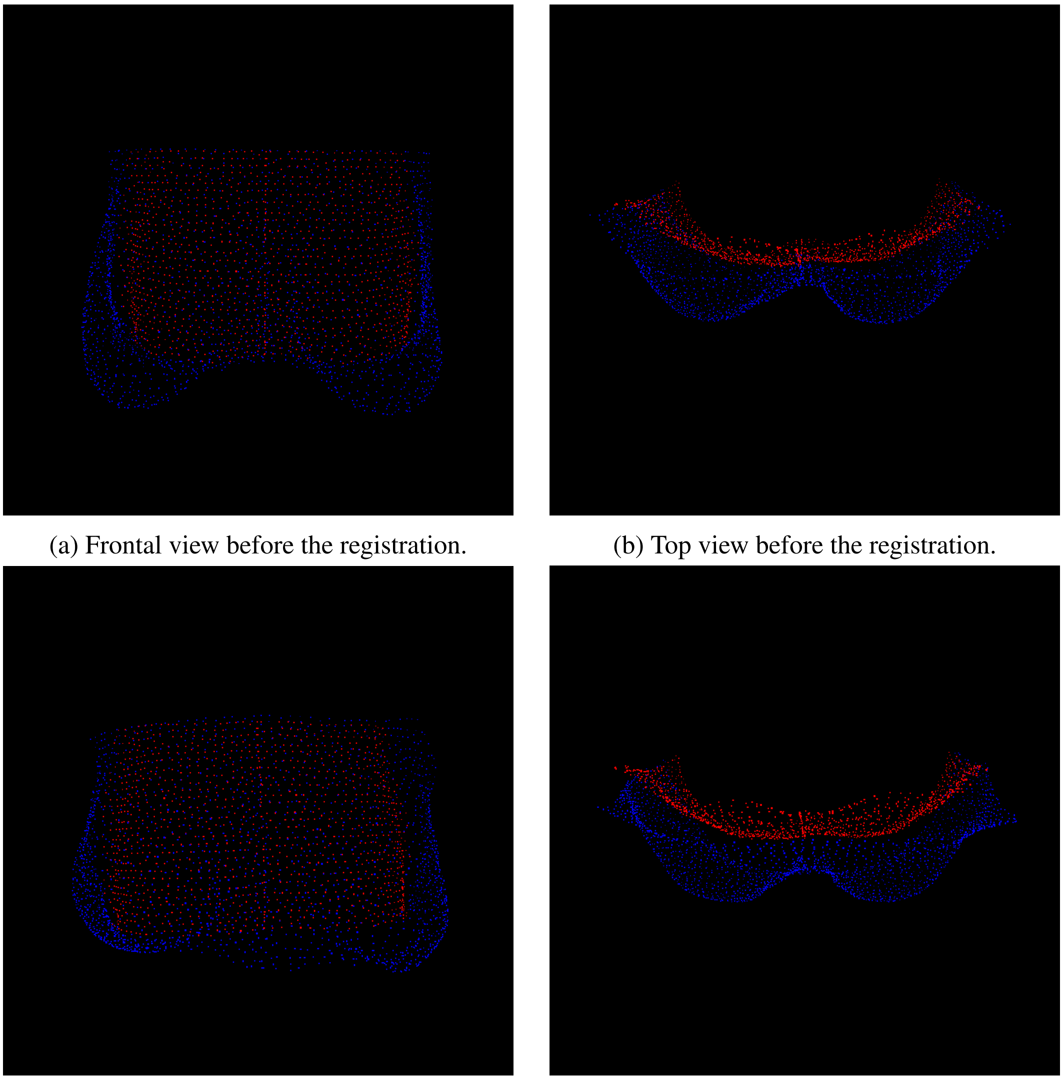

(a) Frontal view before the registration.

(b) Top view before the registration.

(c) Frontal view after the registration.

(d) Top view after the registration.

Figure 5.24: Representation of the torso with the pectoral muscle for patient 20.

line. When analyzing the mean value of all the six different methodologies, it can be concluded that the lower mean TRE is set for the methodology number 5, using a normal ICP for the rigid registration and the [6,6,6] grid for the FFD. This methodology's highest error values are also considerably lower than in the other methodologies.

In Figure 5.26(b), it can be seen that there is a higher maximum error for the LP comparing to MP, X and SN, proving that the medial points will have lower displacements than the lateral points. The same also applies to reference points such as the O4 and Od, more external points in the nipple, that have a higher TRE than the medial points O3 and Oa, as shown in Figure 5.26(a). The AP and LVP points do not have any matches for any of the patients, although they can be found in the surface, they are hard to pinpoint in the MRI. AP is positioned in the armpit, and LVP is a very low point inserted in the inframammary fold zone.

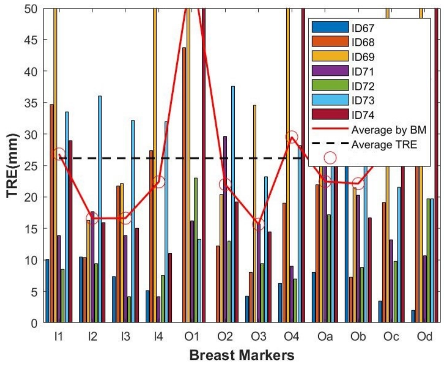

(a) Results using a single breast, normal ICP and a [8,8,8] grid for the FFD.

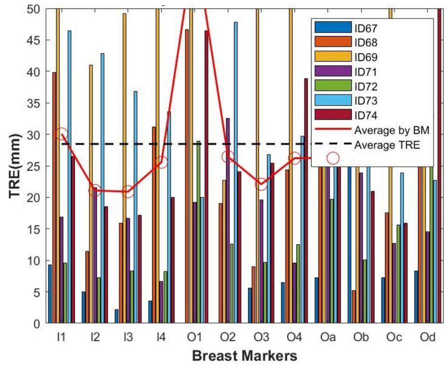

(b) Results using a single breast, geometric ICP and a [8,8,8] grid for the FFD.

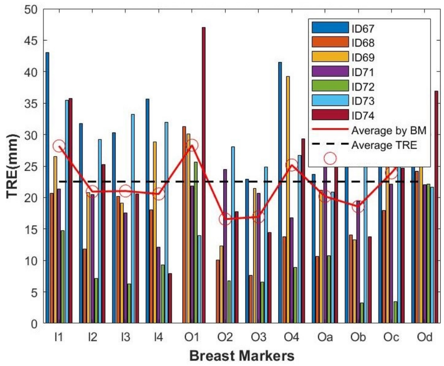

(c) Results using the complete torso, normal ICP and a [8,8,8] grid for the FFD.

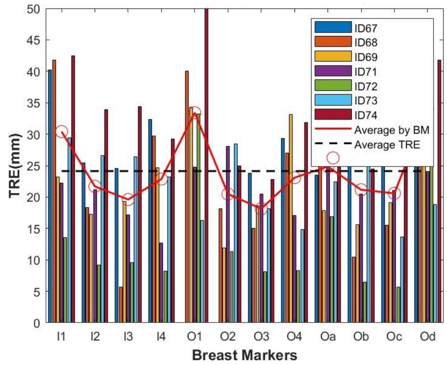

(d) Results using the complete torso, geometric ICP and a [8,8,8] grid for the FFD.

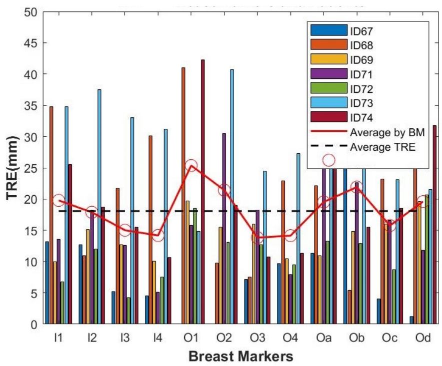

(e) Results using a single breast, normal ICP and a [6,6,6] grid for the FFD.

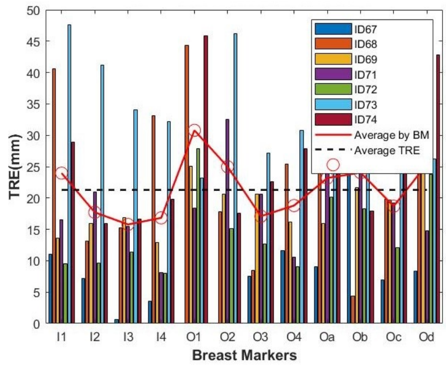

(f) Results using a single breast, geometric ICP and a [6,6,6] grid for the FFD.

Figure 5.25: TRE values by breast marker and by patient (Oa, Ob, Oc, Od correspond respectively to O5, O6, O7 and O8 in Figure 4.7).

Table 5.1 shows the mean values for each breast marker in the breasts 1 and 2, considering all the seven patients of the dataset.

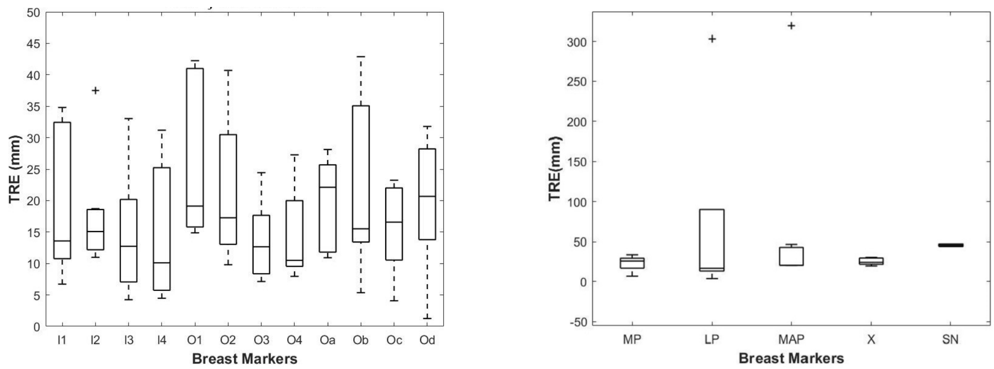

(a) TRE values for each breast marker for the markers around the nipple (O1, O2, O3, O4, I1, I2, I3, I4, Oa, Ob, Oc, Od).

(b) TRE values for the MP, LP, MAP, X and SN values.

Figure 5.26: TRE values for each breast marker, when using a single breast, normal ICP and a [6,6,6] grid for the FFD.

5.4 Prone vs. Upright

The previous results presented in this Chapter were all relative to the patient in an upright position, but for the best case scenario mentioned in the previous Section, the algorithm was also performed with the patient in a prone position. Using the prone position has the advantage of skipping the pose transformation step before the rigid and non-rigid registration, since the MRI is acquired in a prone position. Although it saves some time, the breast in a prone position has a very different shape, comparing to the upright position in which the surface is acquired, because the patient is lying down and the gravity will affect differently in both cases. The compression applied to the patient during the prone position and the position of the arms are also factors that will modify the shape of the breast.

Figure 5.27 shows the results for the best methodology in a prone position. The mean Euclidean distance for this case is 1.07±0.22mm, which is higher than the results for the upright position in the same conditions, and also higher than the cases with an [8,8,8] grid, although in the case of a [6,6,6] grid there are no cases of deformed PCLS after the non-rigid registration.

Looking at Figure 5.28, it can be seen that the breast in a prone position is more compressed than in the upright position, and the volume of the breast will be lower at the end of the registration for the prone position. The breast registered in a prone position also has some points below the breast that are deviated from the region that corresponds to the volume of the breast, because the FFD was not able to match these points to region below the breast mound due to their position after the rigid registration.

5.5 Discussion

The rigid registration is an essential step to the successful performance of the non-rigid transformation. It is impossible to make a good registration when the PCLs are very further apart, and

Table 5.1: Mean TRE value for each breast marker using a single breast, with a normal ICP and a [6,6,6] grid for the FFD.

	1	2
I1	14.99	22.52
I2	19.40	19.65
I3	13.10	18.41
I4	13.35	16.26
O1	21.59	25.90
O2	21.67	23.16
O3	12.53	17.27
O4	13.68	13.91
Oa	18.42	21.59
Ob	25.13	19.99
Oc	11.88	21.22
Od	18.73	21.70
MP	25.41	25.14
LP	16.34	86.18
MAP	78.31	74.39
AP	NaN	NaN
LVP	NaN	NaN
X	25.17	25.17
SN	45.61	45.61

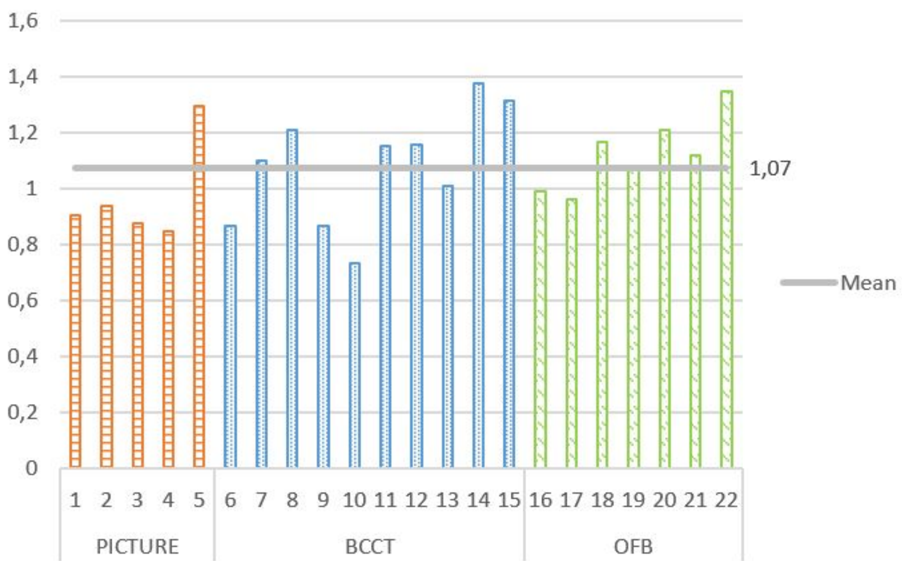

Figure 5.27: Results for the implementation with the patient in a prone position for a single breast, using the normal ICP and a [6,6,6] grid for the FFD.

the ideal approach is to approximate the most the PCLs that are going to be registered.

To overcome the problem of the different positioning of the patient through the data acquisition, the data will be rotated and then aligned through the xy plane, which will place all of the patients in the same conditions.

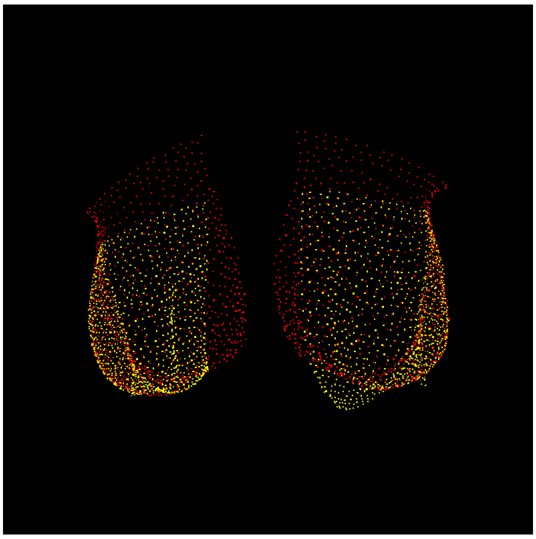

Figure 5.28: Comparison between the results for patient 20 in a prone and upright position. The PCL in yellow represents the breast in a prone position and the PCL in red represents the breast in an upright position, both after the non-rigid registration.

Translation through the breast mound is not a very reliable method, due its lack of robustness and the dependence on factors such as the way the PCL of the scan of the patient is cut, the size of the breast and the size of the stomach. Although it can perform the translation successfully most of the times, or with small deviations, some bad detections can occur, which will worsen the results.

In order to improve the robustness of the algorithm, the detection of the breast mound for the translation should be improved, by manually indicating the breast mound. This could be done as an intermediate step, by asking the clinician to validate if the breast mounds detected by the algorithm were coincident with the real breast mounds. If not, the clinician could manually indicate through the plot of the PCLs where they should be.

A comparison between the implementation of the normal and geometric ICP was made and both have similar errors: 6.41$\pm$1.28mm for the normal ICP, and 7.60$\pm$1.84mm for the geometric ICP. Using the geometric ICP will be valuable mostly to breasts with a bigger ptosis because it will give more weight to the points of that region providing a better fitting between the surface and the MRI PCL.

The number of control points used in the FFD showed to have some influence in the final results, preventing situations where the breast gets completely deformed after the implementation of the FFD. Using a smaller 3D grid of [6,6,6] points leads to results where there are no deformations, even though the mean Euclidean distance is bigger in this case, the TRE distance results show that the matching between the reference points is better in this case.

The cost function of the FFD will attribute the same weight to every point independent of their localization in the PCL. When there are holes in the inframammary fold of the breast, and they are reconstructed, the density of points in that zone is considerably smaller than in the rest of the PCL. When giving additional degrees of freedom to the FFD, that lack of density will lead to deformities that are not plausible.

The registration using the complete torso will lead to some deformations below the sternum, when the fitting before the non-rigid registration is not well performed. The points that do not fit with the region of the ptosis of the breast will match with its surrounding areas, resulting in a higher point density in the region below the sternum. Results using the geometric ICP and the complete torso will not be so deformed due to the better matching in the region below the breast mound.

The registration of the tumor could be analyzed through the comparison of a visual result with a diagram of the real localization of the breast. Even though the results show that the tumor is close to its real localization after the registration, metrics must be implemented in order to understand the accuracy of this registration.

Although the geometric ICP showed greater results, since there were less deformations for this implementation, when testing with the validation dataset the normal ICP showed better results. Even if this dataset only has seven patients, the implementation of the methodology with:

- Single breast
- Upright position
- Normal ICP
- Grid of [6,6,6] points for the FFD.

will be considered the best methodology in future works due to the results obtained.

The registration made with the PCL in a prone position provides good results, but still not better than the results with the upright position and for that it will not be considered.

Chapter 6

Conclusions

Breast cancer is a highly spread disease among women, and although it has a low mortality rate, its high incidence and the consequences of the treatment can have a big impact on women's lives. Its low mortality rate can be justified with the very well set screening program for the early detection of breast cancer and the available options to remove the tumor in these cases. The removal surgery can although lead to some deformations in the breast that will impact the personal life of the patient, leading to feelings of lack of self-confidence and satisfaction that will disturb the normal life of the patient.

To avoid these complications after the surgery, a tool to help guiding the surgery and to communicate better with the patient was built. This tool will match data from the patient coming from the MRI results and from surface data acquired with the patient in an upright position. This tool provides a model that only has a 1.11 ± 0.16mmm deviation from the real shape of the breast. This result is obtained by matching the MRI data with the surface data using a rigid and a non-rigid registration.

The rigid registration is essential to the good performance of this algorithm because it will correctly align the data before the non-rigid registration, allowing its correct performance. This rigid registration consists on the implementation of affine transformations, such as rotations and translations and an implementation of an ICP algorithm. The non-rigid registration consists on the implementation of an FFD algorithm. In the scope of this dissertation, many factors were studied in order to obtain the best of these strategies and the best visualization possible of the breast, to make the model as close to reality as possible, such as the:

- Implementation of a step to correct the orientation of the breast;
- Usage of a geometric ICP in order to correctly align the points with a higher curvature in the breast that did not have a great fitting using the normal ICP;
- Usage of the complete torso for the registration comparing to the usage of a single breast;
- Insertion of the tumor inside the breast;
- Registration of the pectoral muscle;

- Registration of the MRI in a prone position comparing to the upright position;
- Usage of different sizes of grids to the FFD implementation.

In the end these strategies are validated using a validation dataset with landmarks both in the surface and in the MRI PCL that led to the conclusion that the best implementation of this algorithm will come when using only a single breast for the registration, the normal ICP for the rigid registration and an FFD with a [6,6,6] grid for the non-rigid registration.

When using this implementation, all of the patients from the used datasets will have great results, with barely no deformations after the complete registration, providing a reliable tool for clinical usage. The clinical implementation of this algorithm is not yet viable though, since this is not yet a completely automatic process.

6.1 Future Work

Although the results are very promising for a clinical implementation, there are still some changes that could improve the performance of this algorithm.

The translation through the breast mound is the least robust step, that could be improved by manually selecting the breast mound. An intermediate step that asks the clinician to approve the choice of the algorithm for the breast mound would guarantee a correct translation for all the patients.

The impact of the choice of some values used in the pipeline of the algorithm, such as the number of iterations and the threshold used in the ICP and FFD, should be studied in order to understand which values provide better results.

The implementation of evaluation metrics to analyze the registration of the tumor is necessary, since the only way to analyze the current results is purely visual and can be subjective.

The calculation of the volume of the breast is a future step that should be implemented. By calculating the volume of the breast it is possible to compare the variance of the volume through the entirety of the pipeline and check if the transformations are still physically plausible, confirming that larger breasts will have larger displacements in the MAP reference point.

Appendix A

Additional Information

Table A.1: Results after normal ICP with single breast.

Dataset	ID	Laterality	Euclidean Distance	Hausdorff
PICTURE	1	1	7.75	30.70
		2	6.88	34.61
	2	1	7.05	41.99
		2	7.28	39.36
	3	1	5.22	18.78
		2	4.65	20.54
	4	1	7.80	27.97
		2	7.38	29.95
	5	1	4.92	23.78
		2	5.10	19.00
BCCT	6	1	8.45	34.28
		2	8.34	34.69
	7	1	6.48	20.75
		2	6.58	19.51
	8	1	7.90	22.86
		2	8.40	25.29
	9	1	7.47	19.63
		2	7.96	19.33
	10	1	6.20	17.00
		2	6.57	17.34
	11	1	5.51	29.04
		2	6.45	39.73
	12	1	7.43	35.92
		2	6.90	32.99
	13	1	5.12	17.63
		2	5.50	22.02
	14	1	4.89	16.20
		2	5.42	16.80
	15	1	6.07	25.83
		2	6.66	28.72
OFB	16	1	4.16	15.22
		2	4.64	15.38
	17	1	6.43	29.26
		2	4.24	19.56
	18	1	5.76	17.29
		2	6.82	20.53
	19	1	4.43	21.74
		2	4.64	17.06
	20	1	6.60	19.34
		2	6.51	25.87
	21	1	8.89	32.60
		2	8.60	40.65
	22	1	5.95	28.43
		2	6.17	35.79
Mean			6.41	25.48
Std			1.28	7.76
Min			4.16	15.22
Max			8.89	41.99

Table A.2: Results after the geometric ICP with single breast and 100% of the points below the breast mound.

Dataset	ID	Laterality	Euclidean Distance	Hausdorff
PICTURE	1	1	9.29	40.94
		2	7.44	43.42
	2	1	8.66	53.97
		2	9.16	45.99
	3	1	5.68	20.41
		2	6.34	21.82
	4	1	8.27	34.46
		2	8.09	31.92
	5	1	8.61	31.46
		2	6.00	23.07
BCCT	6	1	12.71	46.34
		2	11.76	37.14
	7	1	6.76	24.97
		2	6.61	22.50
	8	1	8.92	36.51
		2	9.16	38.89
	9	1	7.91	22.77
		2	8.17	26.55
	10	1	7.83	33.76
		2	7.89	37.12
	11	1	6.73	32.11
		2	7.88	44.75
	12	1	9.24	47.73
		2	7.23	36.85
	13	1	5.57	20.73
		2	6.40	29.72
	14	1	5.34	20.07
		2	6.17	21.53
	15	1	6.92	25.57
		2	7.90	39.15
OFB	16	1	4.42	15.49
		2	4.67	18.00
	17	1	9.09	42.65
		2	5.42	27.61
	18	1	5.97	18.30
		2	7.11	24.05
	19	1	4.54	22.58
		2	4.86	20.08
	20	1	7.92	31.59
		2	7.53	32.65
	21	1	10.36	45.23
		2	9.96	49.71
	22	1	7.69	43.16
		2	10.36	46.59
Mean			7.60	32.50
Std			1.84	10.23
Min			4.42	15.49
Max			12.71	53.97

Table A.3: Results after the geometric ICP with single breast and 80% of the points below the breast mound.

Dataset	ID	Laterality	Euclidean Distance	Hausdorff
PICTURE	1	1	8.55	35.70
		2	7.52	44.77
	2	1	8.87	53.85
		2	9.32	45.66
	3	1	5.69	19.55
		2	5.64	21.07
	4	1	8.15	39.50
		2	8.16	33.32
	5	1	8.21	29.93
		2	6.59	25.15
BCCT	6	1	13.71	40.28
		2	11.75	38.11
	7	1	7.23	24.22
		2	6.81	22.39
	8	1	8.85	33.10
		2	9.01	32.73
	9	1	9.33	25.31
		2	8.31	22.90
	10	1	7.88	36.66
		2	8.23	39.70
	11	1	6.99	33.80
		2	8.05	47.12
	12	1	7.70	40.76
		2	7.24	38.48
	13	1	5.45	20.20
		2	6.41	31.55
	14	1	5.43	21.50
		2	6.28	25.04
	15	1	6.44	26.65
		2	7.89	38.29
OFB	16	1	4.87	15.19
		2	4.69	18.66
	17	1	8.74	40.92
		2	5.40	26.57
	18	1	5.80	19.96
		2	7.07	23.01
	19	1	4.55	21.79
		2	4.83	20.34
	20	1	7.83	28.02
		2	7.58	32.50
	21	1	10.35	42.67
		2	9.38	49.51
	22	1	7.14	42.45
		2	10.57	42.45
Mean			7.60	32.08
Std			1.88	9.65
Min			4.55	15.19
Max			13.71	53.85

Table A.4: Results after the geometric ICP with single breast and 60% of the points below the breast mound.

Dataset	ID	Laterality	Euclidean Distance	Hausdorff
PICTURE	1	1	8.53	35.75
		2	7.62	44.51
	2	1	9.14	54.16
		2	9.40	45.01
	3	1	6.41	21.98
		2	5.23	17.69
	4	1	8.04	39.77
		2	7.91	34.76
	5	1	6.57	26.61
		2	6.32	25.83
BCCT	6	1	15.09	38.64
		2	12.70	41.05
	7	1	7.81	22.64
		2	7.36	26.90
	8	1	9.82	30.76
		2	9.06	26.97
	9	1	10.04	35.76
		2	8.88	23.66
	10	1	7.50	34.38
		2	8.13	36.86
	11	1	7.07	35.83
		2	7.80	47.17
	12	1	7.75	41.66
		2	7.36	40.34
	13	1	5.40	22.01
		2	6.93	32.38
	14	1	5.89	26.85
		2	6.41	26.31
	15	1	6.56	27.30
		2	7.52	34.78
OFB	16	1	4.56	14.55
		2	4.84	22.24
	17	1	7.40	31.61
		2	5.46	27.05
	18	1	5.84	18.79
		2	7.05	22.70
	19	1	4.61	21.49
		2	4.91	20.15
	20	1	8.07	26.53
		2	7.98	32.79
	21	1	10.16	40.61
		2	10.38	50.09
	22	1	7.36	41.18
		2	10.75	46.42
Mean			7.72	32.15
Std			2.08	9.42
Min			4.56	14.55
Max			15.09	54.16

Table A.5: Results after the geometric ICP with single breast and 40% of the points below the breast mound.

Dataset	ID	Laterality	Euclidean Distance	Hausdorff
PICTURE	1	1	8.56	37.14
		2	7.70	44.82
	2	1	9.76	56.22
		2	9.43	44.91
	3	1	6.29	23.51
		2	5.72	23.11
	4	1	9.04	39.33
		2	8.64	35.42
	5	1	6.37	28.15
		2	6.69	26.34
BCCT	6	1	15.83	40.25
		2	13.25	40.80
	7	1	7.80	26.50
		2	8.03	30.63
	8	1	9.17	32.55
		2	10.79	39.36
	9	1	10.17	34.51
		2	9.65	37.82
	10	1	7.51	30.27
		2	9.02	33.35
	11	1	7.78	40.41
		2	7.51	45.76
	12	1	7.77	40.14
		2	7.79	42.91
	13	1	6.48	26.88
		2	7.14	32.30
	14	1	5.97	26.36
		2	6.70	26.09
	15	1	7.47	28.51
		2	7.83	33.00
OFB	16	1	4.68	13.44
		2	4.94	23.64
	17	1	8.29	33.72
		2	5.62	26.22
	18	1	5.94	17.49
		2	8.74	37.84
	19	1	4.78	22.03
		2	5.30	20.44
	20	1	8.84	31.27
		2	8.78	34.06
	21	1	14.68	54.05
		2	10.15	48.19
	22	1	9.69	40.83
		2	10.76	46.83
Mean			8.25	34.03
Std			2.35	9.33
Min			4.68	13.44
Max			15.83	56.22

Table A.6: Results after non-rigid registration with normal ICP and single breast.

Dataset	ID	Laterality	Euclidean Distance	Hausdorff
PICTURE	1	1	0.92	6.45
		2	0.82	4.89
	2	1	0.93	3.98
		2	0.97	8.69
	3	1	0.83	3.56
		2	0.74	3.23
	4	1	0.75	5.97
		2	0.70	2.90
	5	1	0.87	5.37
		2	0.85	4.12
BCCT	6	1	1.54	19.18
		2	34.80	958.01
	7	1	0.89	4.61
		2	0.77	3.94
	8	1	0.84	5.78
		2	1.55	21.40
	9	1	0.88	5.38
		2	0.89	5.00
	10	1	0.75	3.88
		2	0.81	4.99
	11	1	1.14	5.75
		2	0.93	6.25
	12	1	0.99	5.72
		2	0.98	5.18
	13	1	0.84	0.85
		2	4.50	4.78
	14	1	0.93	6.08
		2	0.78	4.52
	15	1	1.05	5.35
		2	1.03	6.21
OFB	16	1	0.78	4.20
		2	0.80	4.11
	17	1	0.72	0.81
		2	1149.63	2318.48
	18	1	0.97	5.76
		2	16.44	579.37
	19	1	0.95	5.34
		2	0.90	5.58
	20	1	1.04	5.77
		2	0.95	7.52
	21	1	1.02	4.61
		2	0.93	4.31
	22	1	2.82	44.57
		2	1.98	28.60
Mean			28.30	94.34
Std			171.09	376.64
Min			0.70	0.81
Max			1149.63	2318.48

Table A.7: Results after the non-rigid registration using geometric ICP with single breast and 100% of the points below the breast mound.

Dataset	ID	Laterality	Euclidean Distance	Hausdorff
PICTURE	1	1	0.79	5.90
		2	0.80	4.73
	2	1	0.59	2.82
		2	0.79	3.59
	3	1	0.84	6.55
		2	0.68	2.97
	4	1	0.78	4.81
		2	0.67	3.30
	5	1	0.94	6.37
		2	0.84	4.40
BCCT	6	1	0.79	4.49
		2	1.25	8.95
	7	1	0.90	4.01
		2	0.71	2.50
	8	1	0.92	5.85
		2	0.85	5.53
	9	1	0.82	5.24
		2	0.88	4.69
	10	1	0.71	3.04
		2	0.85	4.31
	11	1	1.19	5.94
		2	1.03	8.79
	12	1	1.14	7.05
		2	0.97	5.42
	13	1	0.92	4.63
		2	0.86	4.08
	14	1	1.02	6.13
		2	0.77	5.14
	15	1	1.03	6.65
		2	1.00	6.06
OFB	16	1	0.80	4.31
		2	0.86	5.71
	17	1	0.80	3.90
		2	1.27	9.72
	18	1	0.85	4.17
		2	22.59	943.36
	19	1	0.98	5.49
		2	0.87	5.89
	20	1	1.11	5.96
		2	0.99	6.60
	21	1	1.10	7.65
		2	0.99	6.11
	22	1	2.12	18.06
		2	1.03	6.78
Mean			1.43	26.99
Std			3.24	139.77
Min			0.59	2.50
Max			22.59	943.36

Table A.8: Results after the non-rigid registration, using a single breast and a grid of [6,6,6] points for the FFD, after a normal ICP implementation.

Dataset	ID	Laterality	Euclidean Distance	Hausdorff
PICTURE	1	1	1.16	9.23
		2	1.02	6.51
	2	1	1.31	8.27
		2	1.25	12.59
	3	1	0.90	4.21
		2	0.81	2.98
	4	1	0.96	8.23
		2	0.90	4.41
	5	1	1.17	7.09
		2	1.06	5.06
BCCT	6	1	1.05	7.49
		2	1.11	5.27
	7	1	1.07	5.40
		2	0.88	3.06
	8	1	1.11	6.20
		2	0.93	5.17
	9	1	1.02	5.22
		2	1.10	5.49
	10	1	1.00	5.64
		2	1.14	7.00
	11	1	1.48	7.71
		2	1.18	6.06
	12	1	1.13	5.76
		2	1.30	5.86
	13	1	1.18	5.26
		2	1.03	4.22
	14	1	1.16	6.27
		2	1.03	4.49
	15	1	1.20	6.65
		2	1.32	7.90
OFB	16	1	0.99	3.88
		2	1.02	3.53
	17	1	0.88	4.44
		2	0.97	4.64
	18	1	1.14	5.34
		2	0.90	4.14
	19	1	1.31	5.60
		2	0.97	5.72
	20	1	1.37	7.32
		2	1.20	8.28
	21	1	1.40	8.81
		2	1.42	7.55
	22	1	1.22	6.91
		2	1.28	5.78
Mean			6.41	25.48
Std			1.28	7.76
Min			4.16	15.22
Max			8.89	41.99

Table A.9: Results after the non-rigid registration, using a single breast and a grid of [6,6,6] points for the FFD, after a geometric ICP implementation.

Dataset	ID	Laterality	Euclidean Distance	Hausdorff
PICTURE	1	1	1.04	8.55
		2	1.03	6.09
	2	1	0.48	2.27
		2	0.82	4.67
	3	1	0.94	4.16
		2	0.76	2.98
	4	1	1.05	7.86
		2	0.95	4.86
	5	1	1.16	8.00
		2	1.08	5.63
BCCT	6	1	1.19	11.75
		2	1.58	11.41
	7	1	1.06	4.64
		2	0.85	2.32
	8	1	1.14	7.47
		2	1.11	7.49
	9	1	1.00	6.38
		2	1.06	5.65
	10	1	0.94	3.77
		2	1.24	4.95
	11	1	1.51	8.55
		2	1.26	11.84
	12	1	1.16	7.44
		2	1.29	5.48
	13	1	1.18	5.11
		2	1.08	4.97
	14	1	1.19	6.24
		2	1.04	4.03
	15	1	1.27	8.25
		2	1.29	7.23
OFB	16	1	1.01	4.81
		2	1.03	3.69
	17	1	0.99	5.16
		2	0.97	4.69
	18	1	1.05	5.69
		2	0.90	4.02
	19	1	1.31	6.02
		2	0.97	5.35
	20	1	1.44	7.36
		2	1.32	9.15
	21	1	1.51	11.03
		2	1.53	10.25
	22	1	1.28	7.03
		2	1.41	7.94
Mean			1.13	6.37
Std			0.22	2.43
Min			0.48	2.27
Max			1.58	11.84

Table A.10: Results after the non-rigid registration, using the complete torso and normal ICP.

Dataset	ID	Laterality	Euclidean Distance	Hausdorff
PICTURE	1	1	1.46	10.03
		2	1.56	11.79
	2	1	2.05	16.60
		2	2.22	18.36
	3	1	1.19	6.01
		2	1.15	5.99
	4	1	0.92	7.04
		2	1.02	5.02
	5	1	1.33	7.40
		2	1.30	6.80
BCCT	6	1	1.92	13.21
		2	1.61	12.80
	7	1	1.40	6.11
		2	1.37	5.98
	8	1	1.48	9.03
		2	1.42	7.44
	9	1	1.28	6.71
		2	1.38	8.06
	10	1	1.34	7.77
		2	1.50	8.25
	11	1	1.63	12.45
		2	1.73	14.42
	12	1	1.20	8.99
		2	1.59	6.41
	13	1	1.21	6.95
		2	1.19	6.66
	14	1	1.37	6.68
		2	1.29	7.75
	15	1	1.37	8.95
		2	1.76	32.57
OFB	16	1	0.92	4.54
		2	0.99	4.09
	17	1	0.92	4.41
		2	0.98	4.29
	18	1	1.41	6.67
		2	1.53	6.54
	19	1	1.48	7.12
		2	1.18	7.50
	20	1	1.50	7.54
		2	1.51	9.76
	21	1	1.34	7.34
		2	1.39	8.69
	22	1	1.79	11.16
		2	1.65	9.16
Mean			1.40	8.89
Std			0.28	4.75
Min			0.92	4.09
Max			2.22	32.57

Table A.11: Results after the non-rigid registration, using the complete torso and geometric ICP.

Dataset	ID	Laterality	Euclidean Distance	Hausdorff
PICTURE	1	1	1.48	10.73
		2	1.50	9.27
	2	1	2.03	15.61
		2	2.23	27.21
	3	1	1.15	6.56
		2	1.14	5.95
	4	1	1.11	7.28
		2	1.09	5.82
	5	1	1.25	8.29
		2	1.25	6.60
BCCT	6	1	1.19	11.75
		2	1.58	11.41
	7	1	1.44	6.10
		2	1.51	5.87
	8	1	1.61	10.21
		2	1.51	7.99
	9	1	1.33	8.09
		2	1.43	9.27
	10	1	1.41	9.74
		2	1.47	10.01
	11	1	1.79	12.99
		2	1.79	14.49
	12	1	1.40	7.65
		2	1.38	6.56
	13	1	1.19	7.70
		2	1.18	7.07
	14	1	1.26	6.40
		2	1.32	7.77
	15	1	1.74	11.33
		2	1.72	13.76
OFB	16	1	1.27	5.17
		2	1.39	6.29
	17	1	1.21	5.19
		2	1.14	4.94
	18	1	1.15	6.24
		2	1.13	6.76
	19	1	1.23	6.34
		2	1.12	7.27
	20	1	1.58	8.22
		2	1.48	9.62
	21	1	1.72	8.71
		2	1.54	9.38
	22	1	1.92	11.53
		2	1.87	10.91
Mean			1.44	9.00
Std			0.27	3.79
Min			1.09	4.94
Max			2.23	27.21

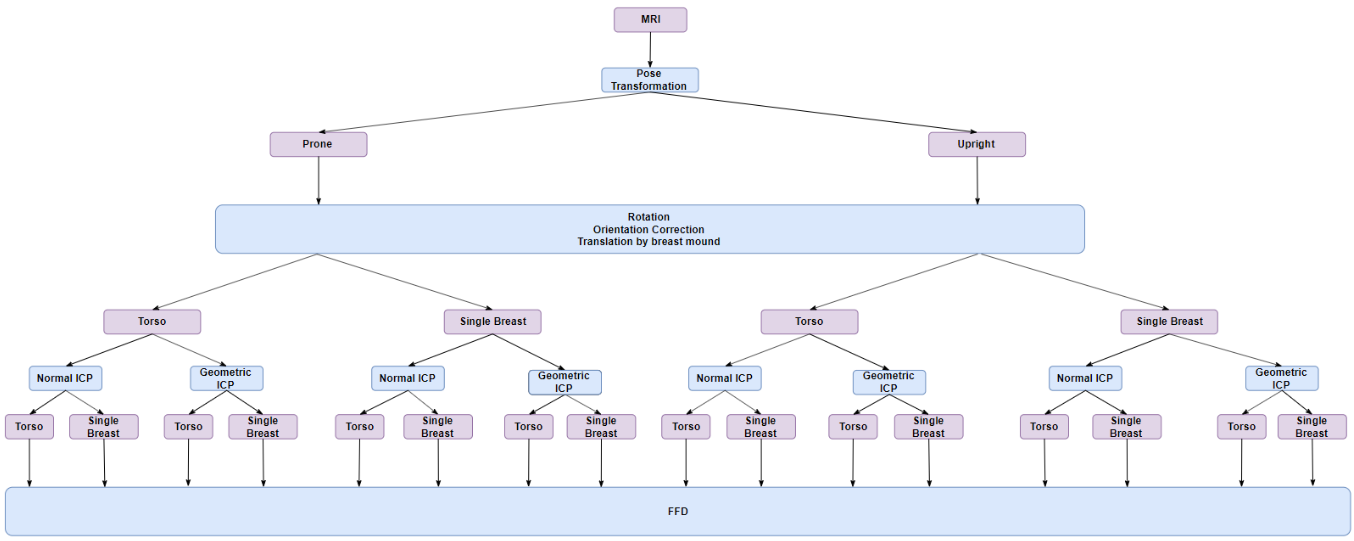

Figure A.1: Diagram with algorithm options.

References

[1] WHO World Health Organization. *World Cancer Report 2008*, volume 133. IARC Press, Lyon, France, 2014.

[2] U.S. Preventive Services Task Force*. Screening for breast cancer: U.s. preventive services task force recommendation statement. *Annals of Internal Medicine*, 151(10):716–726, 2009.

[3] M. Y. Hajeer, D. T. Millett, A. F. Ayoub, and J. P. Siebert. Current products and practices. *Journal of Orthodontics*, 31(1):62–70, 2004. PMID: 15071154.

[4] Kirsti Numminen, Outi Sipilä, and Heikki Mäkisalo. Preoperative hepatic 3D models: Virtual liver resection using three-dimensional imaging technique. *European Journal of Radiology*, 56(2):179–184, 2005.

[5] International Agency for Research on Cancer. Breast Cancer Incidence and Mortality Statistics. 876:6–7, 2018.

[6] National Cancer Intelligence Network. The Second All Breast Cancer Report. *Group*, pages 1–47, 2011.

[7] Carol H. Lee, D. David Dershaw, Daniel Kopans, Phil Evans, Barbara Monsees, Debra Monticciolo, R. James Brenner, Lawrence Bassett, Wendie Berg, Stephen Feig, Edward Hendrick, Ellen Mendelson, Carl D'Orsi, Edward Sickles, and Linda Warren Burhenne. Breast Cancer Screening With Imaging: Recommendations From the Society of Breast Imaging and the ACR on the Use of Mammography, Breast MRI, Breast Ultrasound, and Other Technologies for the Detection of Clinically Occult Breast Cancer. *Journal of the American College of Radiology*, 7(1):18–27, 2010.

[8] Monica Morrow, Janet Waters, and Elizabeth Morris. MRI for breast cancer screening, diagnosis, and treatment. *The Lancet*, 378(9805):1804–1811, 2011.

[9] Olga Pawluczyk, Bindu J. Augustine, Martin J. Yaffe, Dan Rico, Jiwei Yang, Gordon E. Mawdsley, and Norman F. Boyd. A volumetric method for estimation of breast density on digitized screen-film mammograms. *Medical Physics*, 30(3):352–364, 2003.

[10] Valerie A Mccormack and Santos Silva. Breast Density and Parenchymal Patterns as Markers of Breast Cancer Risk : A Meta-analysis. 15(June):1159–1170, 2006. doi:10.1158/1055-9965.EPI-06-0034.

[11] D Rotten and JM Levaillant. The value of ultrasonic examination to detect and diagnose breast carcinomas. analysis of the results obtained in 125 tumors using radiographic and ultrasound mammography. *Ultrasound in Obstetrics and Gynecology*, 2(3):203–214, 1992.

[12] Kevin M. Kelly, Judy Dean, W. Scott Comulada, and Sung Jae Lee. Breast cancer detection using automated whole breast ultrasound and mammography in radiographically dense breasts. *European Radiology*, 20(3):734–742, 2010.

[13] Jerry L. Prince and Jonathan M. Links. *Medical Imaging Signals and Systems*. Pearson Education, New Jersey, 1 edition, 2006.

[14] R. M. Mann, C. K. Kuhl, K. Kinkel, and C. Boetes. Breast mri: guidelines from the european society of breast imaging. *European Radiology*, 18(7):1307–1318, Jul 2008.

[15] Rhadika Sivaramakrishna. 3D breast image registration - A review. *Technology in Cancer Research and Treatment*, 4(1):39–48, 2005.

[16] Sachin Prasad N and Dana Houserkova. THE ROLE OF VARIOUS MODALITIES IN BREAST IMAGING. 151(2):209–218, 2007.

[17] Subbhuraam Vinitha Sree. Breast imaging: A survey. *World Journal of Clinical Oncology*, 2(4):171, 2011.

[18] Helga Henseler, Balvinder S. Khambay, Adrian Bowman, Joanna Smith, J. Paul Siebert, Susanne Oehler, Xiangyang Ju, Ashraf Ayoub, and Arup K. Ray. Investigation into accuracy and reproducibility of a 3D breast imaging system using multiple stereo cameras. *Journal of Plastic, Reconstructive and Aesthetic Surgery*, 64(5):577–582, 2011.

[19] Helder P. Oliveira, Jaime S. Cardoso, Andre Magalhaes, and Maria J. Cardoso. Methods for the Aesthetic Evaluation of Breast Cancer Conservation Treatment: A Technological Review. *Current Medical Imaging Reviews*, 9(1):32–46, 2013.

[20] Joost M. Riphagen, Johan W. Van Neck, and Leon N A Van Adrichem. 3D surface imaging in medicine: A review of working principles and implications for imaging the unsedated child. *Journal of Craniofacial Surgery*, 19(2):517–524, 2008.

[21] Fabio Remondino. Image-Based 3D Modelling : a Review. *The Photogrammetric Record*, 21(September):269–291, 2006.

[22] António Pintor. *A Rigid 3D registration framework of women body RGB-D images*. PhD thesis, Faculdade de Engenharia da Universidade do Porto, 2016.

[23] J. S. Wheat, S. Choppin, and A. Goyal. Development and assessment of a Microsoft Kinect based system for imaging the breast in three dimensions. *Medical Engineering and Physics*, 36(6):732–738, 2014.

[24] Tepper O.M., Karp N.S., Small K., Unger J., Rudolph L., and Pritchard A. Three-dimensional imaging provides valuable clinical data to aid in unilateral tissue expander-implant breast reconstruction. *Breast Journal*, 14(6):543–550, 2008.

[25] Andrea M. Covelli, Nancy N. Baxter, Margaret I. Fitch, David R. McCready, and Frances C. Wright. 'Taking Control of Cancer': Understanding Women's Choice for Mastectomy. *Annals of Surgical Oncology*, 22(2):383–391, 2014.

[26] Eric M. Horwitz, Alexandra L. Hanlon, Wayne H. Pinover, Penny R. Anderson, and Gerald E. Hanks. Impact of surgery and chemotherapy on the quality of life of younger women with breast carcinoma: A prospective study. *Cancer*, 92(5):1288–1298, 2001.

[27] L. Aerts, M. R. Christiaens, P. Enzlin, P. Neven, and F. Amant. Sexual functioning in women after mastectomy versus breast conserving therapy for early-stage breast cancer: A prospective controlled study. *Breast*, 23(5):629–636, 2014.

[28] Minna Salakari, Liisa Pylkkänen, Lauri Sillanmäki, Raija Nurminen, Päivi Rautava, Markku Koskenvuo, and Sakari Suominen. Social support and breast cancer: A comparatory study of breast cancer survivors, women with mental depression, women with hypertension and healthy female controls. *Breast*, 35:85–90, 2017.

[29] Lisa Gottesfeld Brown. A survey of image registration techniques. *ACM Comput. Surv.*, 24(4):325–376, December 1992.

[30] Yujun Guo, Radhika Sivaramakrishna, Cheng Chang Lu, Jasjit S. Suri, and Swamy Laxminarayan. Breast image registration techniques: A survey. *Medical and Biological Engineering and Computing*, 44(1-2):15–26, 2006.

[31] V.R.S R S Mani, Dr.S. Rivazhagan, and S Arivazhagan. Survey of Medical Image Registration. *Journal of Biomedical Engineering and Technology*, 1(2):8–25, 2013.

[32] Francisco P.M. Oliveira and João Manuel R.S. Tavares. Medical image registration: A review. *Computer Methods in Biomechanics and Biomedical Engineering*, 17(2):73–93, 2014.

[33] Evert Jan D. Pol and Max H. Viergever. Medical Image Matching—A Review with Classification, 1993.

[34] J. Nissanov, L. Bertrand, N. Kiryati, and S. Gefen. Planar-to-curved-surface image registration. In *2006 Conference on Computer Vision and Pattern Recognition Workshop (CVPRW'06)(CVPRW)*, volume 00, page 72, 06 2006.

[35] Benbellekens, Vincentspruyt, Rafaelberkvens, and Rudipenne. A Benchmark Survey of Rigid 3D Point Cloud Registration Algorithms. *InternationalJournalonAdvancesinIntelligentSystems*, 8(1):118–127, 2015.

[36] Neil D. McKay Paul J. Besl. Method for registration of 3-d shapes, 1992.

[37] Ying He, Bin Liang, Jun Yang, Shunzhi Li, and Jin He. An Iterative Closest Points Algorithm for Registration of 3D Laser Scanner Point Clouds with Geometric Features. *Sensors*, 17(8):1862, 2017.

[38] Xu Tingting and Wei Ning. Non-rigid Multi-modal Medical Image Registration: A Review. *Proceedings of 3rd International Conference on Multimedia Technology(ICMT-13)*, pages 950–957, 2013.

[39] Yujun Guo, Jasjit Suri, and Radhika Sivaramakrishna. Image registration for breast imaging: A review. *2005 IEEE Engineering in Medicine and Biology 27th Annual Conference*, 4:3379–3382, 2006.

[40] Nenad Vujovic and Dragana Brzakovic. Establishing the correspondence between control points in pairs of mammographic images. *IEEE Transactions on Image Processing*, 6(10):1388–1399, 1997.

[41] Rhadika Sivaramakrishna. *Breast Image Registration using a Textural Transformation*. PhD thesis, University of Manitoba, 1997.

[42] Frédéric J.P. Richard and Laurent D. Cohen. A new image registration technique with free boundary constraints: application to mammography. *Computer Vision and Image Understanding*, 89(2):166 – 196, 2003.

[43] William M. Hsu, John F. Hughes, and Henry Kaufman. Direct manipulation of free-form deformations. *ACM SIGGRAPH Computer Graphics*, 26(2):177–184, 1992.

[44] Thomas W. Sederberg and Scott R. Parry. Free-form deformation of solid geometric models. *Proceedings of the 13th annual conference on Computer graphics and interactive techniques - SIGGRAPH '86*, 20(4):151–160, 1986.

[45] Romain Raffin. *Free Form Deformations or Deformations Non-Constrained by Geometries or Topologies*, pages 49–74. Springer Netherlands, Dordrecht, 2013.

[46] D. Rueckert, C. Hayes, C. Studholme, P. Summers, M. Leach, and D. J. Hawkes. Non-rigid registration of breast MR images using mutual information. (July):1144–1152, 1998.

[47] Julia Anne Schnabel, Christine Tanner, Anthony D. Smith, Andreas Degenhard, Carmel Hayes, Martin O. Leach, D. Rodney Hose, Derek L. G. Hill, and David John Hawkes. Validation of non-rigid registration of contrast-enhanced mr mammography using finite element methods. 2007.

[48] Nicole V. Ruiter, Rainer Stotzka, Tim Oliver Müller, Hartmut Gemmeke, Jürgen R. Reichenbach, and Werner A. Kaiser. Model-based registration of X-ray mammograms and MR images of the female breast. *IEEE Transactions on Nuclear Science*, 53(1):204–211, 2006.

[49] Julia Krüger, Jan Ehrhardt, Arpad Bischof, and Heinz Handels. Breast compression simulation using ICP-based B-spline deformation for correspondence analysis in mammography and MRI datasets. 8669:86691D, 2013.

[50] Thomy Mertzanidou, John Hipwell, Stian Johnsen, Lianghao Han, Bjoern Eiben, Zeike Taylor, Sebastien Ourselin, Henkjan Huisman, Ritse Mann, Ulrich Bick, Nico Karssemeijer, and David Hawkes. MRI to X-ray mammography intensity-based registration with simultaneous optimisation of pose and biomechanical transformation parameters. *Medical Image Analysis*, 18(4):674–683, 2014.

[51] Joaquim Salvi, Carles Matabosch, David Fofi, and Josep Forest. A review of recent range image registration methods with accuracy evaluation. *Image and Vision Computing*, 25(5):578–596, 2007.

[52] Pedro Costa, João P. Monteiro, and Hélder P. Oliveira. Tessellation-based coarse registration method for 3D reconstruction of the female torso. *Proceedings - 2014 IEEE International Conference on Bioinformatics and Biomedicine, IEEE BIBM 2014*, 2014.

[53] L. Han, J. H. Hipwell, B. Eiben, D. Barratt, M. Modat, S. Ourselin, and D. J. Hawkes. A nonlinear biomechanical model based registration method for aligning prone and supine mr breast images. *IEEE Transactions on Medical Imaging*, 33(3):682–694, March 2014.

[54] Hamed Khatam, Gregory P. Reece, Michelle C. Fingeret, Mia K. Markey, and Krishnaswamy Ravi-Chandar. In-vivo quantification of human breast deformation associated with the position change from supine to upright. *Medical Engineering and Physics*, 37(1):13–22, 2015.

[55] Christian Behrenbruch, Christian Behrenbruch, Kostas Marias, Kostas Marias, Pa Armitage, Pa Armitage, N Moore, N Moore, J Clarke, J Clarke, J Michael Brady, and J Michael Brady. Prone-Supine Breast MRI Registration for Surgical Visualisation. *Medical Imaging Understanding and Analysis*, pages 4–7, 2001.

[56] A. Pérez del Palomar, B. Calvo, J. Herrero, J. López, and M. Doblaré. A finite element model to accurately predict real deformations of the breast. *Medical Engineering and Physics*, 30(9):1089–1097, 2008.

[57] B. Eiben, L. Han, J. Hipwell, T. Mertzanidou, S. Kabus, T. Buelow, C. Lorenz, G. M. Newstead, H. Abe, M. Keshtgar, S. Ourselin, and D. J. Hawkes. Biomechanically guided prone-to-supine image registration of breast MRI using an estimated reference state. *Proceedings - International Symposium on Biomedical Imaging*, pages 214–217, 2013.

[58] Pedro Henrique Moreira and Queirós Carvalho. Multimodal Breast Image Registration: Mapping MRI and Surface Data. 2018.

[59] Michael A Wirth, Jay Narhan, and Derek W. S Gray. Nonrigid mammogram registration using mutual information. *Proceedings of SPIE*, 4684(1):562–573, 2002.

[60] J A Schnabel, C Tanner, A D Castellano-Smith, A Degenhard, M O Leach, D R Hose, D L G Hill, and D J Hawkes. Validation of nonrigid image registration using finite-element methods: Application to breast mri images. *IEEE Transactions on Medical Imaging*, 22(2):238–247, 2003.

[61] Helga Henseler, Sarah Kim Bonkat, Peter Maria Vogt, and Bodo Rosenhahn. The kinect recording system for objective three- and four-dimensional breast assessment with image overlays. *Journal of Plastic, Reconstructive Aesthetic Surgery*, 69(2):e27 – e34, 2016.

[62] F. Bernardini, J. Mittleman, H. Rushmeier, C. Silva, and G. Taubin. The ball-pivoting algorithm for surface reconstruction. *IEEE Transactions on Visualization and Computer Graphics*, 5(4):349–359, Oct 1999.

[63] Hooshiar Zolfagharnasab. *Toward a 3D Planning Approach for Breast Conserving Surgery*. PhD thesis, 2018.

[64] C.J. D'Orsi and Acr. *2013 ACR BI-RADS Atlas: Breast Imaging Reporting and Data System*. American College of Radiology, 2014.

[65] Vasileios Vavourakis, Bjoern Eiben, John H. Hipwell, Norman R. Williams, Mo Keshtgar, and David J. Hawkes. Multiscale mechano-biological finite element modelling of oncoplastic breast surgery - Numerical study towards surgical planning and cosmetic outcome prediction. *PLoS ONE*, 11(7), 2016.

[66] J.B.Antoine Maintz and Max A. Viergever. A survey of medical image registration. *Medical Image Analysis*, 2(1):1 – 36, 1998.

[67] P. J. Besl and N. D. McKay. A method for registration of 3-d shapes. *IEEE Transactions on Pattern Analysis and Machine Intelligence*, 14(2):239–256, Feb 1992.

[68] Hugues Hoppe, Tony DeRose, Tom Duchamp, John McDonald, and Werner Stuetzle. *Surface reconstruction from unorganized points*, volume 26. ACM, 1992.

[69] L. Han, J. H. Hipwell, B. Eiben, D. Barratt, M. Modat, S. Ourselin, and D. J. Hawkes. A nonlinear biomechanical model based registration method for aligning prone and supine mr breast images. *IEEE Transactions on Medical Imaging*, 33(3):682–694, March 2014.

[70] Alireza Javaheri, Catarina Brites, Fernando Pereira, and Joao Ascenso. Subjective and Objective Quality Evaluation of 3D Point Cloud Denoising Algorithms. (July):1–6, 2017.

[71] D. P. Huttenlocher, W. J. Rucklidge, and G. A. Klanderman. Comparing images using the hausdorff distance under translation. In *Proceedings 1992 IEEE Computer Society Conference on Computer Vision and Pattern Recognition*, pages 654–656, June 1992.

[72] Sílvia Bessa, Pedro Carvalho, and Hélder P. Oliveira. Breast Image Registration of MRI and Kinect Data Based on 3D Surface Matching, INESC TEC Faculty of Sciences , University of Porto. *The IEEE International Symposium on Biomedical Imaging*, 2018.

[73] J Michael Fitzpatrick and Jay B West. The Distribution of Target Registration Error in Rigid-Body Point-Based Registration. 20(9):917–927, 2001.